PILOT SEISMIC HAZARD ASSESSMENT OF THE GRANITE CITY, MONKS MOUND, AND COLUMBIA BOTTOM QUADRANGLES, ST. LOUIS METROPOLITAN AREA, MISSOURI AND ILLINOIS

FINAL TECHNICAL REPORT

USGS NEHRP External Grant: 07HQGR0012

J. David Rogers and Deniz Karadeniz

Department of Geological Sciences and Engineering
Missouri University of Science & Technology
(formerly University of Missouri-Rolla)
Rolla, MO 65409-0230
Phone: 573-341-6198
Fax: 573-341-6935
E-mail: rogersda@mst.edu

Key words: Seismic hazard analyses, site response, sensitivity, amplification

ABSTRACT

Three 1:24000 scale quadrangles were selected for a pilot program intended to evaluate seismic site response across the spectrum of geologic conditions underlying the St. Louis Metropolitan area, using the Granite City, Monks Mound and Columbia Bottom quadrangles. These evaluations included assessments of: i) site amplification distributions; ii) probabilistic hazard analysis of PGA, 0.2 second and 1.0 second spectral accelerations for 2%, 5% and 10% probability of exceedance in 50 years; iii) two scenario earthquakes and their associated PGA, 0.2 sec, and 1 sec spectral accelerations; and v) sensitivity and uncertainty analyses. These hazard maps were prepared using a fully-probabilistic approach, which considered uncertainties in the input data and in the predicted site amplification.

The results indicate that the variations of the soil conditions in the St. Louis area exert; i) a significant influence on the amplitude, and ii) contrasting shaking characteristics for each of the ground motion parameters. Accurate estimates of the soil cap thickness are most important for assessing amplification. The other important parameter affecting site amplification was the input earthquake time histories. The thickness and shear wave velocity of the weathered bedrock horizon (below the soil cap) appears to have little impact on site amplification, or upon the associated uncertainties. This study included the effects of the underlying geologic conditions, using virtual borings on a 500 meter grid. It has been predicted that on loess covered uplands, earthquake forces may be most severe for short period structures, while in the flood plains underlain by alluvium, earthquake forces can be expected to be more severe for long period structures.

ACKNOWLEDGMENTS

We would like to express our gratitude to Dr. Chris Cramer, for his recommendations and review of the hazard mapping process. He guided us through much of the process and always kept an eye on us during the course of this study.

We also owe a debt of thanks to the St. Louis Earthquake Hazard Mapping Program - Technical Working Group for their technical oversight, suggestions, and much of the needed data for this project.

Thank you also to the U.S. Geological Survey – National Earthquake Hazard Reduction Program, which provided funding for this project through the award of an external research grant. The USGS Center for Earthquake Research and Information in Memphis also provided continual support, especially, through the many valuable materials posted on their website, which relate the earthquake hazards in the Central and Eastern United States.

1. INTRODUCTION

When a building is subjected to ground shaking from an earthquake, elastic waves travel up into the structure. Some of this wave energy is reflected at each floor in the building frame and the remainder reflected from the top of the structure (Frankel, 1999). As the shaking continues, the structure begins to shake and vibrate at various frequencies. Wide ranges of ground motion frequencies are generated by earthquakes, depending on epicentral distance, depth, and the vertical and horizontal components of the ground motion, and position (on hanging or footwall side of the causative fault). The geologic conditions at the site of interest also exert enormous influence on damping or amplification of incoming seismic energy, especially at distances > 100 km. The frequencies of vibration experienced by structures can vary from hundreds to tens of cycles per second, usually expressed as Hertz (Hz). Most man-made structures have fundamental periods of vibration between 0.1 and 20 Hz. As an example, a typical 2-story building has a natural frequency around 5 Hz (0.2 sec period) and 10-story building has a natural frequency around 1 Hz (1 sec period). Structures are most sensitive to ground motions with frequencies that nearly coincide with their natural frequency, because of resonance (Chopra, 2001). As a consequence, structural damage depends on the building's dynamic properties as well as the characteristics of the incoming seismic wave train such as: peak acceleration and velocity, duration, frequency content, and kinetic energy. These characteristics of the earthquake ground motion are usually influenced by trigger factors, such as, the magnitude, distance from the source, rock type and composition, presence of the fractures in rock, and properties of the soil cover capping the bedrock. According to Anderson et al. (1996), a significant portion of these characteristics are affected by the near-surface conditions, even though those materials only typically comprise 0.3% of the energy travel path. It is of particular importance to building codes and engineering design to accurately estimate the depth and character of the unconsolidated soils capping the underlying bedrock, because these control the fundamental site period at any given location. In a subsequent section the methods and techniques for estimating seismic propagation through the unconsolidated materials will be explained. It is widely accepted that "soil sites" tend to amplify ground motions more than "rock sites," particularly at frequencies less than ~ 2 Hz, because of the soft, unconsolidated nature of these young soils. However, past earthquake experiences and laboratory experiments have demonstrated that soil behavior becomes nonlinear at the high strains achieved in the near-field

area of larger magnitude earthquakes. Such nonlinear behavior would reduce the amplitude of seismic waves at frequencies >~2 Hz and lower resonant frequencies caused by the soil cover.

As the practice currently exists, it is usually desirable to estimate the fundamental site period through analysis of wave propagation. The natural site period of sites capped by unconsolidated soils are typically in the range of 0.5 to 1.0 second, about the same period as most structures between 3 and 10 stories high. When the site period and a structure's fundamental periods coincide there is a high probability for a state of resonance to develop, which can wreck havoc on any structure. Therefore, to develop a cogent design strategy for structures subjected to earthquake motion, it is usually desirable to estimate the fundamental periods of the structure and of the site so a comparison can be made to see if the probability of resonance exists. The building codes (such as NEHRP Recommended Provisions for Seismic Regulations for New Buildings and Other Structures, 1997, 2000, and 2003 editions), ASCE 7 Standard, Minimum Design Loads for Buildings and Other Structures (1998, 2002, and 2005 editions); and International Building Code, 2000, 2003, and 2006 editions) account for these effects using the United States Geological Survey National Seismic Hazard Maps. The National Hazard Maps show the areal distribution of earthquake shaking levels that have a specified probability of occurring in the United States (typically, 2% and 10% PE in 50 yrs).

It is known that strong earthquakes are less frequent in the Central and Eastern United States than in California. This is why damage in Central and Eastern U.S. could be catastrophic in a powerful temblor, because most buildings and other structures there have not been constructed to withstand any earthquake shaking. A FEMA (Federal Emergency Management Agency) study estimated seismic risk in all regions of the United States using the probabilistic seismic hazard data developed by USGS in 1996. This study (FEMA, 2001) revealed that the annualized earthquake loss to the national building stock is $4.4 billion per year. 84 % of average annual loss is located on the west coast and 16 % of annual loss is distributed throughout the rest of the U.S. The FEMA report predicted that the states surrounding the New Madrid Seismic Zone have moderate to high annual loss ratios (between $50 to 500 million), Missouri being one of the highest. In this area, the St Louis Metro Area has the highest annualized earthquake losses (between $20-50 Million).

The national hazard maps developed by the USGS (Frankel et. al., 1996, 2002) are directly referenced by the National Earthquake Hazards Reduction Program (NEHRP)

Recommended Provisions and most of the other building codes. National maps delineating earthquake shaking hazard levels provide information essential to creating and updating the seismic design provisions of the building codes used in the United States (Frankel, 1999). Unfortunately, these hazard maps do not include the effects of local geologic conditions, which can greatly affect seismic site response. Because of their scale and coverage, these maps assume the average shear wave velocity of the upper 30 m to be 760 m/s (roughly equal to NEHRP soil profile type B-C, V_s = 2500 ft/sec). The unconsolidated sediments in the upper Mississippi Embayment typically exhibit shear wave velocities less than 250 m/s (Romero and Rix, 2001; Gomberg et al. 2003; Williams et al., 2003, 2007). In order to account for these local site effects, a team of scientists funded by the USGS developed a series of seismic hazard maps for Memphis, TN. Memphis was selected because it is the most densely populated urban area in close proximity to the New Madrid Seismic Zone. Memphis is underlain by a 1-kilometer-thick sequence of loosely consolidated sediments deposited in the Mississippi Embayment. This thick sequence of soil-like materials tends to damp high frequency motions and amplify low frequencies. Cramer et al. (2004) oversaw preparation of the seismic hazard maps for a six-quadrangle area in and around Memphis, accounting for site effects.

In response to earthquake hazard potential in other parts of the Midwest, in 2004 the United States Geological Survey Central Eastern U.S. (USGS-CEUS) office organized a St. Louis Area Seismic Hazard Mapping Project, which is guided by a Technical Working Group (SLAHMP-TWG). The SLAHMP-TWG convenes four times a year to discuss mutual goals and assignments for the five-year NEHRP Earthquake Hazards Program (EHP) study focusing on evaluating relative seismic risks and ground shaking hazards posed to the St. Louis Metropolitan area, which encompassed an area of about 4,000 km^2 on 29 USGS 7.5-minute quadrangles. The long term objectives of this project are to: i) to create a detailed map of earthquake hazards in the St Louis metro area; ii) to create a three-dimensional database of geologic and geotechnical information; and iii) to enlist practical input from stakeholder and end users of the hazard maps (engineers, geoscientists, utilities, planners, investors, building and zoning officials, insurers, financiers, etc.).

The principal short-term goal of the SLAHMP-TWG is to compile available geodata for three pilot quadrangles (Granite City, Monks Mound, Columbia Bottom) to ascertain what level of effort and cost will be required to prepare seismic hazard maps of the 29 quadrangles in the St.

Louis Metro area, using a similar format to that established by the USGS CEUS office for the Memphis/Shelby County Seismic Hazard Mapping project, completed in 2004. These maps should also serve as example work products for what the 5-year NEHRP-EHP in St. Louis could develop, to allow geoscientists and engineers to use the 1997 NEHRP Provisions in the 2003 International Building Code (IBC), recently adopted by the City and County of St. Louis and St. Charles County, which are also being considered by 11 other municipalities in the immediate area.

Recent reviews of water well logs and geotechnical borings in the pilot quadrangles reveals that the Mississippi flood plain actually exhibits a wide array of soil profiles and depths to bedrock, ranging from as little as 2 m to as much as 76 m, with a variety of materials, ranging from peats and fat clay to dense gravelly sands. These differences in material thicknesses and physical properties soon revealed problems with estimating seismic site-response based on the 1:250,000 scale surficial materials maps, making them untenable.

2. RESEARCH OBJECTIVES

The greater St. Louis metropolitan area is a densely populated urban zone, bounded by extensive deposits (up to 76 m deep) of unconsolidated sediments (mostly sands) underlying well-defined flood plains. St. Louis is located near the intersection of two major rivers (Mississippi and Missouri Rivers) and it is about 200 to 340 km north of the New Madrid Seismic Zone (Figure 1).

The overarching goal of this study was to prepare credible seismic hazard maps for three pilot quadrangles felt to be representative of the geologic conditions across the entirety of the St. Louis Metropolitan area. These included the Granite City, Monks Mound, and Columbia Bottom quadrangles, which encompass downtown St. Louis and the area to the north, on both sides of the Mississippi River, and the entire Mississippi flood plain, extending onto the fluvio-glacial outwash blanketing the uplands east of the flood plain in Illinois. The contrasting geologic conditions underlying these areas would allow the TWG to make preliminary evaluations that would be useful tests of the codified seismic design protocol contained with the 2003 IBC. These results should be of interest to expected end users such as: state and federal agencies; academic researchers; public agencies (such as state departments of transportation), local agencies (including building and safety officials), private sector businesses (consultants and insurance

companies), and the general public. This study also should serve as a "baseline" work, so the SLAHMP-TWG can ascertain the reality of proceeding with the original goal of assessing 29 quadrangles in the greater St. Louis Metro area.

This report documents the following maps separately for each quadrangle under investigation (Granite City, Monks Mound and Columbia Bottom):

1. Site amplification maps for ten different ground shaking levels;
2. 2% probability of exceedance in 50 years in terms of PGA;
3. 5% probability of exceedance in 50 years in terms of PGA;
4. 10% probability of exceedance in 50 years in terms of PGA;
5. 0.2 second spectral accelerations for 2%, 5% and 10% probabilities of exceedance in 50 years;
6. 1 second spectral accelerations for 2%, 5% and 10% probabilities of exceedance in 50 years;
7. Two scenario earthquakes (M 7.2 and M6.5) and their associated PGA and 0.2 sec-SA and 1 sec-SA.

In summary, 10 amplification maps and 15 seismic hazard maps were developed for each of the three pilot 1:24,000 scale quadrangles. This resulted in 30 site amplification and 45 seismic hazard maps for the three pilot quadrangles, encompassing a land area of about 415 km^2.

3. SITE AMPLIFICATION MAPS

3.1. INTRODUCTION

It has been known for many years now that many of the most damaging earthquakes have been ascribable to local variations in geologic site conditions. Some of the most notable examples include: Mexico City during the 1985 Michoacán earthquake (Zeevaert, 1991; Romo and Seed, 1986; Singh et al. 1988; Resendiz and Roesset, 1988; Anderson, 2003); San Francisco Bay margins during the 1989 Loma Prieta earthquake (Seed et al. 1990; Aki 1993); and Avcilar-Turkey during the 1999 Izmit and Duzce earthquakes (Tezcan et al., 2002; Cranswick et al., 2000). All these earthquakes emphasized the necessity of accurately estimating the effects of site conditions on amplification of the incoming ground motions.

The relatively unconsolidated "soil cap" overlying more coherent "bedrock" crust materials not only influences peak ground motion parameters, but alters the frequency content of

the ground motion. For example, Seed et al. (1976) compiled the response spectra of ground motions for four categories of site conditions: rock sites, stiff soil sites, deep cohesionless soil sites, and soft to medium stiff clay sites. The response spectra were normalized to peak ground acceleration to allow comparison of different site spectrums. The differences in spectrum were significant. Their results indicated that deep and soft soil cover sites were capable of amplifying long period (periods above 0.5g) ground motions. Studies conducted in the St. Louis area also indicate that large amplifications can be expected in the major river channels filled with unconsolidated alluvium (Rogers et al., 2007b). These researchers calculated 6 to10 times of maximum amplification for various periods and noted increasing amplification for progressively weaker ground motions. The amplification of seismic energy through a soil column is greater in lower magnitude earthquakes because these ground motions are of insufficient amplitude to trigger an inelastic response of the soil cap, which could cause substantive damping of incoming seismic energy. This phenomenon results in greater percent amplification of incoming seismic energy for smaller magnitude events.

Even within a section of a city, the intensity of ground shaking and its effects may vary considerably during any given earthquake (Seed and Idriss, 1969a and 1969b). This variation in shaking intensity can be a result of different geologic conditions underlying the city (Rogers and Figuers, 1991; Goodman and Appuhn, 1966; Duke, 1958; Gutenberg, 1956). Modern seismic hazard analyses are based primarily on accurate assessments of site amplification that incorporate considerations of actual geologic conditions underlying any study area. The uncertainties associated with the amplification calculations will add additional uncertainties in the seismic hazard maps. Therefore, special attention was directed to accurately quantify the expected site amplification in the St. Louis Metro area and determine the parameters that appear to most influence the shaking hazard.

Amplification (or deamplification) is defined as the modification of the earthquake wave frequency content and amplitude as it propagates upward through a soil medium. The amount of modification depends on a few factors, the physical properties of the "soil cap" being the most important. Amplification spectra compare the response of a 'soil site' relative to a 'rock site.' Site amplification is the ratio of the response spectra (or the ground acceleration) of a soil site to the response spectra (or the rock acceleration) of a rock site, at the same epicental distance.

The distribution of site-specific amplifications is of great import in crafting probabilistic /deterministic hazard maps, which are intended to highlight zones of asymmetrical site response. These sites portend the greatest hazard to long-period structures, such as tall buildings, multi-span bridges, and buried pipelines. These site amplification maps are intended to be used with modern building codes, such as the 2003 IBC, which recognize the importance of impedance contrasts and the shear wave velocity profiles in the upper 30 m, which is of great importance in the Midwest because of the low attenuation of seismic energy.

3.2. METHODOLOGY

The methods used to calculate site amplification were similar to those employed in the Memphis seismic hazard maps, summarized in Cramer et al. (2004). For site amplification calculations the following parameters were used: i) soil type and boundaries; ii) shear-wave velocity (V_s); iii) saturated unit density (ρ_s); iv) dynamic soil properties (in terms of shear modulus and damping); and v) acceleration-time histories at the bedrock-soil interface. The first two parameters are necessary to calculate the amplifications. The unit density, dynamic soil properties, and selected input time histories will be described later in this chapter. The above explained parameters were input into the one-dimensional site-response software program SHAKE91 which calculates the propagation of the wave through the soil column and estimates the site-specific amplification factors.

Anytime we perform a series of calculations that utilize a series of input variables, uncertainties with each of those variables will be compounded, leading to a greater range of uncertainty, bracketing the calculated/reported values. In the assessment of site amplification, uncertainties exist in the following input parameters:

1. natural variations in shear-wave velocity (e.g. horizontal versus vertically propagating shear waves; effects of fracture intensity, weathering, etc.)
2. natural variations in bulk density (especially, with preferential weathering)
3. the techniques used to estimate the depth and thickness of the soil layers
4. the differences in the earthquake time-history records used in the 1-D shaking analyses

When combined together, these uncertainties may cause large differences in amplification calculations. To account for this variability and uncertainties, a random sampling method is usually applied. For example, Romero and Rix (2005), Toro and Silva (2001) and Cramer et al. (2004) calculated the soil response by randomly sampling profiles from a range of soil boundaries, shear-wave velocity values, and dynamic soil properties, before estimating site-amplification. Toro and Silva (2001) used the median site amplification values to calculate the hazard; while Cramer et al. (2004) used the amplification distributions to account for the uncertainties associated with the amplification calculations. Cramer (2003) asserted that the latter method of calculating the hazard was the most dependable because it incorporates the uncertainties in the amplification factor. When a truly probabilistic site-specific ground motion is desired, a state-of-the-art approach would be to estimate the site specific amplification factor distributions and use them in the probabilistic calculations (Cramer, 2003; Cramer, et al. 2004).

In this chapter the methodology and resulting site amplification maps for peak ground acceleration, 0.2 sec. and 1 sec. spectral accelerations are presented. The site amplification calculations were performed using the site amplification code (siteampunc.f) provided by Chris Cramer. In this code, input site response parameters are randomly selected from a range of Vs profiles, dynamic soil properties, geologic boundaries, and a set of earthquake acceleration time-histories. The code then inputs these randomly selected parameters into Shake91 and calculates the response. A flow chart summarizing the steps on generating site amplification distributions is shown in Figure 2. The process for selecting input parameters is explained in the following sections and the results are summarized.

The amplification distributions were calculated based on a grid of 0.005˚ or for about every 500 m (Figure 3). There were total of 1974 grid points encompassing the study quadrangles. For every grid point the site amplifications and distributions calculated first, then the seismic hazard calculations. The amplification distributions were generated for two distinct geologic units (floodplain deposits and upland deposits), and 0.5 km is thought to be sufficient enough to capture the differences between these two units. The amplification values were then smoothed in GIS and drawn as smooth color contours.

The free surface effect in the rock outcrop motions as mentioned earlier must also be accounted for in the calculations, because the acceleration time-histories used as input are assumed to be at the bedrock soil interface. Since the displacement amplitude caused by the free

surface effect is doubled at the surface, the input time-histories were reduced by a factor of 2 changing the rock outcrop motion to the rock-soil interface motion (Cramer, 2006c; Cramer et al., 2004).

3.2.1. Input Earthquake Time Histories. Site amplification is usually inversely proportional to earthquake magnitude because of non-linear response of unconsolidated soils in larger magnitude quakes (>M 5.0), because of their increased duration, which engenders more equivalent cycles of loading. When shaking becomes increasingly severe, shear strain accumulates within the unconsolidated soil layers. When this strain reaches a certain threshold, the soil begins to behave nonlinearly, often undergoing plastic deformation. Soil nonlinearity is characterized by reduction of shear rigidity and, hence, reduction of shear-wave velocity, with increased damping. In terms of site response, this results in higher predominant periods and lower amplification factors. Therefore, the frequency content and amplitude of the ground motion input are important parameters and should be selected using considerable caution.

In this study 12 recordings from 6 real earthquake ground motions were selected in an attempt to capture the complexity of earthquake-time histories at epicentral distances close to 200 km. These recordings were obtained from the PEER strong motion (http://peer.berkeley.edu/products/strong_ground_motion_db.html), COSMOS strong motion (http://db.cosmos-eq.org/scripts/default.plx), and Turkish General Directorate of Disaster Affairs (http://www.deprem.gov.tr/) strong motion databases. In addition to these earthquake recordings, two synthetically generated M7.5 and M8.0 records, from Atkinson and Bresnev (2002), and M7.0 and M7.5 records using the SMSIM v. 2.2 code of Boore (2003), were selected. These synthetic recordings were chosen because they were felt to more representative of the Central and Eastern United States (CEUS) source characteristics and attenuation/damping properties. Table 1 lists the earthquake magnitudes and their respective distance from causative source. St. Louis is located approximately 200 km from the New Madrid and Wabash Valley Seismic Zones and, hence, recordings located at a distance of 180-220 km were selected, with magnitudes as close to ~7.5 as possible.

The acceleration-time histories (for rock) are presented in Figures 4 through 7. Note that the vertical scale (acceleration) is held constant for purposes of comparison. The peak

acceleration values of the time-histories, mean, and maximum periods, of the overall frequency content of the time-histories are summarized in Table 2.

3.2.2. Scaling of the acceleration-time histories. Scaling refers to multiplying a recorded or simulated time-history by a constant factor at each time increment. This approach has the advantage that the time histories maintain the natural phasing of the recorded motion, with realistic peaks and troughs in the spectral shape. The disadvantage is that a large number of time-histories need to be used to obtain a reliable estimate of the average response of the structure (Shakal et al., 2002). It is also important to select records with similar site conditions to the project site whenever scaling is performed. In this study, we searched for time histories recorded on dense soil to soft rock to hard rock. We soon found that they were very few strong motion records available for epicentral distances greater than 180 km, and we were obliged to assume that the crustal characteristics of the wave propagation were more or less similar to those in the CEUS, which is an approximate assumption, at best. We attempted to balance these uncertainties by including synthetic ground motions generated for the crustal characteristics of the CEUS.

The magnitude of site amplification depends on the amplitude and frequency of the input ground motions, due to its nonlinear nature (Cramer at al., 2004). As mentioned previously, the soil properties are important in the amplification process, but the amount of seismic energy propagating through the soil column also governs behavior. Smaller amplitude waves tend to cause higher amplifications and smaller amplitude waves tend to trigger smaller amplifications due to the nonlinear characteristics of the soil cap. In order to characterize the shaking intensity in a fully probabilistic approach, the areal distribution of site amplification was required. In order to capture the amplification distributions, the above mentioned earthquake time-histories were scaled. This was accomplished on the actual ground-motion records at ten different shaking levels (0.01, 0.05, 0.1, 0.2, 0.3, 0.4, 0.5, 0.6, 0.8, and 1.0g) at specific frequencies (PGA, 0.2 sec SA, and 1.0 sec SA) to obtain input, or base rock, ground-motions. The Shake91 program was run for each of these shaking levels and the predicted site amplifications were determined for each level.

3.2.3 Dynamic Soil Properties. The seismic wave propagation is effected by many factors as explained in the previous sections which included the density and shear-wave velocity in large

part. Of these, soil properties such as stiffness and damping characteristics are the most important, because they relate to the nonlinear soil behavior in site response and are affected by the strain level induced by the earthquake. Therefore, the susceptibility of a soil deposit to ground motion amplification is mainly governed by the dynamic soil properties. These properties are known as the shear modulus and damping characteristics of the soil. Shear modulus is a measure of the stiffness of a material and damping is the ability of the material to dissipate energy.

The propagation of seismic waves is affected by a variety of factors, including density and shear-wave velocity. Soil stiffness and damping characteristics usually exert the greatest influence on nonlinear soil behavior, which is controlled by the strain level induced by the earthquake. As a consequence of this "trigger mechanism", the susceptibility of a soil deposit to ground motion amplification is governed, in large part, by the dynamic soil properties. These properties are described by the shear modulus and damping characteristics of the soil. Shear modulus is a measure of the stiffness of a material and damping is the ability of the material to dissipate energy that passes through it.

In this study the shear modulus and damping ratio relations published by EPRI (1993) were used. The 1993 EPRI study summarized the results of numerous resonant column and large-scale triaxial chamber laboratory tests on samples obtained from Gilroy 2 (California), Treasure Island (San Francisco Bay Area), and Lotung, Taiwan. Based on the results of the laboratory tests and literature review, modulus reduction and damping curves were developed for various confining pressures, corresponding to depths ranging from 0 to 305 meters (shown in Figure 8).

3.2.4. Shear-wave velocities. The regional shear-wave velocities were determined for two distinct lithologic units; Holocene age alluvial units and Pleistocene age loess. Local analyses were performed to ascertain variations, uncertainties, and randomness associated with the shear-wave velocity profiles. These data then were grouped based on formation age and stratigraphy. This approach included three locations capped by Holocene age deposits and six locations capped by Pleistocene age materials. The uncertainties in dynamic geophysical properties were then incorporated into a series of regional shear-wave velocity profiles (SWVP) to better approximate the characteristic profile of the Quaternary age cover lying atop the Paleozoic age

basement. The characteristic SWVPs were compiled after correlating this information with the lithologic structure (depth-to-bedrock) recognized in the St Louis area. This study used 76 site-specific shear-wave velocity profiles to compile characteristic SWVPs needed to calculate seismic site amplification across the entire St. Louis Metro area over the next decade.

The characteristic profiles for the Holocene age and Pleistocene age lithologic units are shown in Figure 9 and summarized in Table 3. The alluvial and loessal deposits are divided into six depth increments of 5 meters each to identify the depth dependency of the Vs measurements. The estimated values of shear-wave velocity and associated uncertainties were then input into the site response analysis software (SHAKE91) to calculate the site amplifications.

3.2.5. Surficial material types and their thickness distribution. Granite City, Columbia Bottom and Monks Mound Quadrangles are located in west-southwestern Illinois State and east of Missouri State. This area is mostly contained within the American Bottoms, a large alluvial valley of the Mississippi River containing clay, silt, sand and gravel over bedrock (Grimley et al., 2007). Two geologic units are recognized in the flood plain (alluvial) deposits: Cahokia and Henry Formations. Cahokia Formation is characterized by different facies of floodplain, fan, point bar, levee, oxbow lake, backswamp, tributary and abandoned channel deposits of fine to medium sand (Cahokia sand), and silt to silty clay (Cahokia clay). Of these Cahokia clay overlies Cahokia sand and is the deposition product of oxbow lake and backswamp depositional environments. These environments usually represent fine-grained sediment (CH, CL, ML) lay down during periods of stream flooding. Cahokia sand is the depositional product of point bar, levee, fan and abandoned channel depositional environments. Cahokia sand deposits are generally separated into a fine grained top stratum (clays, silts, silty sands) and a coarser grained substratum (sand and gravel).

The Cahokia Formation is underlain by Henry Formation; a glacial outwash deposit (Wisconsin Episode) predominantly consists of fine-coarse sand to the top and gravel to the bottom (Figures 10). Henry formation rests unconformably on the bedrock valley of the Mississippi River and its thickness ranges from 0 to 20 meters being thickest at the lateral margins of the floodplain in the Monks Mound quadrangle (Smith and Smith, 1984). At these locations, Henry formation is also overlain by thick deposits of fine grained Cahokia clay formation. The boundary between Cahokia and Henry Sand was estimated where the sand

coarsens or at the base of abandoned meander clay plugs (Grimley et al., 2001). Henry Formation also outcrops in the Monks Mound quadrangle locally. In the study area Henry Formation is as thick as 15 to 20 meters below Cahokia Formation.

Flood plain deposits (alluvium) are bounded by the upland deposits (Peoria and Roxana Formation) both on the eastern and western margin of the quadrangles (see Figure 10). Roxana Formation is the older of the two and is distinctively pinkish brown in color, has slightly more sand, coarse silt, and clay compared to the yellow brown Peoria Formation (Grimley and Lepley, 2005). These loess deposits are underlain by highly variable glacial till (Glasford Till) containing mixtures of sand, gravel, silt, and clay and usually unsorted in particle size. Glasford Till is highly variable in composition and texture from fat to lean clay to gravel. It also includes many discontinues sand and gravel lenses that can be tens of meters wide and up to 5 meters thick. In the Granite City quadrangle till may extend to bedrock at depths of 10-23 meters. This is the usual case, however in the southeastern corner of the Monks Mound quadrangle till is underlain by Petersburg Silt and Banner Formation. Petersburg silt is the lake sediment, probably with loessial component and composed of mainly silt and silty materials up to 4 meters thick. Banner Formation is an older till deposition (pre-Illinois Episode) that contains relatively few sandy and gravely materials. Compared to the Glasford till, the Banner till is more clayey, slightly less stiff and has higher moisture content (Grimley and Lepley, 2005). See Table 4 for the comparison of the lithologic units and their ages.

One of the most important parameters in site-response analysis is the thickness of the surficial materials, or depth-to-bedrock values. The ordinary kriging method was used to estimate and interpolate the depth to bedrock boundaries using ArcGIS software version 9.1. The ordinary kriging method uses the information from data points closely surrounding the areas to be estimated by incorporating the autocorrelation structure of the data.

Subsurface information was gleaned from digitized well logs prepared by Missouri and Illinois Departments of Transportation. Stratigraphic interpretations and geologic cross sections were prepared by the Missouri and Illinois geological surveys, based on information gleaned from field exposures, geophysical surveys, and well logs (geotechnical, water wells, mining, environmental). Since all three of the study quadrangles border the Wood River quadrangle, data from this quadrangle was included in the data collection. The spatial distribution of this adjacent

data was needed to reduce 'edge effects' that would otherwise have come to fore in the three study quadrangles.

The primary advantages of the kriging method are its ability to: 1) interpolate an actual value at measured data point; and, 2) to provide kriged estimates and the corresponding uncertainties at unmeasured sites.

Depth-to-bedrock values were estimated by first determining the top-of-bedrock elevation values using the available data points. These top-of-bedrock elevation values were used to construct the kriging map showing the prediction surfaces. Using the spatial analyst tool ArcGIS, the predicted surface of the top-to-bedrock was digitally subtracted from the bedrock elevation using the USGS 30 m DEM (Digital Elevation Model) for the respective quadrangles. The resulting product is an isopach map that is mathematically conformable with both the topographic surface and the bedrock surface, and referred as a 'unit thickness map' or 'depth-to-bedrock' map. The map is shown in Figure 11.

Ordinary kriging was used in this study because of its ability to provide error estimates through known parameters. An error estimate map was constructed for the estimated top-of-bedrock elevation map. According to the calculations, the error ranges from 1.8 to 18.4 meters (Figure 12). The highest error distributions correspond to those areas where there is very little available data.

3.2.6. Bedrock properties. Top-of-bedrock elevations were determined using the kriging method. These elevations are estimates of the top-of-bedrock, and no distinction was made for an intervening 'zone of weathering.' The weathered horizon can exhibit much different dynamic properties from the parent bedrock, depending on a number of factors. Two important aspects of weathering are the thickness of the weathered zone overlying relatively 'fresh' bedrock, and the severity of such weathering, which can significantly reduce the shear-wave velocity in the weathered zone. The severity usually depends on how long the bedrock outcrop was under subaerial exposure (in thousands, or tens of thousands, of years).

Sensitivity analyses were performed to ascertain how these parameters might affect site response, assuming increasing thickness of the "weathered cap," which usually includes residual weathering products. In addition, published literature was reviewed and the SLAHMP-Technical Working Group offered a number of helpful suggestions, based on regional experience.

The thickness of the weathered bedrock was estimated from geological observations gathered by previous workers, including Lutzen and Rockaway (1987), Goodfield (1965), and the ISGS (Grimley, 2006). The thickness of the weathered rock horizon appears to be influenced by geomorphic province, principally, uplands mantled by loess or alluvium deposited in low gradient flood plains. The upland loess sites were then separated into two groups: those east of the Mississippi River in Illinois, which had been glaciated, and those on the Missouri side, which have not been glaciated.

The carbonate rocks are generally susceptible to solution weathering and these weathering products are partly or completely removed. This makes it difficult to describe the severity of weathering in carbonate rocks. The most severe examples of solution weathering and their associated features tend to be manifest in those beds nearest the ground surface, although they may extend to a considerable depth (Lutzen and Rockaway, 1971). The weathering of the Paleozoic carbonate units in and around St. Louis tends to be concentrated along vertical joints and near-horizontal beds that possess the greatest hydraulic conductivity. These "macro pores" tend to become filled with blocks of limestone rubble and pockets of residual clay, often surrounding the blocks. Some of the formations exhibit numerous filled sinks, which are ancient features, and more recent sinkholes, which are oftentimes influenced by ancient filled sinks, which have no apparent relation to current topography or drainage patterns. Filled sinks and reactivated sinkholes are difficult to recognize without subsurface exploration or exposure, so we could not attempt to account for them in this regional hazard assessment, which covered an area of 460 km^2.

The seismic refraction method is generally regarded as one of the most reliable field methods for determining the shear wave velocity of the bedrock close to the ground surface. The USGS dispatched a geophysical field team to St. Louis in 2003 to make a preliminary evaluation of shear wave propagation in the bedrock units underlying the St. Louis Metro area (summarized in Williams et al., 2007). These estimates were based on the reflection/refraction method, and these were used in the site amplification studies described herein. When plotted on a frequency histogram, most of the measured shear wave velocities fall in the range of 1500-2000 m/sec (Figure 13). Using this distribution and the results of recent investigations by ISGS (Bauer, 2007), an average value of 1750 m/sec with a standard deviation of 250 m/s was applied to describe the shear wave velocity in the weathered rock horizon, across the study area. It should

be noted; however, that these observations and the selected Vs value for the weathered rock are not based on the direct outcrop observations or laboratory tests.

The thickness of the weathered rock horizon was estimated in accordance with the geological evidence gathered in the area by various investigators, including Lutzen and Rockaway (1987). As mentioned previously, the thickness of the weathered rock horizon varies significantly, depending on location. The upland deposits are subdivided into two groups based on their paleogeologic history.

There are three recognized sequences of glaciation in the St. Louis Metro area. The oldest is referred to as the 'Pre-Illinoian glaciation' and is believed to have occurred about 450,000 years (450 ka) ago. It is likely originated from east or northeast based on the mapped striations. This glaciation likely extended almost to what is now the Mississippi River flood plain. Geologic conditions west of the Mississippi River suggest that the area west of St. Louis has never been glaciated. Most workers have found scant evidence of glacial-derived sediments underlying the terrain west of the Mississippi River, although a thin and intermittent veneer of glacial till (often queried) material overlies the eroded bedrock surface within 0.5 to 1.5 km of the Mississippi River flood plain (Goodfield, 1965). The warm interglacial period that accompanied this earliest stage of glaciation may have included several cycles with durations on the order of ~240,000 years, which resulted in extensive development of soil residuum (Grimley et al., 2001). In the few bedrock exposures at the ground surface, this residuum is consistently observed lying over the bedrock, reaching thicknesses as great as 10 m.

The next glacial stage has been termed the Illinoian glaciation. It occurred between about 190,000 and 130,000 years ago (Grimley et al., 2001). This glaciation resulted in the deposition of extensive deposits of wind-blown loess and lacustrine (lake) deposits. Soil development was not as extensive as during pre-Illinoian time because the interglacial warming only lasted about ~75,000 years.

The most recent glaciation is known as the Wisconsinan glaciation, which advanced to within ~30 km of what is now St Louis, below the confluence of the Missouri and Mississippi Rivers. However, this stage resulted in the deposition of extensive alluvial deposits carried by discharge from the Upper Mississippi River and Illinois River drainage basins (Curry and Grimley, 2006). The outflow emanating from the northern climes likely carved the modern day flood plain down to bedrock, before the continental glaciers fully retreated. As the glaciers

retreated the rivers systems became increasingly choked with sediment, which began filling the flood plains as sea level and the river's controlling base level, continued rising.

In summary, three different glacial/weathering stages have impacted the study area over the past ~450 ka, leaving a distinctive mark on the weathering profile. The weathered horizons can be subdivided into three major groups, recorded in most of the geotechnical borings across the study area. These are: 1) the western part of the Mississippi River flood plain, which includes loess covered uplands in the Granite City and Columbia Bottom quadrangles; 2) the Mississippi River flood plain, which is filled with alluvial deposits, and: 3) the loess covered uplands east of the Mississippi River, which are underlain by re-worked glacial outwash dating back to ~450 ka. This third area includes the uplands along the eastern fringes of the Monks Mound quadrangle. The thickest sequence of weathered material corresponds with the oldest surficial deposits, the re-worked glacial outwash lying beneath the uplands east of the modern Mississippi River flood plain, which date back to pre-Illinoian time (~450 ka). In this terrain, geotechnical borings suggests that the weathered zone commonly reaches a thickness averaging about ~20 m. We selected 20 m as being a representative thickness to describe the weathered horizon in the uplands on the Illinois side of the Mississippi River flood plain (Figure 14). The only glacial epoch which appears to have encroached the western fringes of the Mississippi River flood plain was during Illinoian time, when an unknown thickness of till was deposited, which was subsequently re-worked and discontinuously eroded, leaving a thin veneer of overconsolidated till, to a maximum depth of 3 m (Grimley et al., 2001). West of the Mississippi River geotechnical borings usually encounter a weathered bedrock horizon (beneath the loess or till veneer) that is only 1 to 2 m thick. For these reasons, a weathered zone 2 m thick was assumed to exist beneath the loess covered uplands west of the Mississippi River for this study (Figure 14). Other observations in the area support this value (Lambert et al., undated).

Borings in the modern Mississippi River flood plain that pierce the bedrock basement consistently exhibit no discernable zone of weathering. Most workers have concluded that the weathered rock horizon was removed during relatively intense erosive cycle that initiated during the Pleistocene-Holocene epoch transition, beginning around ~11 ka (Goodfield, 1965; Grimley, et al., 2001). In this study we have, therefore, assumed the weathered rock horizon is absent beneath the alluvial valleys of the major water courses, such as the Mississippi and Missouri Rivers (see Figure 14).

3.3. CALCULATION PROCEDURE AND RESULTS

For each frequency and amplitude the process of randomly choosing a ground-motion record, scaling it, then, randomly selecting sediment properties from a suite of Vs profiles and soil depths, and, finally, calculating the response of the site, is repeated 100 times. A mean and standard deviation is then derived from these 100 estimates of the amplification product.

The Monte Carlo randomization method is a numerical statistical simulation method where statistical simulation is defined in terms of utilizing sequences of random numbers to perform a simulation. It may include the distribution functions as exponential, Gaussian, Bivariate, lognormal, etc. In this work, the Monte Carlo randomization procedure used to generate site-amplification distributions, and provide an estimate of the uncertainty, in terms of mean, median and standard deviation. These distributions were assumed to be lognormal in form.

As mentioned previously, the amplification distributions were calculated based on a grid of 0.005˚, or, about every 500 m, as shown in Figure 3. There were total of 1,974 grid points encompassing the three study quadrangles. These grid points were divided into two groups to represent the major geologic variations thought to exist in the area. 10 ground-motion levels were coupled with three ground motion parameters (PGA, 0.2sec Sa and 1 sec Sa), and 100 calculations performed on each grid point to obtain an unbiased estimate of site amplification. This required 3000 calculations per grid point. When multiplied to the number of grid points, a total of 5,400,000 calculations were made on the three study quadrangles. Since it took approximately 10 minutes per grid point to make the necessary calculations, the grid points were divided into ten groups and these were run separately. The computations were made using the UMR NIC (Numerically Intensive Calculation) cluster, as well as a personal computer slaved to the computation process. The UMR NIC cluster computations were made on a Dell 1850 (3.2 GHz CPU Xeon EM64T with 2 GB RAM) and the personal computer computations were made on a Dell Precision 690 (Dual Core Intel Xeon EM64T with 2.33 GHz CPU).

The amplification distributions were generated separately for alluvium and loess deposits. The median site amplifications (solid lines) and the 16th and 84th percentile uncertainties (dotted lines) for loess and alluvium are presented in Figure 15 and Figure 16, respectively. These site amplification estimates show that loess and alluvium exhibit contrasting amplification characteristics for ten different ground motions and three ground motion parameters (PGA, 0.2 s

SA and 1.0 s SA). Site amplifications for the alluvial deposits at 1 sec spectral accelerations (SA) are larger than those predicted on loess covered sites. On the other hand, site amplifications estimated for the loess sites at 0.2 sec spectral accelerations and peak ground accelerations are higher than those on alluvial sites. If ground motions are sufficiently severe to trigger nonlinear behavior of the soil cap, then there may be greater nonlinear reduction in 0.2 s amplitudes on alluvium, as compared to loess. This is why the loess amplification estimates are higher than those on the alluvium at 0.2 s SA. At 1.0 s spectral acceleration, soil nonlinearity is much less effective, because a lower velocity profile in the alluvium results in greater site amplification.

At low ground motion levels (<0.05g), alluvium shows higher amplifications in peak ground acceleration (amplification between 3-3.5 times) and 1.0 sec spectral acceleration (amplification between 1.5 to 5 times). The difference between amplifications in loess and alluvium decrease with increasing ground motion levels (between 0.05-0.5g), and show similar amplification behavior. At ground motion levels higher than 0.5g, the alluvium starts to deamplify the input rock accelerations. However, loess does not exhibit deamplification, even at the highest ground motion levels (~1.0g), because it is so stiff.

The associated uncertainties in all these cases tends to increase with increasing ground motion level, and both the loess and alluvium exhibit a similar range of uncertainties. These amplification factors are summarized in Table 4. The differences in predicted site amplification between loess and alluvium tend to increase with increasing thickness of the respective units, between 10 and 30 m.

In addition to the site amplification distributions, the amplification factors were plotted for specific shaking levels (0.01, 0.05, 0.1, 0.2, 0.3, 0.4, 0.5, 0.6, 0.8, and 1.0) and these maps are presented in Figures 18 through 47. These figures suggest that as the shaking level increases, site amplifications decreases due to increasing non-linear behavior of the soil profile. At higher levels of shaking (> ~0.5 to 0.6g) alluvium exhibits a tendency towards deamplifying the ground motion. The largest amplifications in alluvium (up to 5 times) were noted at 1 second spectral accelerations, and this increases with the increasing unit thickness. Site amplifications were consistently greater in the alluvium (PGA, 0.2 sec SA and 1 sec SA) for the smallest ground motion levels, ~0.01g.

In Figure 17 site amplification was compared to the thickness of the geologic units for peak ground acceleration, 0.2 sec spectral acceleration, and 1 sec spectral acceleration for a

ground motion level of 0.01g. This plot suggests that the site amplification increases with the thickness of the low velocity soil cap, an expected result. The amplifications in peak ground acceleration (PGA) was found to be more or less constant when the cap thickness exceeds 30 m, for loess and alluvium. At 1 sec spectral accelerations the amplifications in loess and alluvium continues to increase with increasing thicknesses. The greatest increase in amplification (~400%) was noted in alluvium, when its thickness increases from 5 m to 55 m. At 0.2 sec spectral accelerations, however, there does not appear to be any linear relation between site amplification and unit thickness, with a very asymmetrical distribution.

4. SEISMIC HAZARD ANALYSIS

4.1. INTRODUCTION

The primary earthquake hazard is the impact of ground shaking, usually engendered by slow-moving shear waves. Shaking-hazard maps can be combined with building fragility data to estimate expected earthquake damage in an urban area characterized by a particular dominant structure type, over a specified time interval. It is known that strong earthquakes are less frequent in the Central and Eastern United States when compared to similar magnitude quakes in California, which lies along a tectonically-active continental margin. This is why structural damage in the CEUS could be catastrophic in a powerful temblor, because most of the structures in the CEUS were not designed to withstand earthquake shaking.

The general concept of hazard analysis refers to the process of subdividing a region into sectors with similar behavior with respect to a given set of parameters (Roca et al., 2006). These parameters define the characteristics of ground shaking, such as: peak ground acceleration, peak ground velocity, peak ground displacement, spectral accelerations, intensity etc. Seismic Hazard Analysis (SHA) requires the interplay of information gleaned from an array of disciplines, including: seismology, geology, geophysics, geotechnical engineering, and statistics. Seismology is needed to help define the likely earthquake sources, their magnitude, recurrence frequency, and estimate the damping characteristics of seismic energy in a particular region. These parameters are used to evaluate critical factors, such as “where”, “how big”, “how often”, “when”, and “how likely” future earthquakes might be in any given area. Duration is usually governed by the style of rupture (e.g. uniaxial versus bi-modal rupture), depth of the hypocenter,

dip of the rupture surface, and areal extent of any offset, along the fault(s). Geology is necessary to define the regional tectonic setting, the location, size and spatial distribution (geometry) of the causative faults, their past and present rupture patterns, and physical properties (including hypocentral depth, rupture area, sense of initial motion, etc.). Geology also aids in understanding the subsurface geologic materials, their structure, and likely stress history. Geophysics is often used to help identify and characterize seismic sources not readily observed at the earth's surface, using methods such as seismic, electrical, and magnetic profiling. Geotechnical engineering is increasingly applied to estimate the local soil conditions and help define their potential impact on site response (ground motions) at the ground surface. Finally, statistical techniques are used to evaluate disparate information from the above-listed disciplines and present it with appropriate limitations and degree of confidence, so end users are properly appraised of range in expected results, resulting from an incomplete body of information (Reiter, 1990).

Seismic hazard assessments can be performed by applying either of two fundamentally different concepts: Probabilistic or Deterministic methods. There are significant differences between these approaches and each possesses its own advantages and disadvantages, which are described in Section 6.

The St. Louis Metro area is located between 200 km (closest) to 400 km (furthest) from two recognized intraplate seismic source zones (New Madrid and Wabash Valley). Damaging earthquakes can be expected to occur less frequently in these intraplate source zones, when compared to seismic zones along plate boundaries, such as the Circum-Pacific "ring of fire." Even though the frequency of damaging earthquakes is less in the CEUS, there is a high risk of damage and significant consequences because the regional infrastructure has not been designed to resist earthquake ground motions. St. Louis is a densely populated urban zone with 2,801,033 people (US Census Bureau, 2007). The city is located just downstream of the confluence of the Mississippi and Missouri Rivers, and bounded by extensive deposits of unconsolidated sediment (mostly sands) underlying well-defined flood plains and wind blown loess covering the adjacent uplands. These deposits may cause differential site response due to differing site conditions. One goal of this study was to examine the differences in predicted site response, the hazard potential, and the expected range of accelerations.

The hazard calculations were made using both probabilistic and deterministic approaches. The following maps were created for each of the three study quadrangles (Granite City, Monks

Mound, and Columbia Bottom):

1. 2% probability of exceedance in 50 years in terms of PGA;
2. 5% probability of exceedance in 50 years in terms of PGA;
3. 10% probability of exceedance in 50 years in terms of PGA;
4. 2% probability of exceedance in 50 years in terms of 0.2 sec SA;
5. 5% probability of exceedance in 50 years in terms of 0.2 sec SA;
6. 10% probability of exceedance in 50 years in terms of 0.2 sec SA;
7. 2% probability of exceedance in 50 years in terms of 1.0 sec SA;
8. 5% probability of exceedance in 50 years in terms of 1.0 sec SA;
9. 10% probability of exceedance in 50 years in terms of 1.0 sec SA;
10. Two scenario earthquakes (M 7.7 and M 7.0) and their associated PGAs and 0.2 sec-SA and 1 sec-SA.

The hazard maps were constructed by choosing a frequency of exceedance, and then finding the value of ground motion at that frequency of exceedance from the hazard curve at each grid location and, then, contouring the resulting values (Frankel et al., 1999). These maps correspond to return periods of approximately 500 (10% probability), 1000 (5% probability), and 2500 (2% probability) years. A probability of exceedance of 10% in 50 years corresponds to an annual frequency of exceedance of 2.1×10^{-3}, 5% in 50 years corresponds to 1.03×10^{-3}, and 2% in 50 years corresponds to 4.04×10^{-4}.

In summary, 15 seismic hazard maps were developed for each of the three pilot 1:24,000 scale quadrangles, encompassing a land area of about 460 km^2.

ATTENUATION RELATIONSHIPS

As mentioned in the previous section as stress waves travel away from the source of an earthquake, they spread out and are partially absorbed by the material they travel through causing the energy and consequently amplitude of the wave to decrease. The amount of energy released in an earthquake and its amplitude is strongly related to the magnitude of the earthquake causing variations in wave characteristics such as amplitude, frequency content, and duration.

The relationships that identify these characteristics with a given magnitude and distance are known as the attenuation relationships.

In this study, like the national maps and the Memphis maps, five CEUS ground-motion relationships were employed:

1. Atkinson and Boore (1995)
2. Frankel et al. (1996)
3. Toro et al. (1997)
4. Campbell (2003)
5. Somerville et al. (2001)

The comparisons of these relationships for M5.5, 6.5 and 7.5 earthquakes for PGA and 1 sec SA are given in Figure 48. Like the national and Memphis maps, all five relations are used for the largest New Madrid earthquakes (weighted 0.25, 0.25, 0.25, 0.125, and 0.125 respectively) and only the first four relations are used for the smaller magnitude earthquake events (weighted 0.286, 0.286, 0.286, and 0.143 respectively). The Somerville et al. (2001) relation is a finite fault relation and is not applicable to earthquakes below M6.0 (Cramer et al., 2004).

These relations and weighs assigned to them are expected to change in the near future (Cramer, 2007), therefore as for the national maps, the products of this research may have to be recalculated and updated to follow of the new recommendations.

4.3. METHODOLOGY

The probabilistic and deterministic seismic hazard maps prepared as part of this study include the effects of surficial geology on site response. These maps were generated by incorporating the codes hazFXv3.f, hazDXv3.f, hazgridXv3 and hazsum. The early versions of these codes were used in the generation of the USGS national seismic hazard maps and were prepared by Art Frankel (2000) of the USGS. These codes were modified by Chris Cramer when he was with the USGS Center for Earthquake Research and Information (CERI) at Memphis (He is now on the faculty at the University of Memphis). These codes account for the fully-probabilistic approach in developing the probabilistic maps and apply median of site

amplification estimates to the hard-rock ground motion attenuation relations in the deterministic maps.

All of the seismic hazards were calculated based on a grid of 0.005˚, or about every 500 m, the same spacing employed in the amplification distribution calculations. For every grid point the site amplifications and distributions were calculated first, then the hazard codes were run to generate the respective hazard values. The amplification distributions were generated for two distinct geologic units (floodplain deposits and upland deposits), and 500 m was felt to be an appropriate spacing to capture the differences between these two units. The hazard values were then smoothed in GIS and drawn as smooth color contours.

The probabilistic hazard maps were generated applying the fully-probabilistic approach of Cramer (2001, 2003, 2005a, 2005b, 2006b) and Cramer et al. (2004). Cramer (2003) noted that if the probabilistic ground motions are calculated from a single value median site-specific amplification factor, this implies that there are no uncertainties associated with the amplification. However, it is widely appreciated that the amplification calculations will have uncertainties, due to variations in the soil parameters, as well as earthquake parameters. When this amplification is applied, the calculated probabilistic ground motions are no longer truly probabilistic. One way to solve this problem is to estimate the site amplification distributions with associated uncertainties and use this information to modify the bedrock ground motion attenuation relations prior to the seismic hazard calculation (Cramer, 2003; 2005a). The uncertainties in site amplification distributions are accounted by randomly selecting the input parameters. In this application the site-amplification distribution is assumed to be lognormally distributed with a median value and a logarithmic standard deviation. The site amplification distribution for a ground motion with soil condition (A_s) given an input ground motion on bedrock (A_r) is described as (Cramer, 2003),

$$P(sa) = P\left(A_s \middle| A_r\right) \qquad \text{Eq. 7.9}$$

Where P(sa) is the site amplification distribution. This distribution is used in the cumulative probability density distribution of A_s for given A_r as,

$$P\left(A_s \le A_o \middle| A_r\right) = \int_{A_s:-\infty \to A_o} P\left(A_s = A \middle| A_r\right) dA \qquad \text{Eq. 7.10}$$

Where A is a ground motion parameter expressed either in peak ground acceleration or spectral acceleration, and A_o is the ground motion level to be exceeded (Cramer, 2005b). Cramer (2003) noted the ease and accuracy of using cumulative density distribution in Eq. 7.10 instead of probabilistic density distribution. The problem is solved for a particular motion exceeding a ground motion level, hence the Eq 7.10 becomes (Cramer, 2005b),

$$P(A_s > A_o | M, R) = 1 - \int_{A_r} P(A_s \leq A_o | A_r) P(A_r | M, R) dA_r \qquad \text{Eq. 7.11}$$

This method was applied to the Memphis maps (Cramer et al., 2004) as well as to the entire Mississippi embayment (Cramer, 2002; Cramer, 2006b; Cramer, 2006c) including the areas around St. Louis. Cramer (2003) compared the fully probabilistic approach with the hybrid (which considers median value of the site amplification). His results indicated higher PGA estimations than the hybrid at high ground motion levels, however at low ground motion levels the difference was negligible suggesting the importance of using the entire site-amplification distribution, particularly for larger ground motions (>0.5g).

The St. Louis probabilistic hazard maps in this work are generated by combining the modified national seismic hazard model of Frankel et al. (2002) and the fully probabilistic approach of Cramer (2003). This model included the effect of the surficial geology on site response. It should be noted however that these maps are not sufficiently detailed to capture all the local variations in geology and, hence, are not intended to be site-specific. They can be used to assess the possible effect of geology on the ground motion parameters.

Deterministic analyses were performed for two scenario earthquakes for PGA, 0.2 sec Sa and 1 sec Sa. The median site amplifications were used in the deterministic hazard calculation with the same attenuation relationships and weights used in the USGS national maps. The first scenario earthquake we evaluated was a M 7.7 event occurring on the southwesterly limb of the New Madrid Seismic Zone, about 200 km south of St. Louis. The second scenario earthquake was a M 7.0 event occurring at Marked Tree, Arkansas, at the southwestern limits of the New Madrid Seismic Zone, about 400 km south of St. Louis.

4.4 RESULTS AND DISCUSSIONS REGARDING THE HAZARD MAPS

Probabilistic seismic hazard maps for St. Louis were generated for return periods of approximately 500 (10% probability), 1000 (5% probability) and 2500 (2% probability) years for PGA, 0.2 sec Sa and 1 sec Sa ground motion parameters. The hazard calculations were made for 1,974 grid points spaced 500 m apart. The results were smoothed by averaging each of the neighboring points. These maps then were compared to the previous studies, which encompassed the entire region surrounding St. Louis. The hazard maps of this study were superimposed on the 2002 USGS national and Cramer (2006c) seismic hazard maps, for the same ground motion level to better understand the effect of modeling the actual soil cap on the ground motion parameters. Note that the USGS hazard maps do not include the effects of local geology. Cramer (2006c) incorporated the effects of site geology with the associated uncertainties. However, the calculations were performed at 0.2 degree intervals, much coarser than the USGS national maps.

The hazard maps presented from Figure 49 through Figure 66 clearly show that loess and alluvium exhibit different ground motion shaking characteristics for each of the ground motion parameters (PGA, 0.2 sec Sa and 1 sec Sa) that were considered. The amplification results suggested that amplifications in loess were highest for 0.2 sec spectral accelerations and lowest for alluvium. The hazard analyses reveal the same conclusion where the highest accelerations are experienced by loess at 0.2 sec spectral acceleration.

2% probability of exceedance in 50 years maps for various parameters are compared in Figures 49, 50 and 51. At 0.2 sec Sa, loess covered uplands exhibit higher accelerations than floodplain deposits. On the other hand, higher spectral accelerations are observed in alluvial deposits at 1 sec Sa, where it is at least 300% higher than in the loess covered uplands.

10% probability of exceedance in 50 years maps for various parameters are compared in Figures 52, 53, and 54. The hazard analyses of 10%-in-50 years revealed the same results as the 2%-in-50 for the 0.2 sec Sa where the highest accelerations again are experienced by loess (around 100% higher than alluvium). The difference in site response for different geologic units and geographic locations is higher for 2% in 50 years maps, as compared to 10% in 50 year maps. The results also suggest that the peak ground accelerations are less than 50% for alluvium and loess units for all probabilistic levels. Similar results were gathered for the 5% probability of exceedance in 50 years maps, as shown in Figures 55, 56, and 57.

When compared to the USGS National Maps, the probabilistic hazard levels calculated in this study for alluvium exhibit zero to 200 % greater ground motion levels for PGA, and, between 20 % smaller to 150 % greater, ground motion levels for 0.2 sec Sa; and, 100 to 260 % greater ground motion levels for 1 sec Sa. The probabilistic hazard levels calculated in this study in loess covered uplands exhibit zero to 300 % greater ground motion levels for PGA, 200 % to 250 % greater ground motion levels for 0.2 sec Sa and, zero to 175 % greater ground motion levels for 1 sec Sa.

The results are also compared to the Cramer (2006c) study. These comparisons indicate similar ground motion levels of PGA: 150% smaller ground motion levels for 0.2 sec Sa, and 300% greater ground motion levels for 1 sec Sa as shown in Figures 58, 59, and 60.

The probabilistic results of this study were also compared to Toro and Silva (2001) for 1 sec Sa and PGA for different levels of probabilities as well (see Figure 67). Similar ground motion levels are observed for peak ground acceleration, however, 10 to more than 100% higher ground motion levels were estimated by this study for 1 sec Sa.

The deterministic hazard maps are shown from Figure 61 through Figure 66. The results of the deterministic scenarios suggest that the hazard levels for 0.2 sec Sa in loess are approximately 15% higher than for alluvium. The alluvial sites exhibited consistently higher acceleration levels at 1 sec Sa, similar to the probabilistic maps.

The significant variations in predicted ground motions appear to be ascribable to the more detailed (500 m spacings) characterization of the actual variations in geologic conditions, especially, near the boundaries between loess and alluvial deposits.

Table 6 summarizes the ground motion levels for alluvium and loess for 2%, 5% and 10% probability of exceedance for all three periods (PGA, 0.2 sec Sa, and 1.0 sec Sa) and scenario earthquakes. Results indicate that the response (spectral acceleration value) differences can be attributed to i) the type of surficial material, and ii) the period of interest. In alluvium, 0.2 sec Sa values are usually higher than 1 sec Sa values. In loess, however, 0.2 sec Sa values are always higher than the 1 sec Sa values. When compared with each other, loess deposits seem to be experiencing more acceleration force than alluvium at 0.2 sec Sa period. On the other hand, alluvium deposits seem to be experiencing more accelerations force than loess at 1 sec Sa period. These observations suggest that 0.2 sec period structures situated on loess may experience larger acceleration forces than the same structures situated on alluvium. The same conclusion can be

reached for 1 sec period structures situated on alluvium where the earthquake acceleration forces may be more severe than the same structure situated on loess. It still should be noted that one other major factor affecting the response of the deposits is the variations in thickness and these arguments can only be correct locally and not in all situations.

5. UNCERTAINTY ANALYSIS

5.1. INTRODUCTION

All the civil engineering structures must be planned, designed and constructed to withstand the man-made or natural hazards. In this process, however, uncertainties play a major role, and they effect the decision on the design and planning. Two sources of uncertainties may be recognized: 1) those that are associated with natural randomness called aleatory; and 2) those that are present due to lack of knowledge and interpretation known as epistemic (Ang and Tang, 2007). The aleatory uncertainty is a result of variability in the parameters, heterogeneity of the phenomenon, and randomness and may not be reduced by more or better data. The epistemic uncertainty however is a result of imperfect models, insufficient knowledge of reality which may be reduced by the acquisition of more data or improvements in data acquisition and interpretation (Romero and Rix, 2005). The inevitable consequence of these uncertainties is risk that the engineering system will perform which involves probability and associated consequences.

In dealing with earthquake related problems, uncertainties are unavoidable. One main reason for that is that damage causing large earthquakes are rare events and their occurrence in the future is not known, even though there are physical models that describes them. It is a problem of when, how and where they expect to occur. Another reason is due to heterogeneities in the crustal properties, and how the wave will propagate and how it will attenuate. One last reason is how it will affect the site under consideration, and how the site properties change.

The probabilistic and deterministic maps have uncertainties associated with them on the order of 50% (Cramer, 2001). These uncertainties result due to the insufficient knowledge on the location of the large ruptures, in the choice of ground motion attenuation relations, and in the magnitude of the New Madrid characteristic earthquakes. In particular, since probabilistic and deterministic maps are results of the site amplifications, the controlling factors on site amplification and the degree of effect on the results are discussed in this section.

As mentioned in the previous sections, the uncertainties are present in the site-amplification because of; the variations in the shear-wave velocity, the variations in the density values, the estimation technique of the depth to the soil layers, and the differences in the time-histories. These uncertainties may cause large differences in amplification calculations when combined. To account for these variability and uncertainties randomly sampling method was applied where the input soil properties were selected from range of time-histories, soil boundaries, shear-wave velocity values, and dynamic soil properties and finally estimating a site-amplification. The Monte Carlo randomization technique was applied in the analysis where it also provided an estimate of uncertainty in the calculations.

The uncertainty of the above mentioned parameters are examined first by selecting a specific parameter to be investigated; and second by fixing all other parameters and limiting the Monte Carlo choices. This way, the sensitivity of a specific parameter on the site response was investigated. This section discusses the results of sensitivity analyses conducted for selected input parameters on site amplification results and compares the results for PGA, 0.2 sec Sa and 1 sec Sa.

5.2. SENSITIVITY TO INPUT TIME HISTORY

The amount of amplification depends on the amplitude and frequency of the input ground motions due to its nonlinear nature (Cramer at al., 2004). The soil properties are important in calculating site amplifications, but the amount energy propagating through the soil column also governs the behavior. The smaller amplitude waves will likely cause higher amplifications and smaller amplitude waves will cause smaller amplifications due to the nonlinear characteristics of the soil profile. In this study 12 recordings from 6 real earthquake ground motions were selected to capture the true complexity of the earthquake-time histories. In addition to these earthquake recordings, two synthetically generated M7.5 and M8.0 records from Atkinson and Beresnev (2002), and M7.0 and M7.5 records using the SMSIM v. 2.2 code of Boore (2003) were selected. The properties of these time-histories were shown in 2.

In Figures 4 thru 7, the time-history plots were provided. These plots show the differences in peak accelerations as well as shape and frequency content of the ground motion. Compared to the synthetic ground motions, the actual records from earthquakes have more realistic phase relations (Cramer et al., 2004). The synthetic ground motions are more

homogeneous in nature; however, they can be more representative of CEUS source characteristics and attenuation/damping properties. There is no doubt that the seismic waves can travel longer distances in CEUS than WUS because of the smaller crustal dampings allowing crustal earthquake stress waves to spread laterally over very large areas.

Differences in the above mentioned time-histories cause variations in site amplifications. These effects can be seen in Figure 68 where all eight time-histories are plotted and compared for a ground motion parameter of interest (PGA, 0.2 sec Sa and 1 sec Sa) for a 30 meter assumed soil profile. Figure 68 shows that site amplification results estimated in this study are most sensitive to the selected input time histories. The differences in site amplifications can be up to 90% at small ground motion levels. The differences decrease as the ground motion level increase until 0.2g especially for PGA and 0.2 sec spectral acceleration. The differences in amplifications increase again at higher ground motion levels (~0.2g). These results suggest that for small ground motions (less than ~0.1g) and for very high ground motions (higher than 0.4g) PGA and 0.2 sec spectral acceleration shows greater sensitivity to the choice of input time series than 1.0 sec spectral acceleration. Even though the synthetic time histories show higher peak accelerations up to 17 times, their estimated amplification distributions do not deviate more than 50%, except Chi Chi earthquake. Chi Chi earthquake deviates from the rest of the recordings in all amplification distributions especially in PGA and 0.2 sec Sa.

5.3. SENSITIVITY TO SURFICIAL GEOLOGY THICKNESS

Top of bedrock elevations were determined using the kriging method as explained previously. The primary advantages of the kriging method are its ability to: 1) interpolate an actual value at measured data point and 2) to provide krigged estimates and the corresponding uncertainties at unmeasured sites. The surficial materials thickness maps were spatially calculated by subtracting the predicted top of bedrock elevations from the digital elevation model. Since the digital elevation model is expected yield smaller uncertainties, the uncertainties from the estimation of top-of-bedrock were used in the analysis. These uncertainties range from 1.8 meters to 18.4 meters depending on the location. The highest error or uncertainties correspond to the areas where there is little or no sample data.

Sensitivity analysis is performed to identify the differences in site amplification due to the variations in soil thickness (15m, 30 m and 45 m) and the results are plotted in Figure 69. At

0.2 sec and 1 sec spectral accelerations, the difference in site response is highest at low ground motion levels up to 60% when the maximum error (~18 meters) is considered. At PGA, however, the difference is much lower (<20%) for the highest level of error. These results indicate that the uncertainties in the soil thicknesses are most sensitive to the spectral accelerations (0.2 sec and 1 sec) and are less sensitive to the peak ground acceleration. Clearly site amplifications and associated uncertainties are very sensitive to the variations in the soil thickness.

The plots in Figure 69 also compare site amplifications for the weathered rock horizon, shear wave velocity and corresponding soil cap thickness. The difference between the site amplifications with and without weathered rock is very small in all cases. In this case it appears that additional thickness of the weathered rock unit has negligible additional effect on the site response and amplification.

5.4. SENSITIVITY TO SHEAR WAVE VELOCITY AND THICKNESS OF THE WEATHERED BEDROCK

As mentioned earlier, three different glacial/weathering stages have impacted the study area over the past ~450 ka, leaving a distinctive mark on the weathering profile. The weathered horizons can be subdivided into three major groups,

1) the western part of the Mississippi River flood plain, which includes loess covered uplands in the Granite City and Columbia Bottom quadrangles;

2) the Mississippi River flood plain, which is filled with alluvial deposits, and

3) the loess covered uplands east of the Mississippi River, which are underlain by re-worked glacial outwash dating back to ~450 ka. This third area includes the uplands along the eastern fringes of the Monks Mound quadrangle.

The only glacial epoch which appears to have encroached the western fringes of the Mississippi River flood plain was during Illinoian time. The geotechnical borings in this area usually encounter a weathered bedrock horizon that is between 1 to 2 m thick. For these reasons, a weathered zone 2 m thick was assumed to exist beneath the loess covered uplands west of the Mississippi River for this study.

The thickest sequence of weathered material corresponds with the oldest surficial deposits, the re-worked glacial outwash lying beneath the uplands east of the modern Mississippi River flood plain, which date back to pre-Illinoian time (~450 ka). In this terrain, geotechnical

borings suggests that the weathered zone commonly reaches a thickness averaging about ~20 m. We selected 20 m as being a representative thickness to describe the weathered horizon in the uplands on the Illinois side of the Mississippi River flood plain.

Borings in the modern Mississippi River flood plain that pierce the bedrock basement exhibited no discernable zone of weathering. It has been concluded during the Pleistocene-Holocene epoch transition (~11 ka), the intense erosive cycle likely removed the weathered rock horizon. In this study we have, therefore, assumed zero thickness for the weathered rock horizon beneath the alluvial valleys of the major water courses, along the floodplain of the Mississippi and Missouri Rivers.

Williams et al. (2007) velocity estimates which were based on the reflection/refraction method, varies between 1250 to 3750 m/sec with an error estimate of ~800 m/sec. An average value of 1750 m/sec with a standard deviation of 250 m/s was applied to describe the shear wave velocity for the weathered rock horizon in site amplification analyses, since most of the measured shear wave velocities fall in the range of 1500-2000 m/sec. However, it is evident from the range of velocity measurements that there are large uncertainties associated with the weathered rock properties. Sensitivity analyses were performed for weathered rock horizon to estimate the effect of thickness and shear wave velocity on site amplification.

Full soil response uncertainty sensitivity tests were conducted using an alternative 15 m, 30 m and 45 m soil profile over weathered rock thicknesses of 10, 30, and 50 m with 1000 m/sec, 1500 m/sec and 2000 m/sec shear wave velocities for ground motion parameters, and are shown in Figures 70 thru 72. The results suggest that the differences between the amplifications of three alternative weathered layer thicknesses with three alternative shear wave velocities are highest for the small ground motion levels and this difference decrease for increasing ground motion levels. In particular, at small ground motion levels the differences are highest at PGA and 0.2 Sa, however it is smallest at 1 sec Sa. Clearly there are slight differences in the site amplification especially for small ground motion parameters for small shaking levels. Still, in these plots one would expect to see larger variations with thicker and slower weathered rock layer. However, soil response distributions (median and plus and minus standard deviations) for PGA, 0.2 s, and 1.0 s ground motions were negligibly different (essentially the same) for these three alternative weathered rock thicknesses.

The above mentioned results are also consistent with Cramer (2007) results where he plotted the response spectrum of the input record (an Atkinson and Beresnev, 2002 synthetic record representing a M8.0 in the NMSZ as recorded on hard rock in the St. Louis area) and nine alternative response spectra covering the above weathering layer thickness and shear velocity alternatives for each overall soil thickness of 5, 10, 20, and 30 m. As shown in Figure 73, the more significant variation in soil response among the alternatives is in the period band less than 0.2 s. The thicker the weathered rock layer and the slower the weathered rock velocity, the larger the variation, as one would expect. However, the variations are small to negligible at the periods of interest for the seismic hazard analysis (pga, 0.2 s, and 1.0 s usually) even at 0.1 s period (Cramer, 2007).

5.5. SENSITIVITY TO MODEL CHOICE

This study didn't perform any sensitivity analysis on the choice of the software; however, previous investigations provided convincing results that the choice of the type of analysis software is one of the most important factor affecting the predicted site-amplifications. Cramer (2006c) evaluated several computer codes for calculating the site-amplification calculations including SHAKE91, TREMORKA and DEEPSOIL v.2.5. TREMORKA is an equivalent linear implementation using the frequency dependent damping approach and uses modulus and damping curves as a function of strain. DEEPSOIL is a finite element code and uses a hyperbolic model representation for dynamic soil properties. The details on these codes are given elsewhere (Kausel and Assimaki, 2002; Park and Hashash, 2001). Cramer (2006c) plotted the 5% damped elastic response spectra for the same 0.1g and 0.5g PGA input time series as shown in Figure 74. According to this plot, Cramer (2006c) identified higher response spectra at higher frequencies for TREMORKA on the order of 30%. Cramer et al. (2004) and Cramer (2006c) identified less than 50% difference between the codes for 0.1g input and much higher differences for 0.5g. Their results suggest that the uncertainties of the use of a soil-response program may cause differences in site-amplification in the range of 20-50% which will eventually affect the hazard estimates.

The above mentioned codes resemble each other in that they all are equivalent linear codes. There is however the possible effects of the pore water pressure increase on the estimated site response which can be handled only using a nonlinear model. The estimated site response

can be higher or lower that is liquefaction caused by the pore pressure built up may amplify or deamplify the incoming accelerations. A decrease in site-response is identified at short period (<1 sec) spectral accelerations and an increase is identified at long period (>1 sec) spectral acceleration values (Youd and Carter 2005; Zorapapel and Vucetic 1994). This study did not consider the possible effects of the pore pressure built up in the amplification analysis and in the hazard estimates.

5.6. DISCUSSION

As mentioned earlier, in dealing with earthquake related problems, uncertainties are unavoidable. These uncertainties will cause either higher values or lower values than predicted and must be taken into account before making any kind of smart engineering decision. Some of these uncertainties result due to insufficient knowledge on the earthquake source and attenuation, and some result due to randomness and knowledge on the range of values. A full range of sensitivity analyses were performed part of this study to understand the most sensitive parameters that effect the amplification the most. The analysis also included to understand how much specific ground motion parameters (PGA, 0.2 sec Sa and 1 sec Sa) were effected. Some of the results are summarized in the following paragraphs.

The results on the input time histories indicate that the greater sensitivity on the amplification can come from the selected input time histories. It appears that for small ground motions (less than ~0.1g) and for very high ground motions (higher than 0.4g) PGA and 0.2 sec spectral acceleration shows greater sensitivity to the choice of input time series than 1.0 sec spectral acceleration. The results also indicated that the choice of input time history whether it is an actual record or a synthetic record does not cause a clear difference in the amplifications even though the synthetic time histories show higher peak accelerations up to 17 times.

The sensitivity analysis on the variations of soil thickness indicate that the uncertainties in the soil thicknesses are most sensitive to the spectral accelerations (0.2 sec and 1 sec) and are less sensitive to the peak ground acceleration. The difference in amplification can be up to 60% for the spectral acceleration range and less than 20% for the peak acceleration indicating the importance of the accurately determining the surficial materials thicknesses.

Sensitivity analysis on the thickness of the weathered rock layer and its shear wave velocity value show that sensitivity is highest at the small ground motion levels for small periods

of interest, PGA and 0.2 Sa. The thicker the weathered rock layer and the slower the weathered rock velocity, the larger the variation, one would expect. However, the sensitivity analysis revealed that the variations in amplification due to weathered rock layer variations are small to negligible at the periods of interest for the seismic hazard analysis, PGA 0.2 s, and 1.0 s (Cramer, 2007).

The choice of the site-response program can have up to 20-50% difference in the hazard calculations being higher for high ground motion levels. Cramer (2006c) stated that if this uncertainty incorporated into site-amplification logic tree, the site amplification variability would be increased; increasing the site-specific probabilistic hazard values especially at low probabilities of exceedance. The type of the program whether it is an equivalent linear or a nonlinear may also cause large differences in the site response mainly due to the generation of high pore pressures and liquefaction phenomena.

6. DISCUSSIONS AND CONCLUSIONS

6.1. DISCUSSIONS

Considerable uncertainties exist due to natural variations in the selected parameters and the paucity of information about seismicity in the Central and Eastern United States. Unfortunately, these uncertainties are unavoidable and, when combined, they may cause large differences in amplification calculations and hazard estimates. The uncertainties associated with the amplification calculations were taken into account by creating site-amplification distributions through a process called the randomly sampling method, where the input soil parameters are selected randomly from a range of soil boundaries, shear-wave velocity values, and dynamic soil properties and input bedrock motions from a suite of acceleration time-histories. The uncertainties associated with the hazard calculations were taken into account by applying the probabilistic calculations.

A major concern of this study is the appropriateness of the seismic hazard calculations for use in the existing building codes; including decisions about which level of exposure (probability of exceedance) should be employed and how they should be applied. This is a controversial topic among scientists and engineers because both approaches have intrinsic advantages and disadvantages associated with them. Reiter (1990) pointed out that the issue is not “whether,” but rather “to what extent” a particular approach should be used.

The most favorable aspect of the deterministic approach is the relative ease by which the assessment can be carried out, as compared with fully probabilistic methods. The deterministic assessment is easy to apply and the results have "physical" implications that are easy to digest. In calculating the deterministic hazard, one should know/estimate the maximum magnitude a fault can produce. However, this approach does not take into account the uncertainties originating from the maximum magnitude estimations and may lead to conservative input parameters and, hence, additional economic overburden. The major drawback of a deterministic approach is that it does not consider the frequency of occurrence (Reiter, 1990). This might lead to inconsistent levels of acceptable risk, because faults seldom rupture along their entire length, which is usually assumed in such assessments. The deterministic approach provides a "scenario" event that can be used to identify potentially troublesome areas, however, it requires large number of scenario earthquakes to understand the aggregate effects of a possible earthquake.

The probabilistic approach takes uncertainties into account in terms of frequency of occurrence of earthquakes, distance to source, and earthquake magnitude. The inclusion of these variables is generally perceived as the most acceptable approach, if such data exists. Experience has shown that earthquakes exhibit a lot of variability, depending on a range of physical factors, so any meaningful assessment will be accompanied by no small measure of uncertainties. Experience and judgment will continue to loom large in assessing both the reliability of, and viability of employing, such hazard assessments. Reiter (1990) defined this disadvantage as "loss of transparency," which he defined as the ability to look at a hazard analysis and understand which factors exert the greatest influence on the calculated hazard. The hazard analyses presented in the previous sections are described as a level of expectancy for a given time interval. This level of expectancy does not have any indication on how close the source is or what size the magnitude of the earthquake is. Knowing these factors could be important to the engineer, because the duration and spectral levels will be different for earthquakes of varying magnitude even if similar peak accelerations are predicted. Another disadvantage of probabilistic approaches are how they handle statistical information. The assumed model (Gaussian or lognormal) and the resulting mean, median, and average estimates can deviate from one another and no small measure of "scientific/engineering judgment" is required to select an "appropriate" model and the most realistic mean/median/average values. Another nagging problem with probabilistic analyses is that many people have difficulty understanding the results, because they

have no "physical meaning", in of themselves, standing alone (Wang et al., 2003; Wang, 2005a; Wang 2005b). Probabilistic assessments are only as reliable as the data input into them. Since actual paleoseismic data only exist for a handful of high-visibility faults which broach the land surface, a great dealing of "guesswork" is necessary to realistically account for "lower visibility" seismic sources, such as those emanating from small faults, buried faults, blind thrusts, and distant sources, which should be included in any assessment (Holzer, 2005; Musson, 2005).

6.2. CONCLUSIONS

The following conclusions have been reached for the preliminary estimations of site amplification and the associated hazard estimations. These conclusions are subject to change or revision, as the new data, information, and observations become available.

1. Within the modern floodplains the alluvial thickness is fairly uniform, between 30 and 40 meters, thinning to as little as 5 meters at the lateral margins bounding the elevated uplands. The thickness of the soil cap in the loess covered uplands varies considerably between 5 and 73 meters.
2. The median shear-wave velocity of alluvium is calculated as 200 m/sec, and loess is calculated as 208 m/sec.
3. The variations in shear-wave velocity of Henry formation and Cahokia formations are very similar, despite their age difference suggesting the depth effect on Vs.
4. In order to represent the depth dependency in the Vs estimations, alluvium and loess units were divided into 5 meter depth increments. From 0 to 30 meters the shear wave velocities are estimated as 134, 180, 222, 250, 256, and 286 m/sec, and 179, 241, 325, 443, 481, and 539 m/sec, for alluvium and loess respectively.
5. The site amplification factors on response spectra depend on the input ground motion, and hence, the frequency of the input ground motion.
6. Natural variations and physical characteristics of the "soil cap" overlying the Paleozoic bedrock in the St. Louis area exerts a significant influence on the amplitude and frequency characteristics of the earthquake ground motions at the surface.

7. Alluvium and loess exhibit distinct amplification behaviors for small ground motion levels (<0.01g) for all ground motion parameters: PGA, 0.2 sec spectral acceleration and 1 sec spectral acceleration.
8. The differences in site amplification between alluvium and loess covered sites tends to decrease with increasing ground motion (up to 0.5g).
9. The alluvial profiles exhibited deamplification of ground motions when the rock accelerations exceed 0.5g. Loess did not exhibit deamplification at any input acceleration (between 0.01 and 1.0g).
10. The thickness of the "soil cap" (alluvium or loess, or both) exerts significant influence on site amplification.
11. The measured shear wave velocities in loess and alluvium appear to be a simple function of depth (confinement) and not their geologic age. This was a surprising, but consistent trend, over a wide area, which included channel fills along the lower Ohio River, and within the upper Mississippi Embayment.
12. Accurate estimates of the soil cap thickness (especially, for the alluvium) are essential to allow accurate predictions of site amplification, especially for 1 sec Sa. The greatest site amplification was observed in alluvium; which exhibited a 400% increase, from 5 m to 55 m thickness.
13. The thickness and shear wave velocity of the weathered bedrock horizon (below the soil cap) appears to have little impact on site amplification, or upon the associated uncertainties.
14. The two most important parameters affecting site amplification estimates were the input time histories and the thickness of the soil cap. Differences in soil thickness can cause up to 100 % error, if we assume the maximum uncertainty of ~18 meters.
15. Site-amplification uncertainties may range between 0-100%, depending on the choice of the necessary input parameters.
16. Loess and alluvium exhibit contrasting shaking characteristics for each of the ground motion parameters and EQ scenarios considered.
17. Loess is characterized by large accelerations at 0.2 sec period spectral acceleration for all levels of probability (at some locations up to > 30% greater than in the alluvium). This means, on upland sites underlain by loess, earthquake forces may be most severe for short

period structures (less than five stories high). However, there are still local areas in alluvium that may cause equivalent forces similar to that in loess.

18. Alluvium is characterized by large accelerations at 1 sec period spectral acceleration for all levels of probability. This means, in the natural flood plains underlain by alluvium, earthquake forces may also be severe for long period structures (greater than 10 stories). However, there are still local areas in loess that may cause equivalent forces similar to that in alluvium.
19. The peak ground accelerations are similar for alluvium and loess covered sites, for all probabilistic ground motion levels. In addition, 0.2 sec Sa values are always higher than 1 sec Sa values for loess covered sites and usually higher than 1 sec Sa values for alluvium covered sites.
20. When compared to the USGS National Maps, the probabilistic hazard levels calculated in this study for alluvium sites exhibit zero to 200 % greater ground motion levels for PGA, and between 20 % smaller to 150 % greater ground motion levels for 0.2 sec Sa; and, 100 to 260 % greater ground motion levels for 1 sec Sa.
21. When compared to the USGS National Maps, the probabilistic hazard levels calculated in this study for loess covered sites show zero to 300 % greater ground motion levels for PGA, 200 % to 250 % greater ground motion levels for 0.2 sec Sa and 0 to 175 % greater ground motion levels for 1 sec Sa.
22. When compared to Cramer's 2006c study, with similar ground motion levels of PGA: 150% smaller ground motion levels were estimated for 0.2 sec Sa and 300% greater ground motion levels for 1 sec Sa.
23. The results of the deterministic scenarios suggest that the hazard levels for 0.2 sec Sa in loess covered sites are approximately 15% higher than for alluvial sites. The alluvial sites exhibited consistently higher acceleration levels at 1 sec Sa, similar to the probabilistic maps.
24. The significant variations in predicted ground motions appear to be ascribable to the more detailed (500 meter spacing) characterization of the actual variations in geologic conditions, especially, in the transition zones between loess covered uplands and alluvial filled flood plains.

RECOMMENDATIONS FOR FUTURE WORK

1. Site amplification and seismic hazard depend on the estimated input parameters. Therefore, some of these parameters must be estimated more accurately, i.e., maps showing the predicted thickness of the soil cap.
2. The results suggest that the site amplification on alluvial sites is most influenced by unit thickness. This, points to the importance of borehole data in the alluvial filled flood plains, where few of the borings pierce the planated bedrock surface.
3. The depth to top-of-bedrock (soil cap thickness) map was prepared using kriging methods. There are inherent advantages and disadvantages associated with this methodology. The greater the density of data (surface topography, number and spacing between of borings, etc.), the more accurate the prediction (ignoring 3D effects). Some measure of care should be exercised when making estimations at the upland-floodplain boundary, where the respective units thicken, thin, and interfinger with one another.
4. The thickness and shear-wave velocity estimates of the weathered bedrock horizon are insufficient to ascertain if the selected values are within the acceptable range. However, sensitivity analyses eliminated this as a serious problem because the thickness of the weathered zone is non-existent to small (< 2 m) over most of the study area. In the loess covered uplands east of the Mississippi River flood plain the weathered rock zone increases to an assumed median value of ~20 m, beneath re-worked glacial outwash.
5. The hazard results are based on the 2002 USGS national map model. The USGS will be updating their models and the National Map sometime in 2008. New calculations will need to be performed to evaluate how these changes will compare with the estimates in this study.

Table 1. Selected earthquake recordings (M ~7.5) used in the response analysis

Recording	**Magnitude (M_w)**	**Distance (km)**	**Station**	**Components**
Atkinson and Bresnev (2002)	7.5 and 8.0	200	---	---
Boore's SMSIM v 2.3 (1996) and (2003)	7.0 and 7.5	200	---	---
Landers, CA Earthquake (1992)	7.3	194	VIR	200, 290
Kocaeli, Turkey Earthquake (1999)	7.4	210	BLK	0, 90
Duzce, Turkey Earthquake (1999)	7.2	184	KOER	90, 180
Chi-Chi, Taiwan Earthquake (1999)	7.6	184	KAU082	0, 270
Hector Mine, CA Earthquake (1999)	7.1	194	USGS0141	90, 360
Denali, AK Earthquake(2002)	7.9	196	TASP	39, 309

Table 2. Summary of the earthquake accelerations-time histories used in this study

Earthquake	**Station**	**Peak-acceleration (g)**	**Fourier amplitude spectrum (sec)**	**Mean period (sec)**
Landers, CA Earthquake (1992)	VIR 200	0.017	1.55	0.895
	VIR 290	0.011	1.79	1.115
Kocaeli, Turkey Earthquake (1999)	BLK 000	0.018	0.8	0.862
	BLK 090	0.018	3.23	1.134
Duzce, Turkey Earthquake (1999)	YKP 90	0.004	2.11	0.914
	YKP 180	0.005	1.69	1.214
Chi-Chi, Taiwan Earthquake (1999)	KAU 082-000	0.017	2.61	1.801
	KAU 082-270	0.019	1.71	1.569
Hector Mine, CA Earthquake (1999)	GP 90	0.016	0.79	0.594
	GP 360	0.018	1.08	0.752
Denali, AK Earthquake (2002)	TASP 39	0.016	---	0.698
	TASP 309	0.017	---	0.679
Atkinson and Bresnev (2002)	M 7.5	0.053	0.42	0.494
	M 8.0	0.070	2.29	0.669
Boore's SMSIM (1996) and (2003)	M 7.0	0.030	0.3	0.263
	M 7.5	0.043	0.53	0.257

Table 3. Shear wave velocity variations with associated uncertainties

Geologic unit	No. of Vs	Degrees of freedom	Normal Distribution			Lognormal Distribution			Median Vs (m/sec)	Average Lognor. Standard Deviation (m/sec)
			Total χ^2	Mean Vs (m/sec)	Standard deviation range of (Vs)	Total χ^2	Mean Vs (m/sec)	Standard deviation Range of (Vs)		
Alluvium										
0m-5m	76	7	9.4	139	105-173	3.1	135	107-172	134	33
5m-10m	56	6	1.7	180	149-210	2.5	177	148-212	180	32
10m-15m	45	7	4.9	218	184-251	6.1	215	183-252	222	34
15m-20m	27	8	17.5	262	209-316	12.6	257	212-312	250	50
20m-25m	25	8	8.8	274	221-327	5.3	269	224-324	256	50
25m-30m	21	6	10.5	295	241-348	8.7	290	242-348	286	53
Loess										
0m-5m	201	7	17.1	187	135-240	5.1	180	136-238	179	51
5m-10m	104	10	25.5	265	175-354	12.8	250	179-350	241	86
10m-15m	49	5	9.1	347	225-468	17.5	327	230-463	325	116
15m-20m	69	9	15.2	475	289-659	3.9	443	306-640	443	167
20m-25m	46	9	16.3	522	294-749	4.6	477	310-732	481	211
25m-30m	16	4	4.6	596	381-810	5.0	558	382-816	539	217

Table 4. The lithologic units, classification and their ages (Grimley et al., 2001; Grimley and Lepley, 2005; Smith and Smith, 1984).

Group	**Geologic Unit**	**USC Classification**	**Geologic age (C^{14} years B.P)**
Lowland	Cahokia Clay	CH, CL, MH, ML	Holocene (< 2,400)
	Cahokia Sand	SP to CH, ML	Holocene (8,500 – 2,400)
	Henry Formation	SP, GP, GW	Pleistocene (12,000 – 10,000)
Upland	Peoria and Roxana Formation	SP, CL	Pleistocene (55,000 - 12,000)
	Glacial Till	SP, GP, CH, ML	Pleistocene (190,000 - 130,000)

Table 5. Summary information of median (50th percentile) site-amplification factors for 10, 20, and 30 meter thick loess and alluvium profiles.

	Soil thickness (in meters)					
	Loess			**Alluvium**		
	10	**20**	**30**	**10**	**20**	**30**
Peak Ground Acceleration	2.63	2.78	3.03	2.68	3.00	3.27
0.2 sec spectral acceleration	3.83	3.24	2.92	3.25	2.70	3.86
1.0 sec spectral acceleration	1.12	1.18	1.33	1.18	1.45	1.90

Table 6. Mean, maximum, and minimum values of the estimated peak ground accelerations and spectral accelerations

		Alluvium			**Loess**		
Probability		PGA	0.2 sec SA	1.0 sec SA	PGA	0.2 sec SA	1.0 sec SA
2%	Max	0.383	0.783	0.524	0.547	0.965	0.345
	Min	0.267	0.407	0.132	0.245	0.422	0.131
	Mean	0.333	0.511	0.303	0.423	0.750	0.186
5%	Max	0.249	0.517	0.319	0.335	0.653	0.186
	Min	0.145	0.224	0.076	0.152	0.285	0.074
	Mean	0.217	0.354	0.171	0.260	0.491	0.100
10%	Max	0.175	0.369	0.199	0.219	0.458	0.105
	Min	0.09	0.136	0.045	0.099	0.179	0.044
	Mean	0.155	0.262	0.096	0.171	0.338	0.058
M 7.7	Max	0.146	0.305	0.233	0.174	0.392	0.124
	Min	0.07	0.121	0.051	0.057	0.113	0.052
	Mean	0.130	0.237	0.120	0.135	0.291	0.071
M 7.0	Max	0.051	0.113	0.078	0.05	0.139	0.038
	Min	0.019	0.033	0.016	0.016	0.034	0.017
	Mean	0.046	0.096	0.035	0.040	0.094	0.022

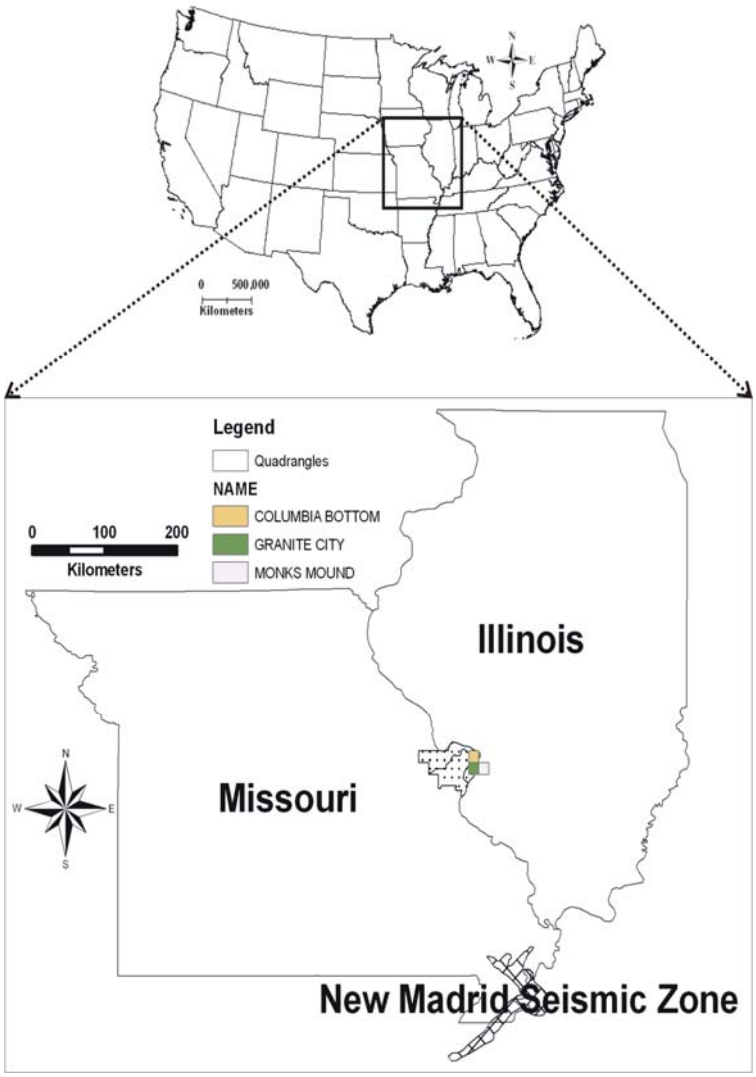

Figure 1. Map showing the location of the three quadrangles studied (Granite City, Monks Mound and Columbia Bottom).

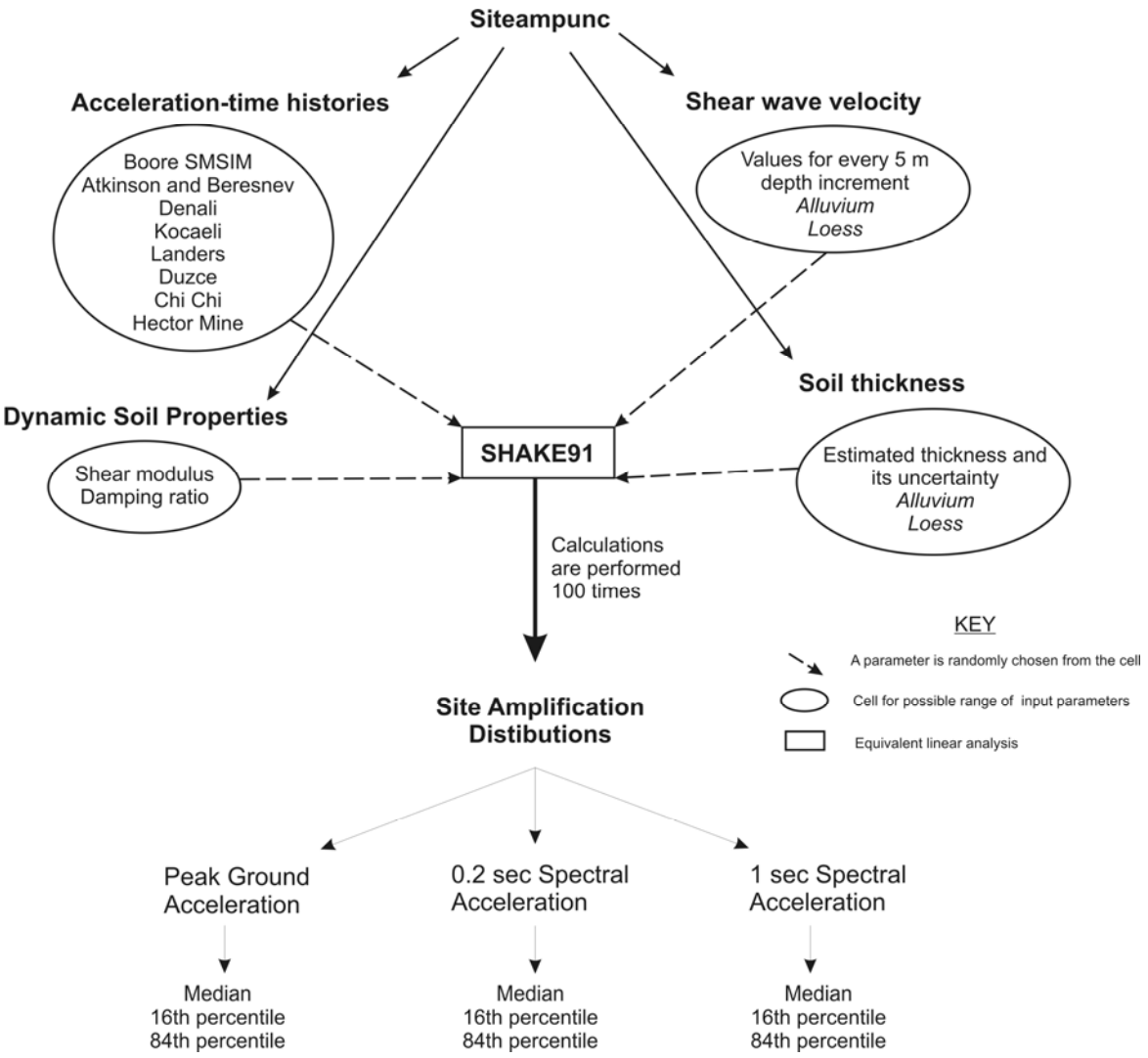

Figure 2. Flow chart showing the steps of the amplification calculations performed in this study.

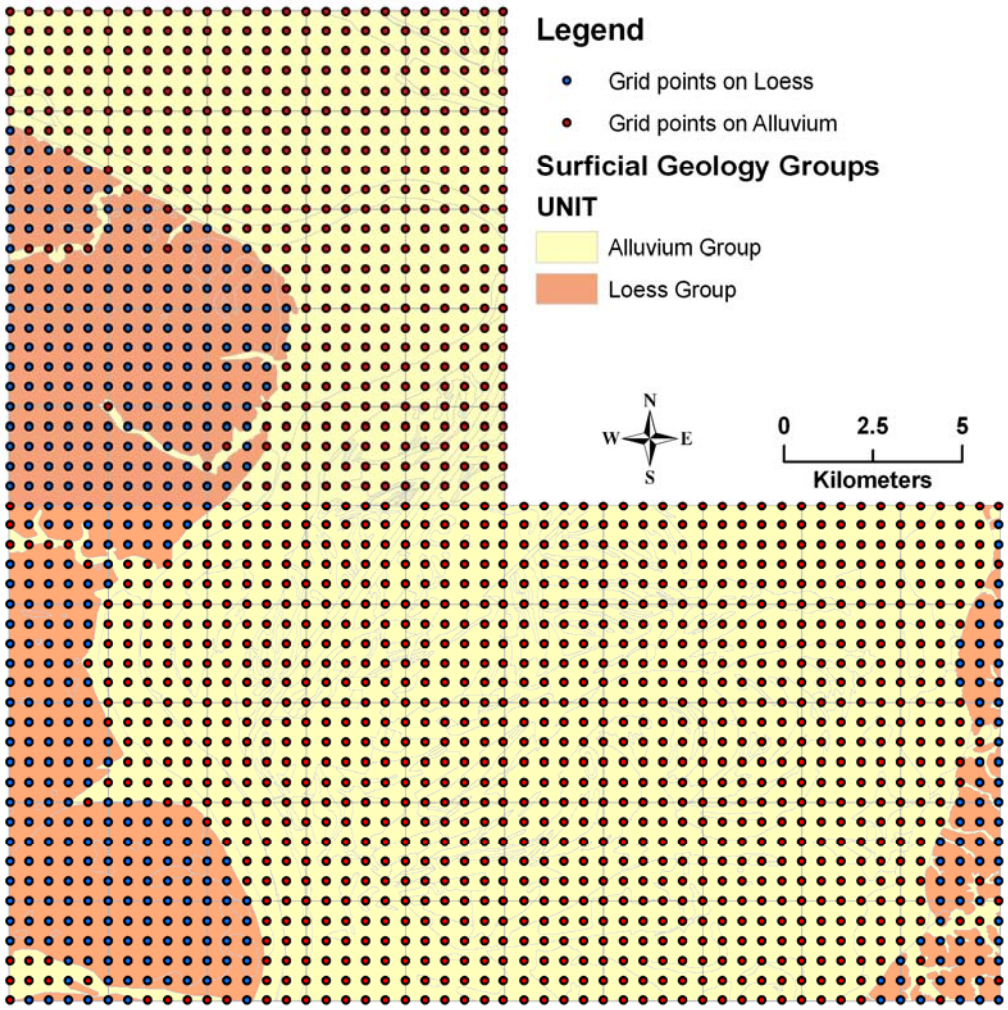

Figure 3. The amplification distributions are calculated based on a grid of 0.005˚ or for about every 500 m. There were total of 1974 grid points encompassing the study quadrangles. The amplification distributions were generated for two distinct geologic units; floodplain deposits (yellow) and upland deposits (orange). The grid points were divided into grid points on alluvium (red color circles) and grid points on loess (blue color circles).

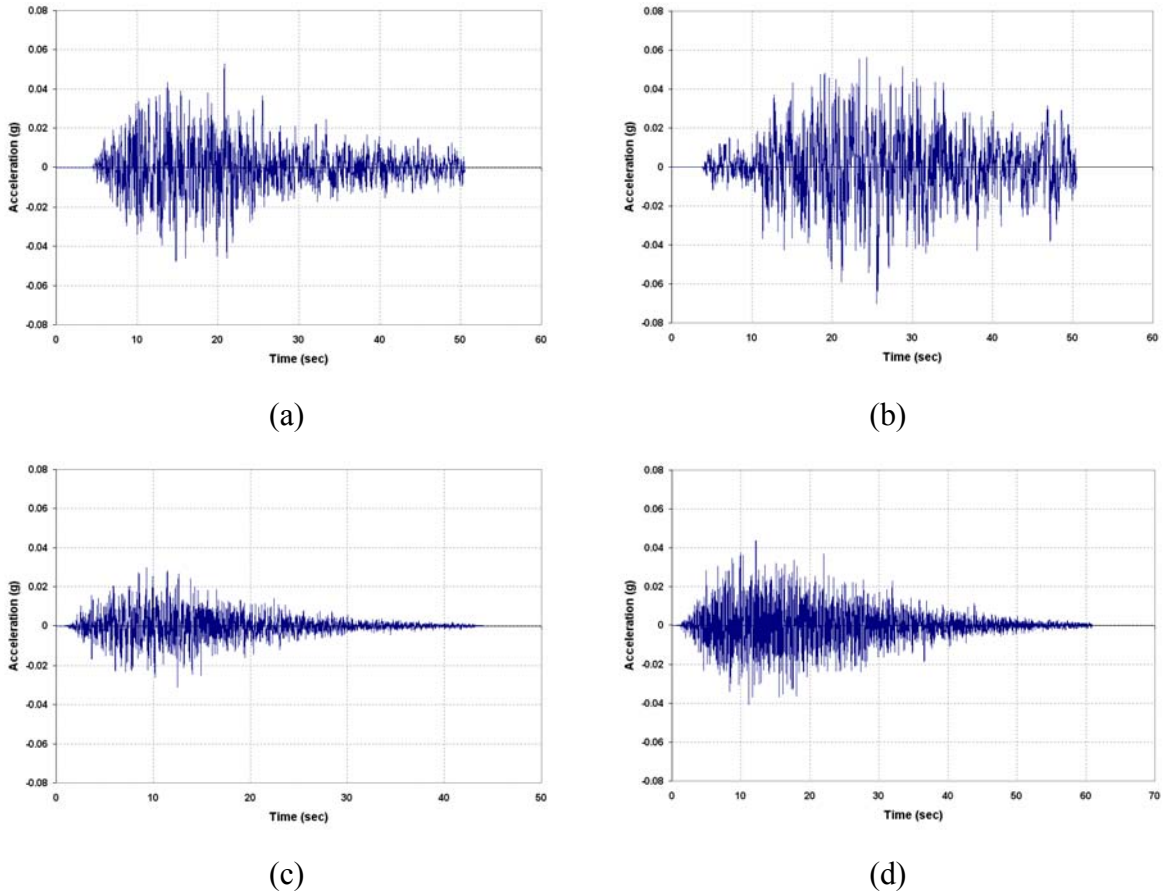

Figure 4. Acceleration time histories of synthetically generated ground motions: (a) Atkinson and Beresnev, 2002 M 7.5, (b) Atkinson and Beresnev, 2002 for M 8.0, (c) Boore SMSIM code v. 2.2, for M 7.0 and (d) Boore SIMSIM code v. 2.2, for M 7.5.

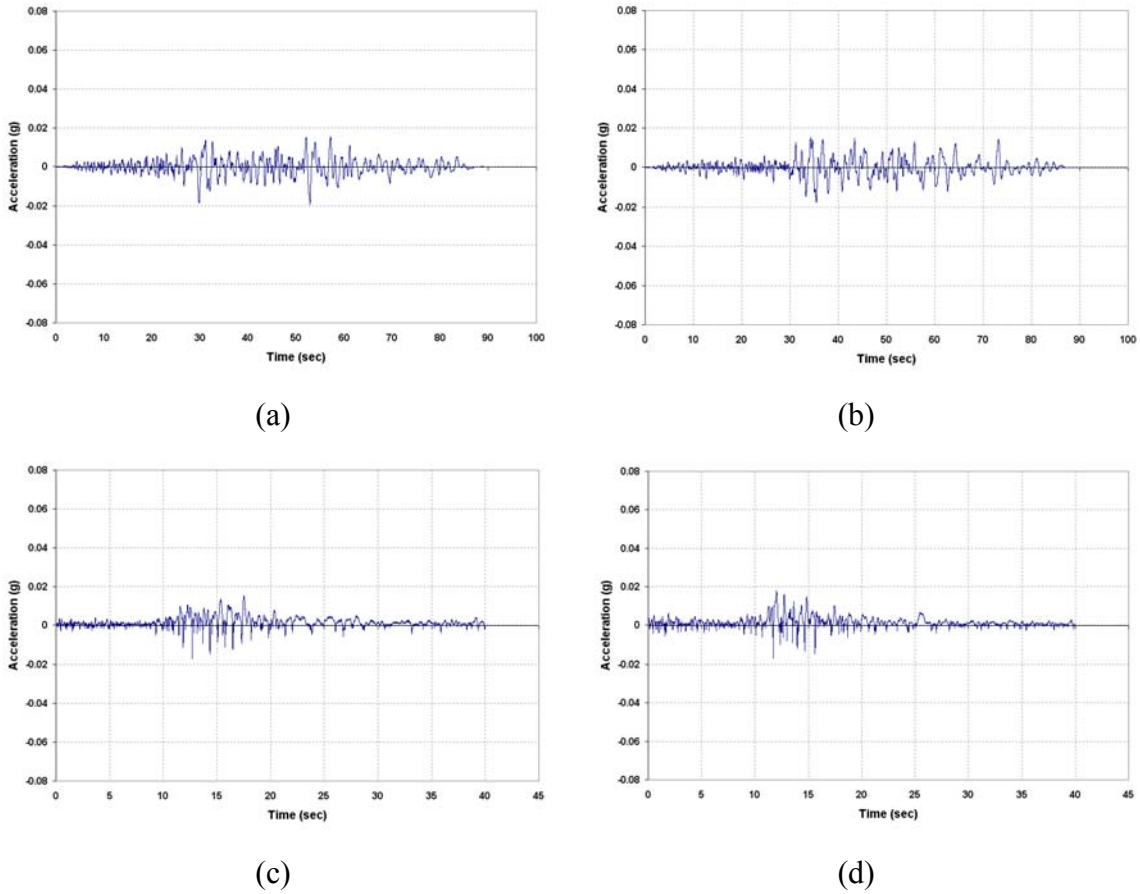

Figure 5. Acceleration time histories of real recordings: (a) Chi Chi 1999 earthquake of M 7.6 North component (b) Chi Chi earthquake of M 7.6 West component, (c) Denali 2002 earthquake of M 7.9, 39˚ component (d) Denali 2002 earthquake of M 7.9, 309˚ component.

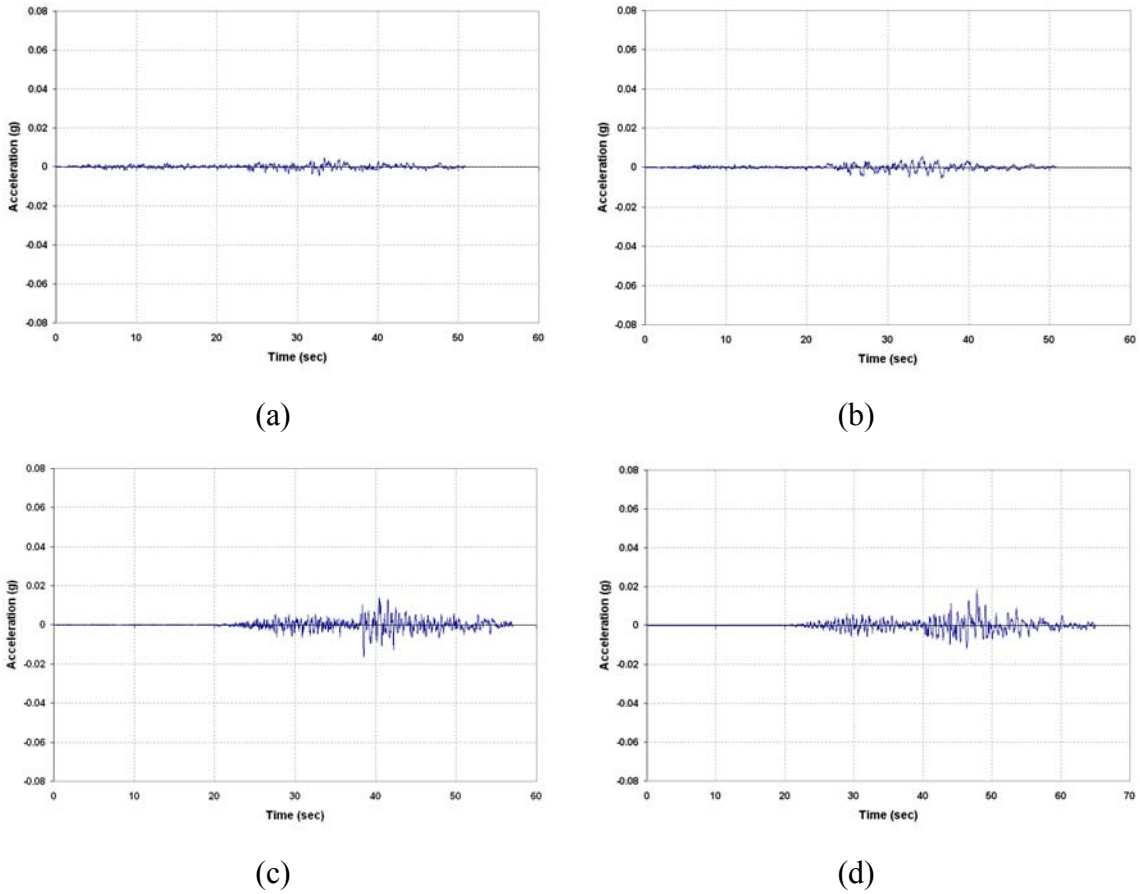

Figure 6. Acceleration time histories of real recordings: (a) Duzce 1999 earthquake of M 7.2, 90˚ component (b) Duzce 1999 earthquake of M 7.2, 180˚ component, (c) Hector Mine 1999 earthquake of M 7.1, 90˚ component (d) Hector Mine 1999 earthquake of M 7.1, 360˚ component.

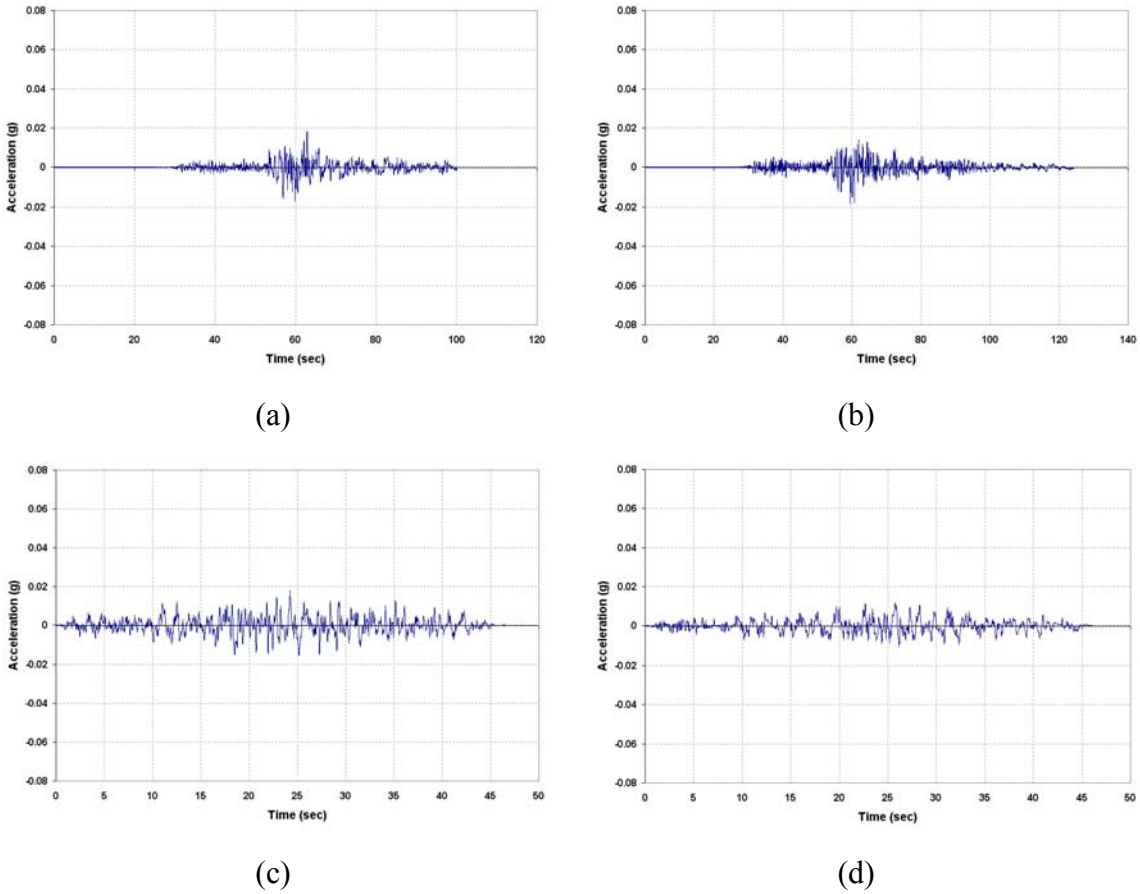

Figure 7. Acceleration time histories of real recordings: (a) Kocaeli 1999 earthquake of M 7.4 East component (b) Kocaeli 1999 earthquake of M 7.4 North component, (c) Landers 1999 earthquake of M 7.3, 200˚ component, (d) Landers 1999 earthquake of M 7.3, 290˚ component.

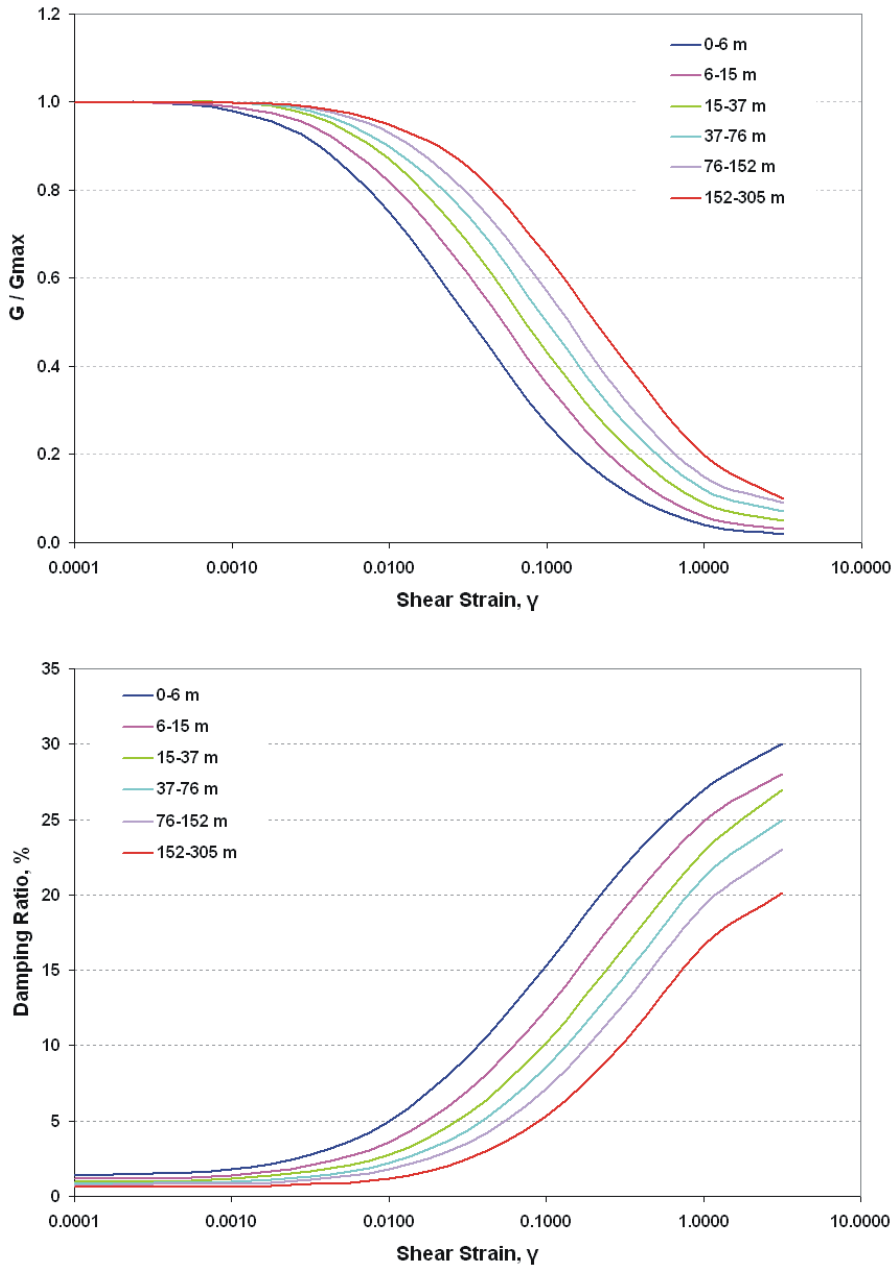

Figure 8. Shear modulus reduction curves (top figure) and the damping ratios (bottom figure), from EPRI (1993).

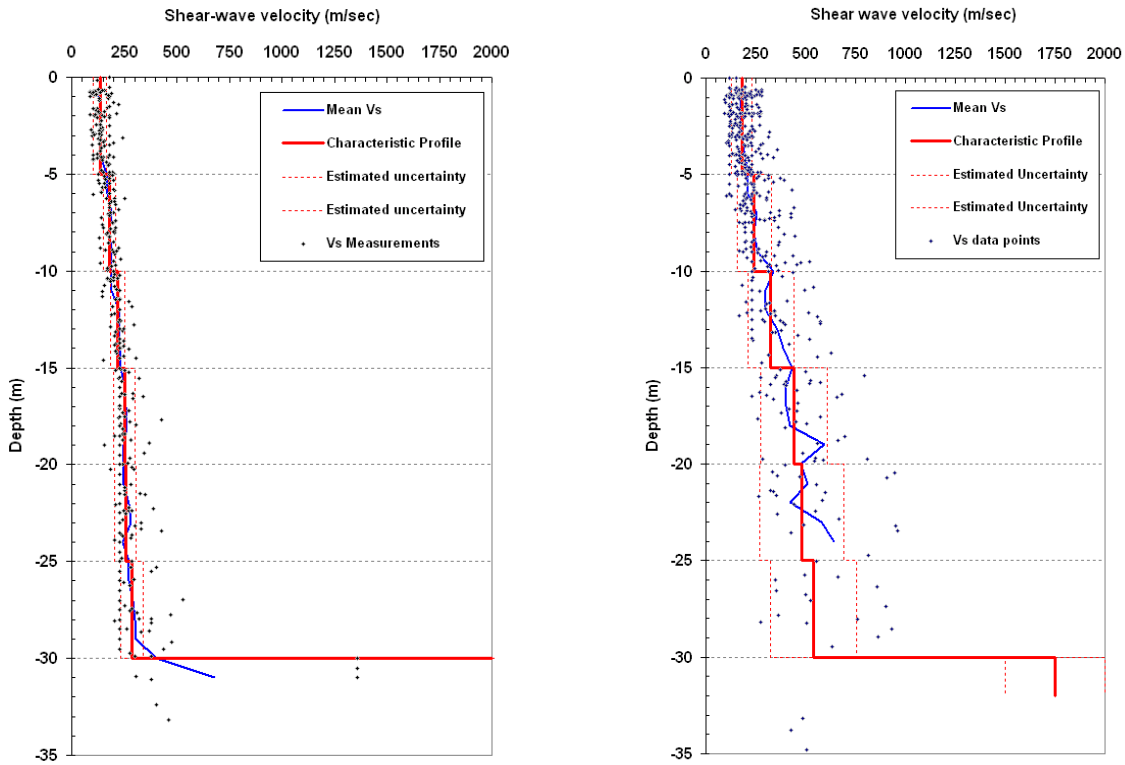

(a) (b)

Figure 9. (a) The estimated characteristic shear-wave velocity profile for flood plain deposits (alluvial deposits), and (b) The estimated characteristic shear-wave velocity profile for upland deposits (loess deposits).

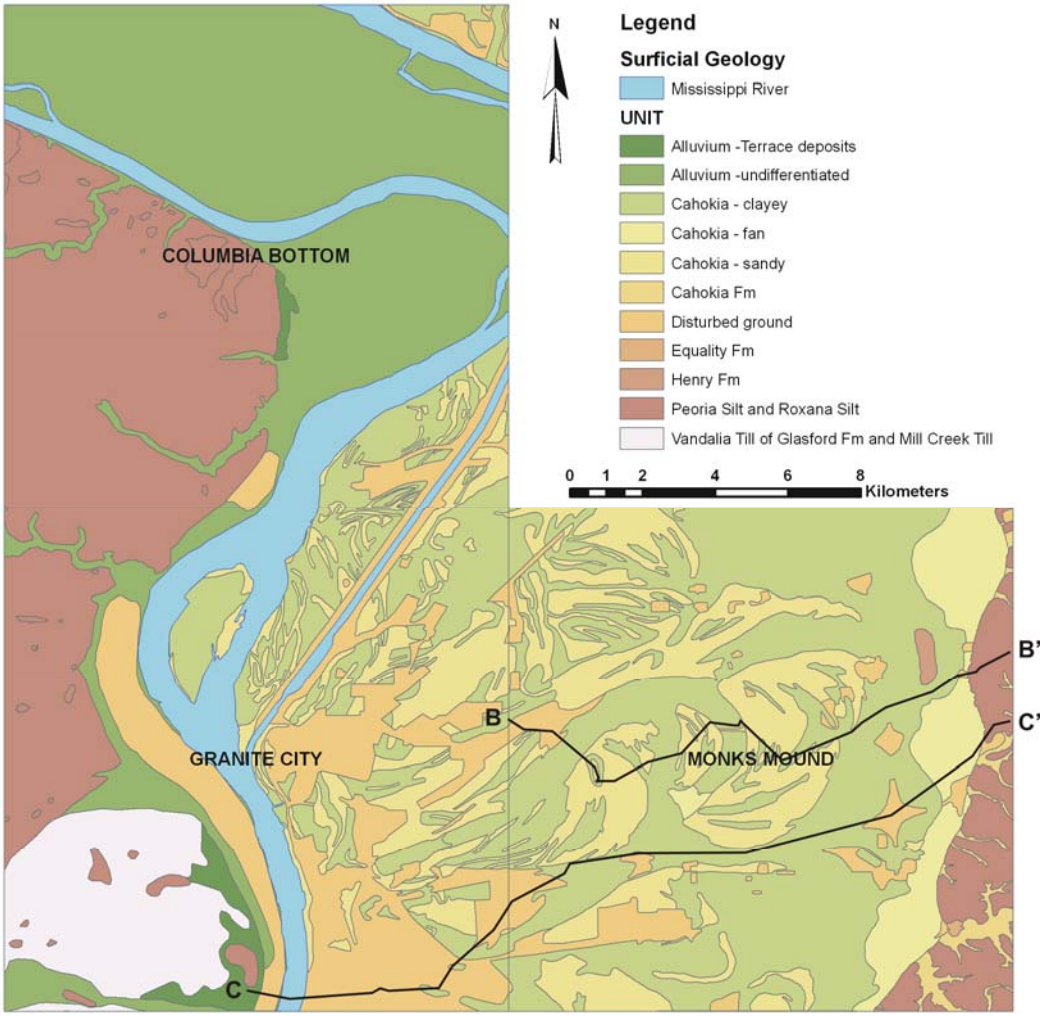

Figure 10. The surficial geologic map of Granite City, Monks Mound and Columbia Bottom Quadrangles. This map is more generalized on the Missouri side of the Mississippi River (see alluvium). On the Illinois side of the river, however, alluvium is subdivided into different facies: Cahokia clay, Cahokia sand, Cahokia fan, and Cahokia formation. The ISGS cross-sections are shown as B-B' and C-C' in Figure 4.3 (Grimley et al., 2007; Phillips et al., 2001).

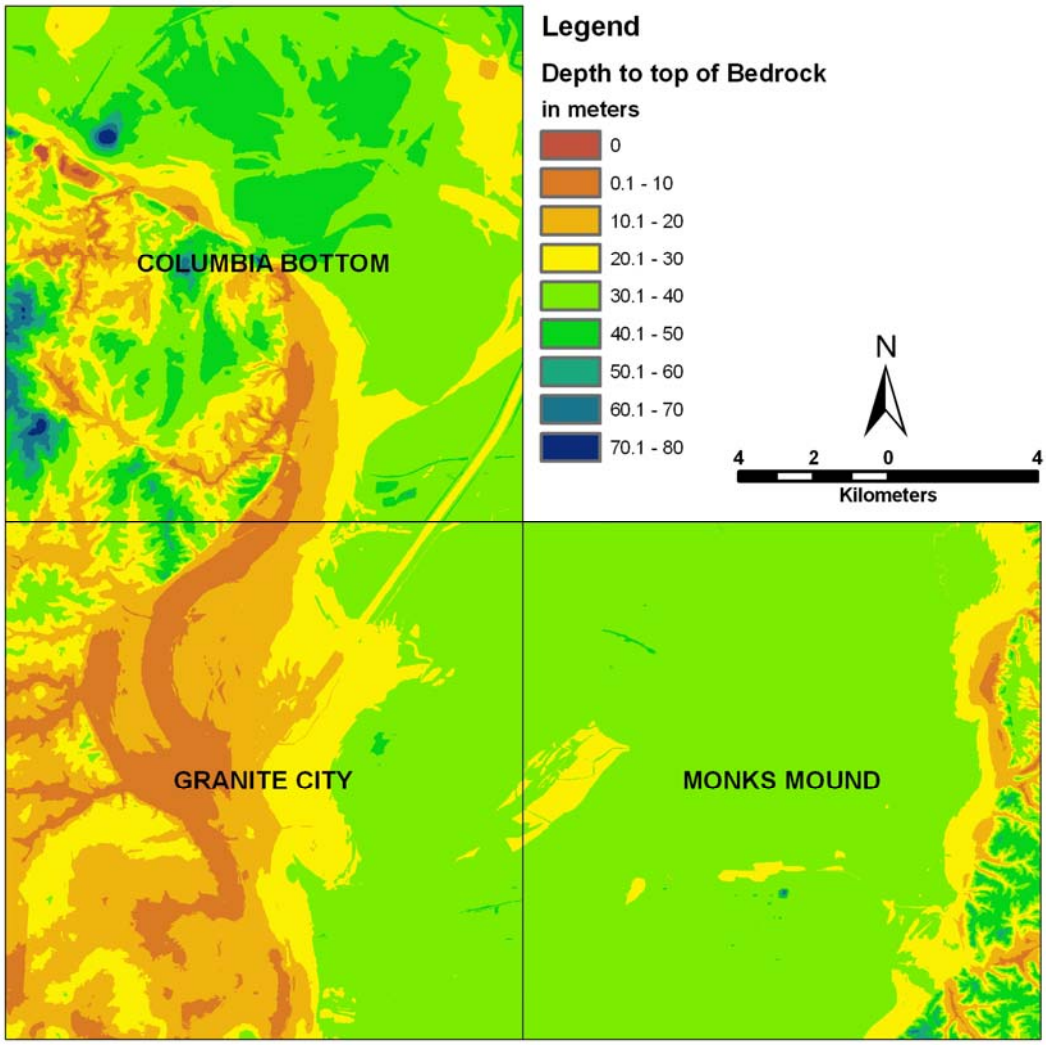

Figure 11. Estimated depths to top of bedrock (or surficial materials thickness). See Section 4 on the preparation procedure of this map

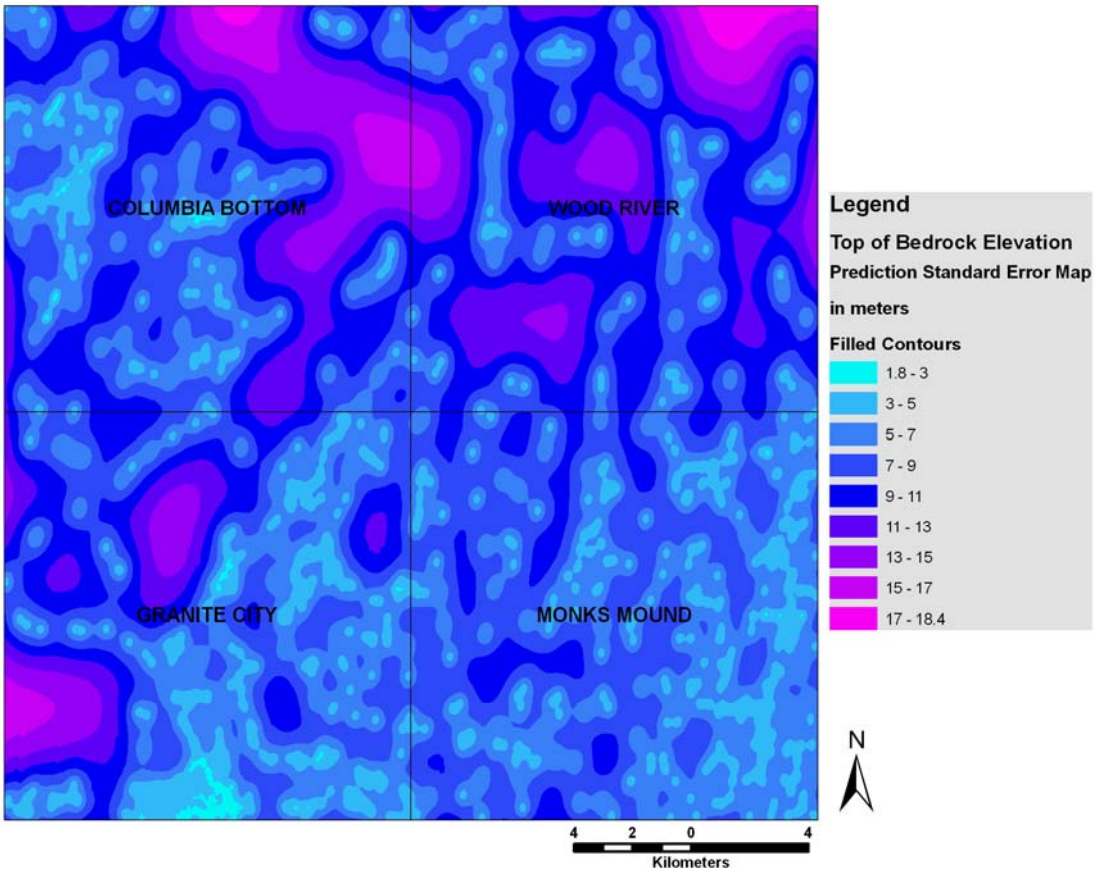

Figure 12. Prediction standard error map of top-of-bedrock elevation map as estimated using the ordinary kriging method.

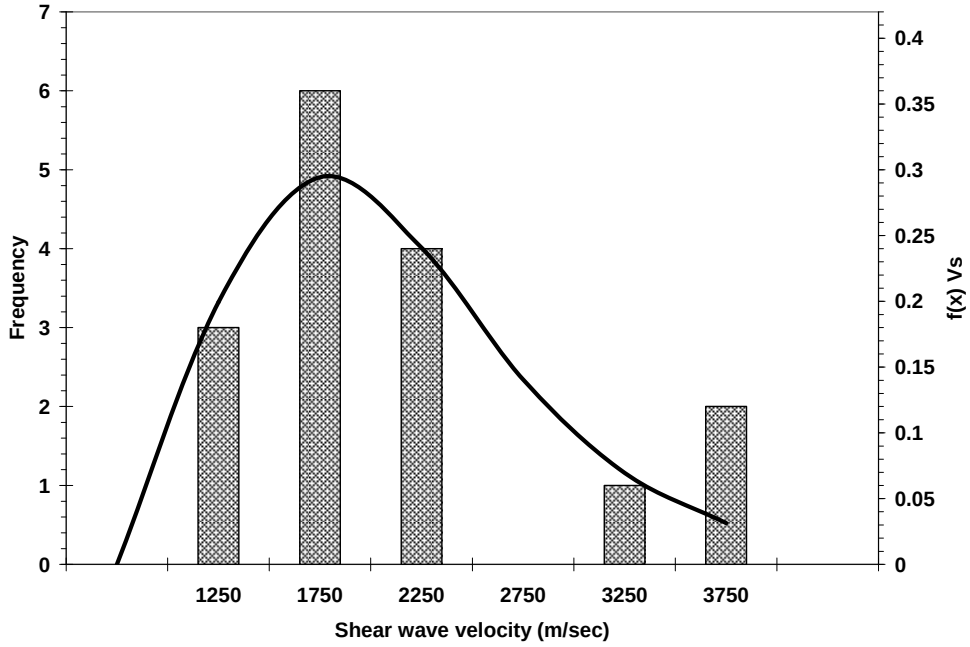

Figure 13. Frequency plot of the shear wave velocity measurements made by Williams (2007).

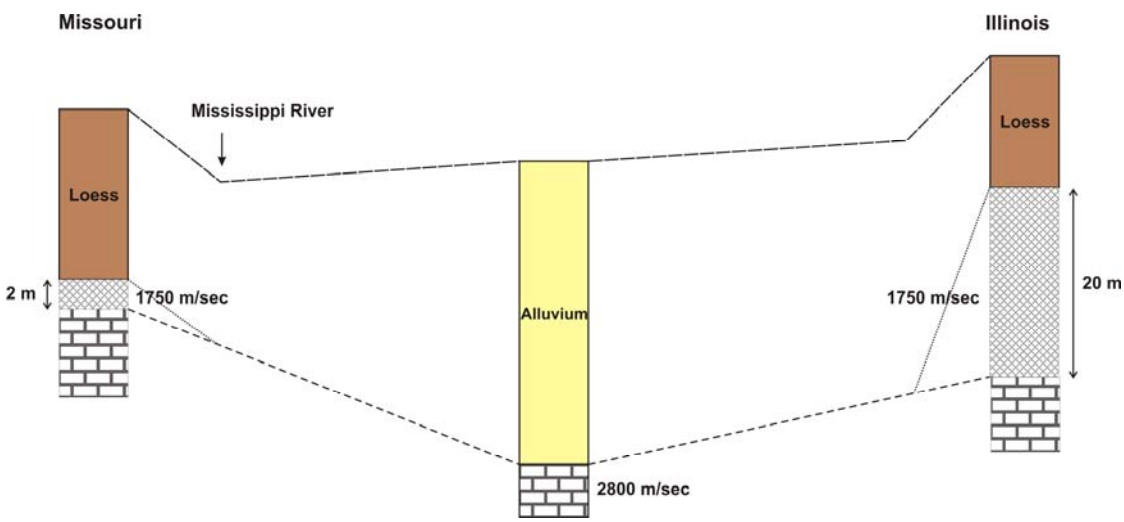

Figure 14. Schematic cross section showing the assumed variations of the weathered rock horizons described in the text.

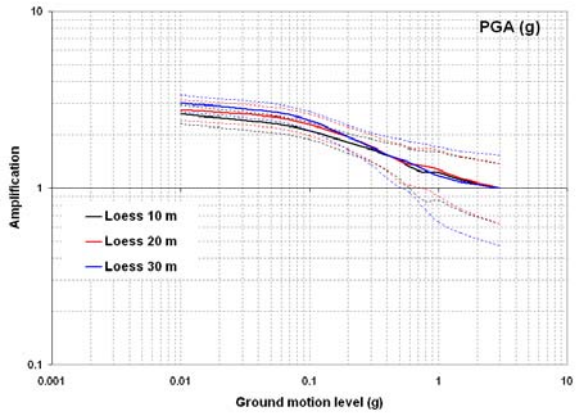

(a)

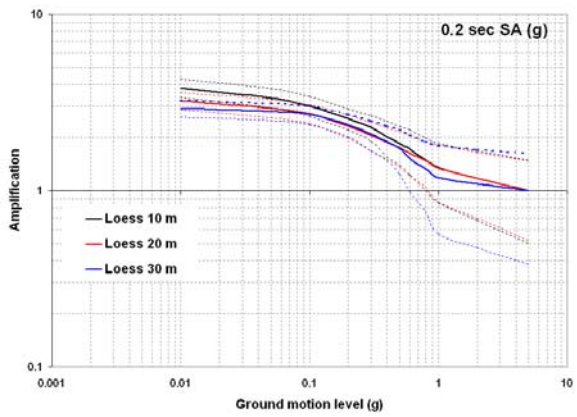

(b)

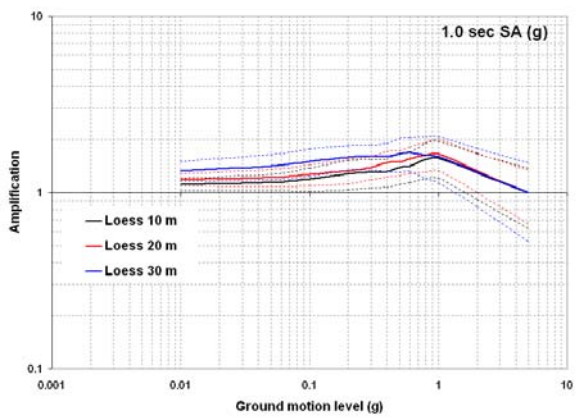

(c)

Figure 15. Median (50th percentile) site-amplification estimates for 10, 20, and 30 meter thick loess profiles are shown as solid lines. The 16th and 84th percentile uncertainties for the same thicknesses are shown as dotted lines.

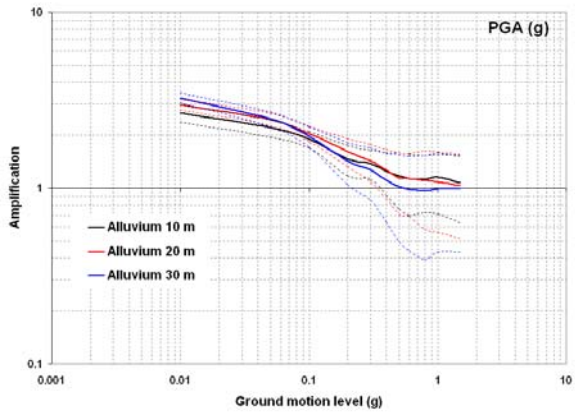

(a)

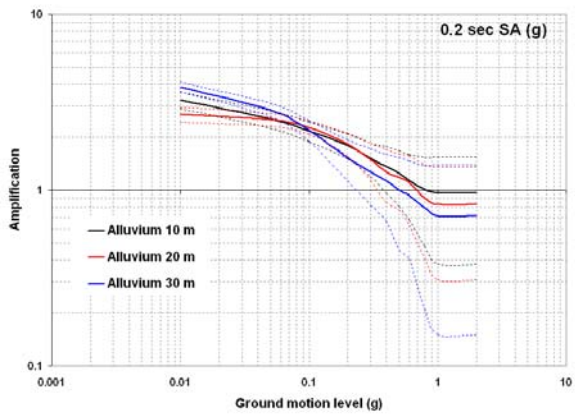

(b)

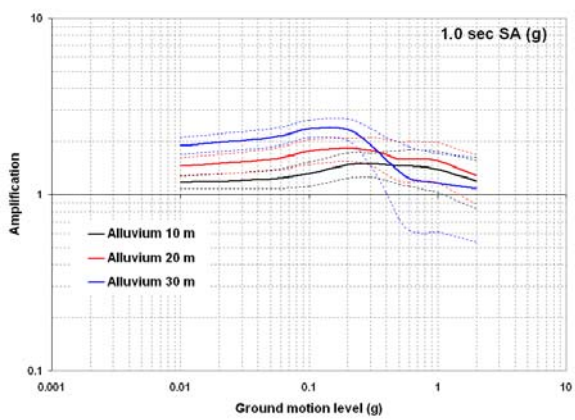

(c)

Figure 16. Median (50th percentile) site-amplification estimates for 10, 20, and 30 meter thick alluvium profiles are shown as solid lines. The 16th and 84th percentile uncertainties for the same thicknesses are shown as dotted lines.

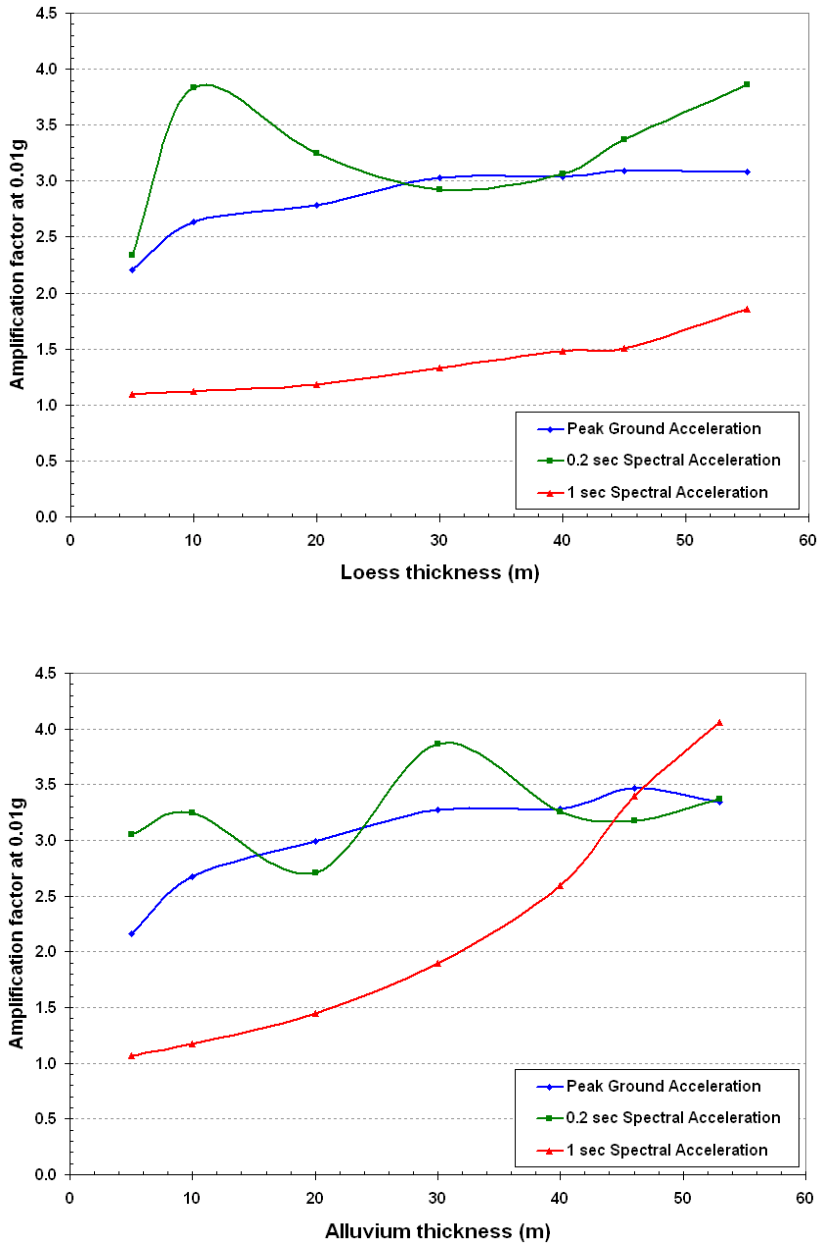

Figure 17. Plots showing the effect of thickness on the peak ground acceleration, 0.2 sec spectral acceleration and 1 sec spectral acceleration of the loessal and alluvial deposits.

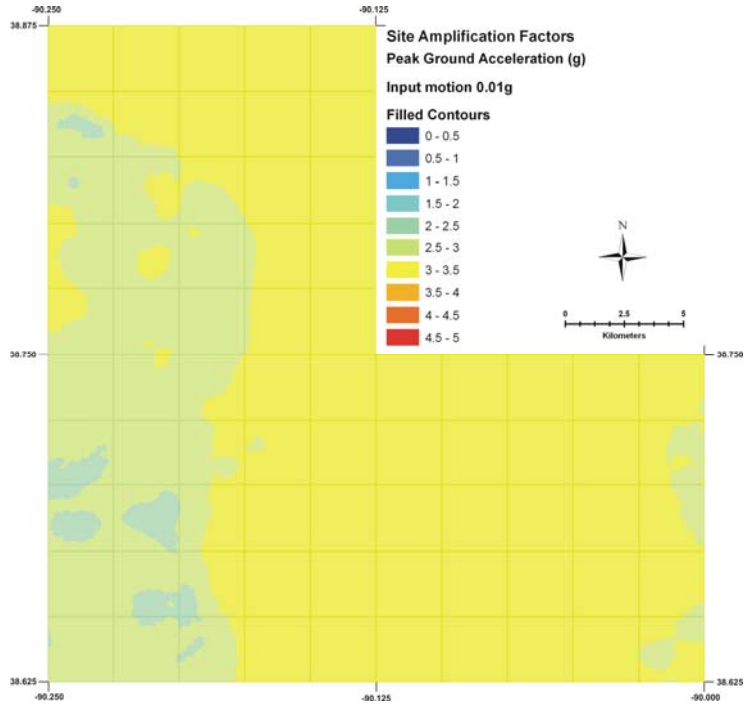

Figure 18. Site amplification map for peak ground acceleration for input ground motion level of 0.01g.

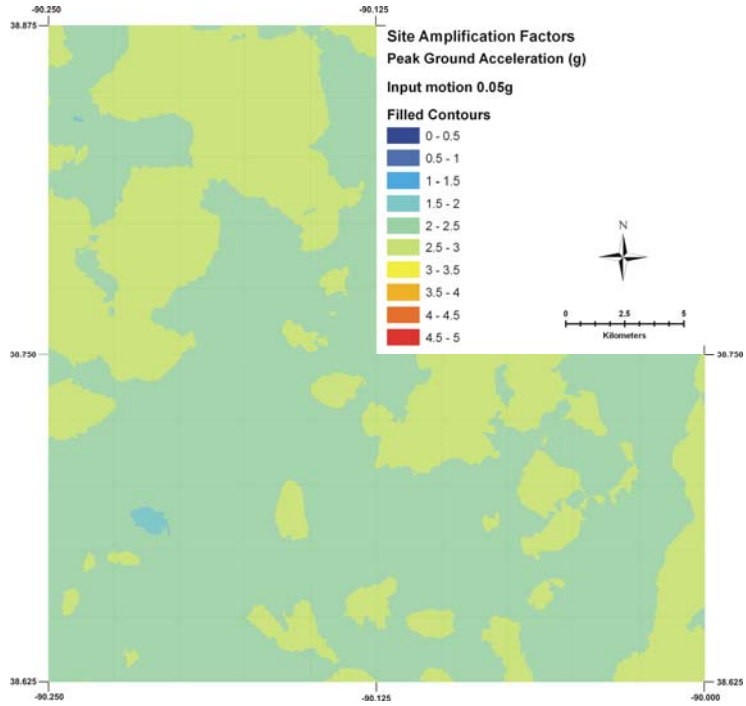

Figure 19. Site amplification map for peak ground acceleration for input ground motion level of 0.05g.

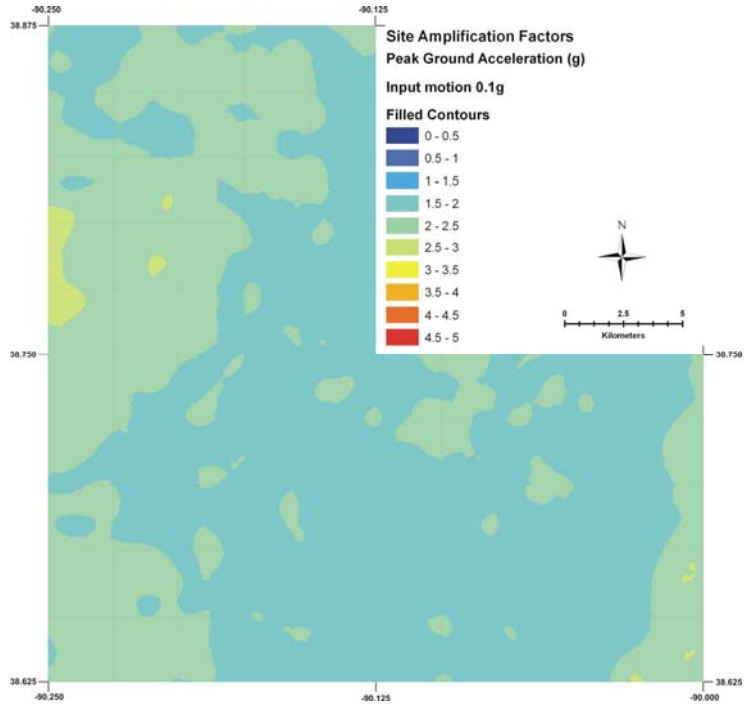

Figure 20. Site amplification map for peak ground acceleration for input ground motion level of 0.1g.

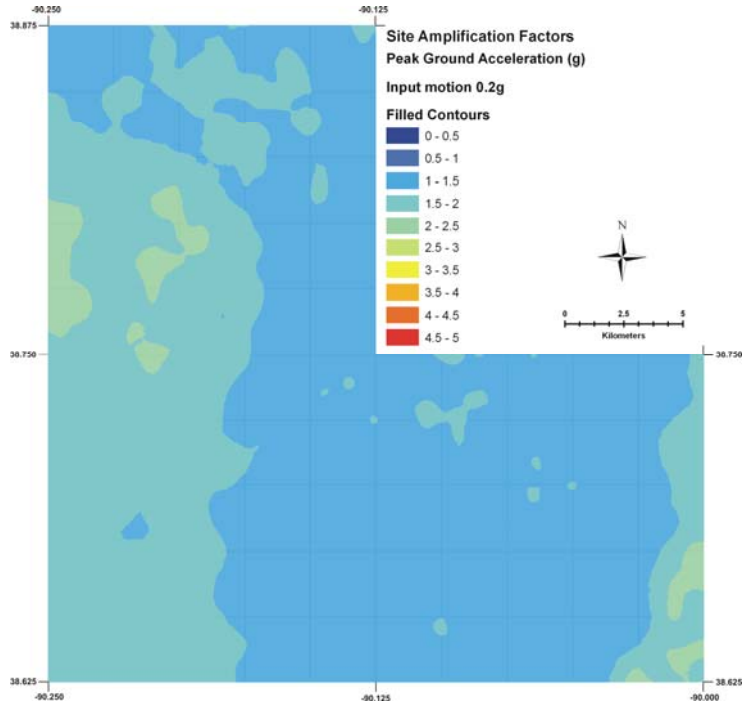

Figure 21. Site amplification map for peak ground acceleration for input ground motion level of 0.2g.

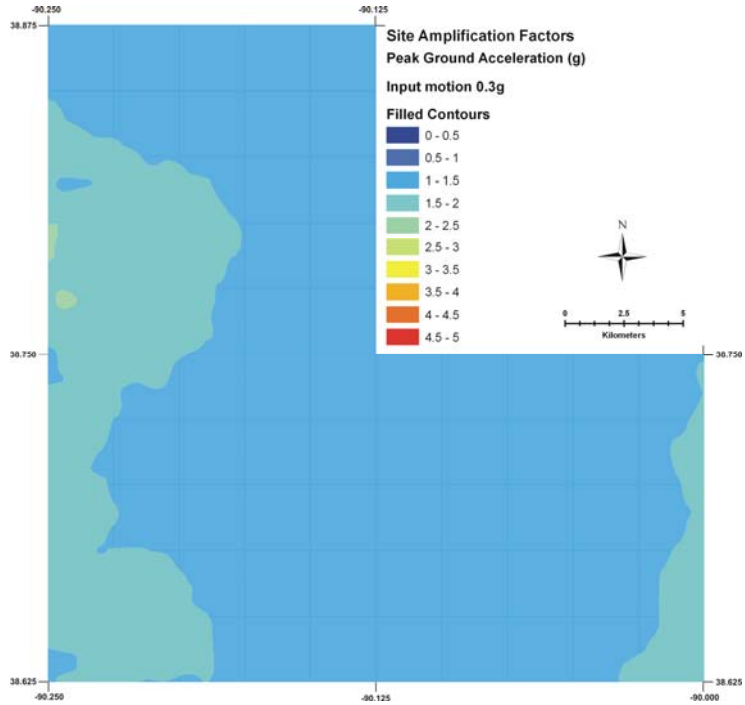

Figure 22. Site amplification map for peak ground acceleration for input ground motion level of 0.3g.

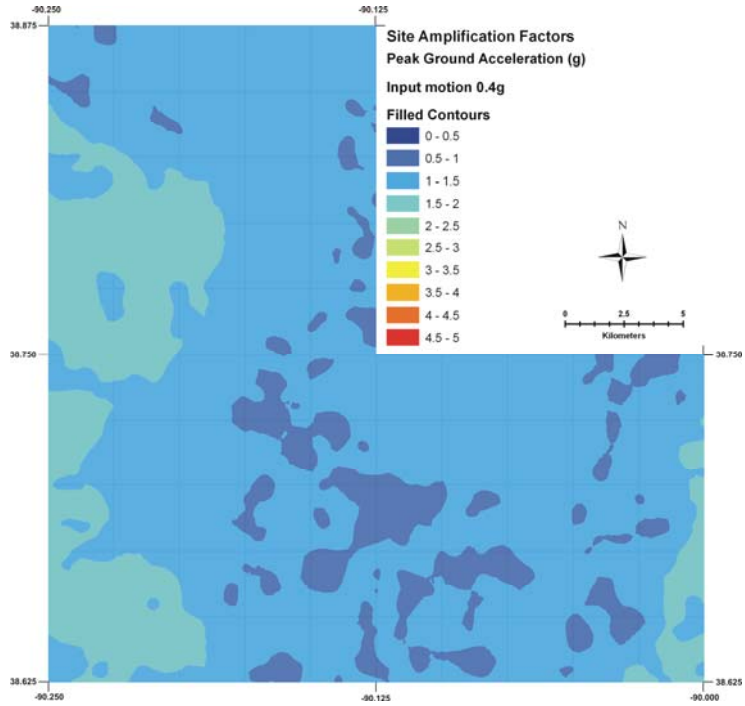

Figure 23. Site amplification map for peak ground acceleration for input ground motion level of 0.4g.

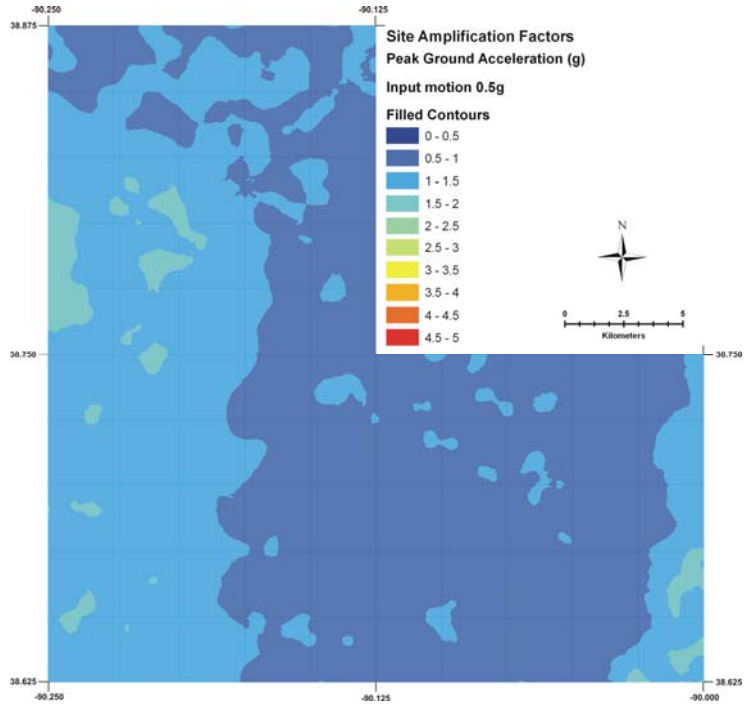

Figure 24. Site amplification map for peak ground acceleration for input ground motion level of 0.5g.

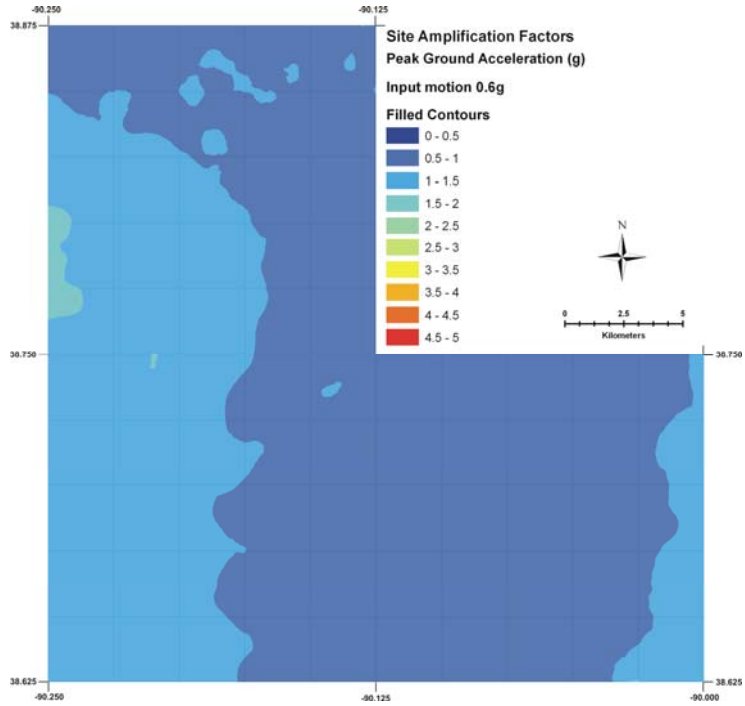

Figure 25. Site amplification map for peak ground acceleration for input ground motion level of 0.6g.

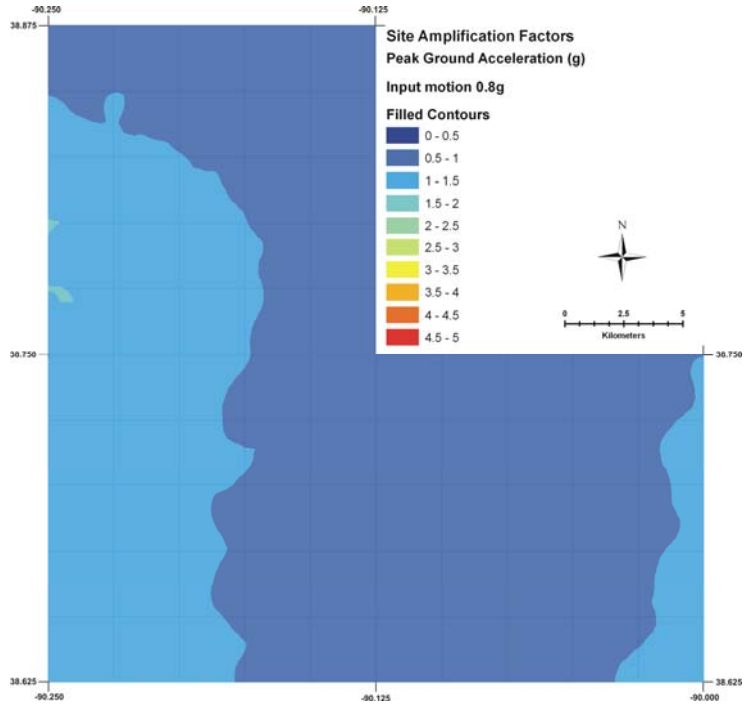

Figure 26. Site amplification map for peak ground acceleration for input ground motion level of 0.8g.

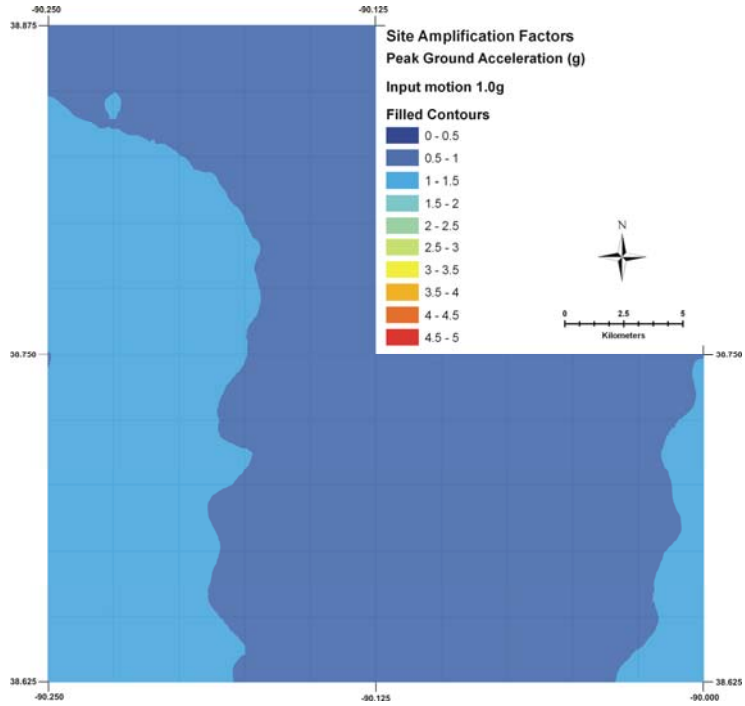

Figure 27. Site amplification map for peak ground acceleration for input ground motion level of 1.0g.

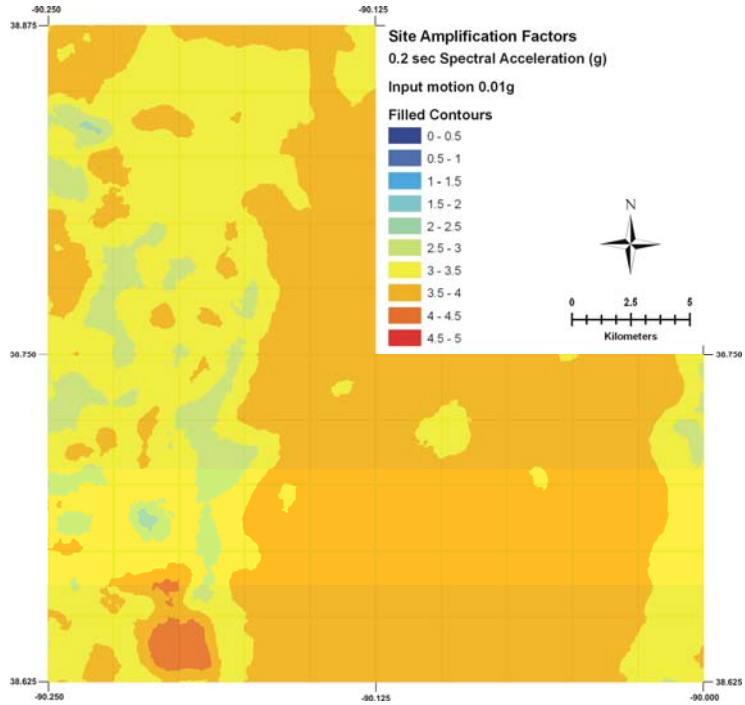

Figure 28. Site amplification map of 0.2 sec spectral acceleration for input ground motion level of 0.01g.

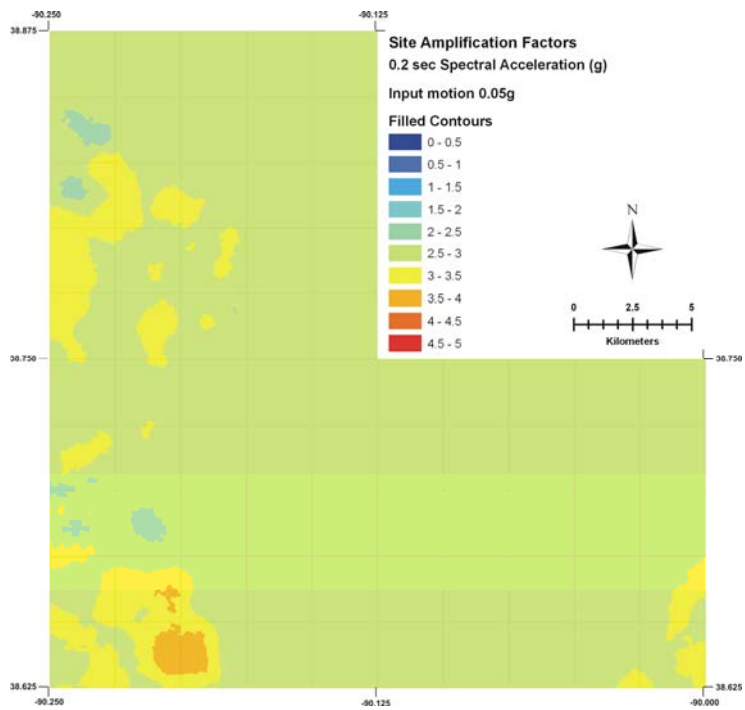

Figure 29. Site amplification map of 0.2 sec spectral acceleration for input ground motion level of 0.05g.

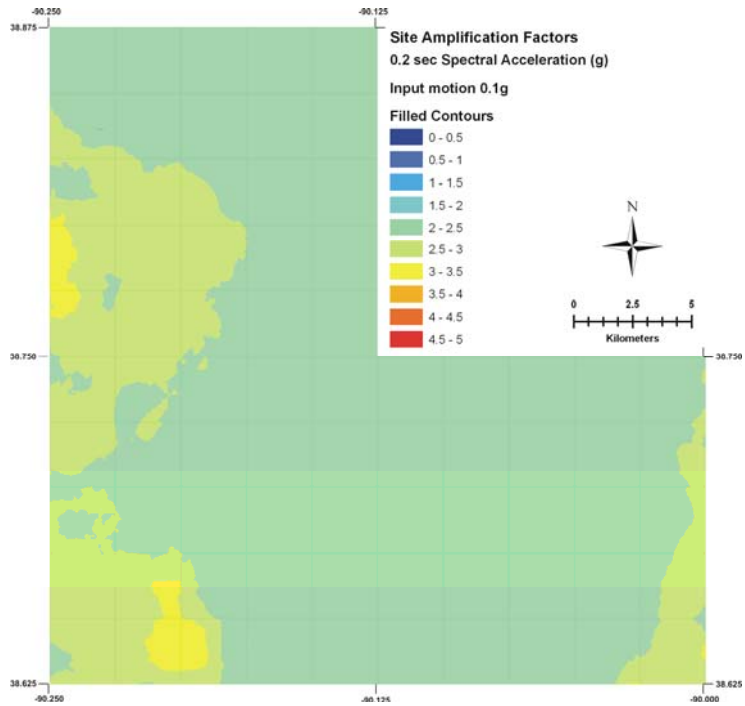

Figure 30. Site amplification map of 0.2 sec spectral acceleration for input ground motion level of 0.1g.

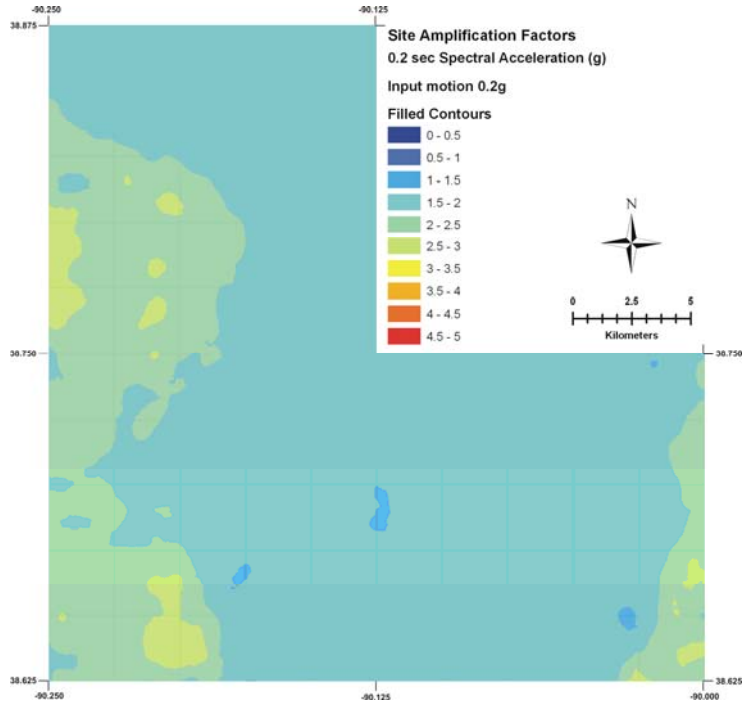

Figure 31. Site amplification map of 0.2 sec spectral acceleration for input ground motion level of 0.2g.

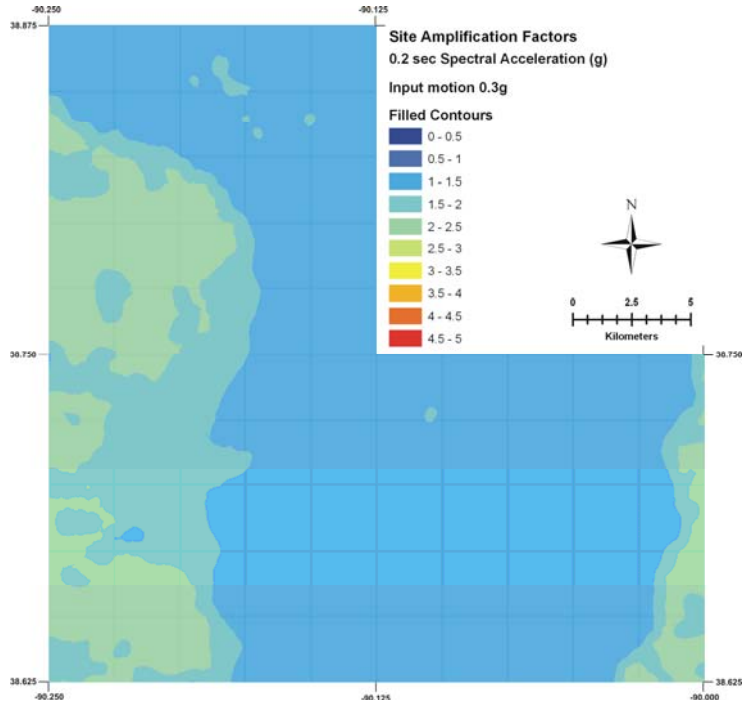

Figure 32. Site amplification map of 0.2 sec spectral acceleration for input ground motion level of 0.3g.

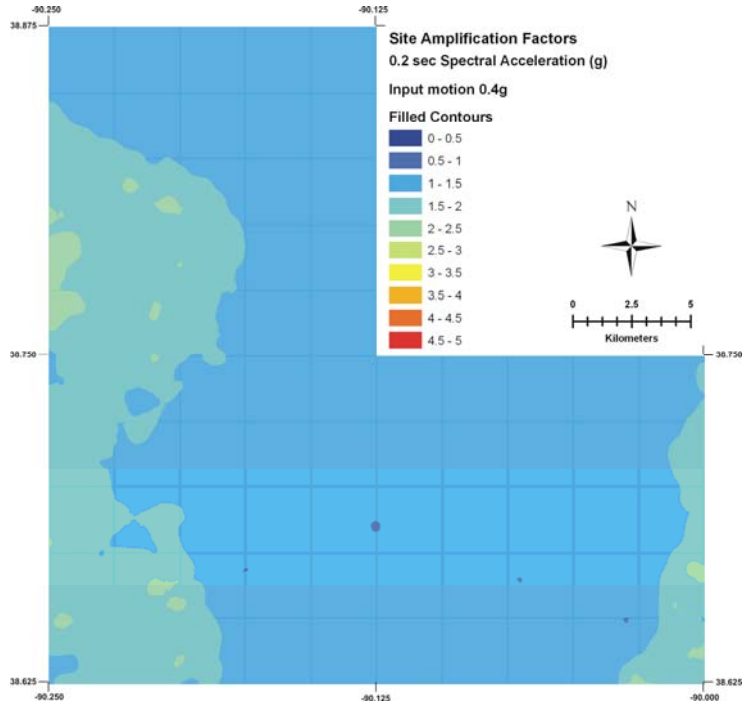

Figure 33. Site amplification map of 0.2 sec spectral acceleration for input ground motion level of 0.4g.

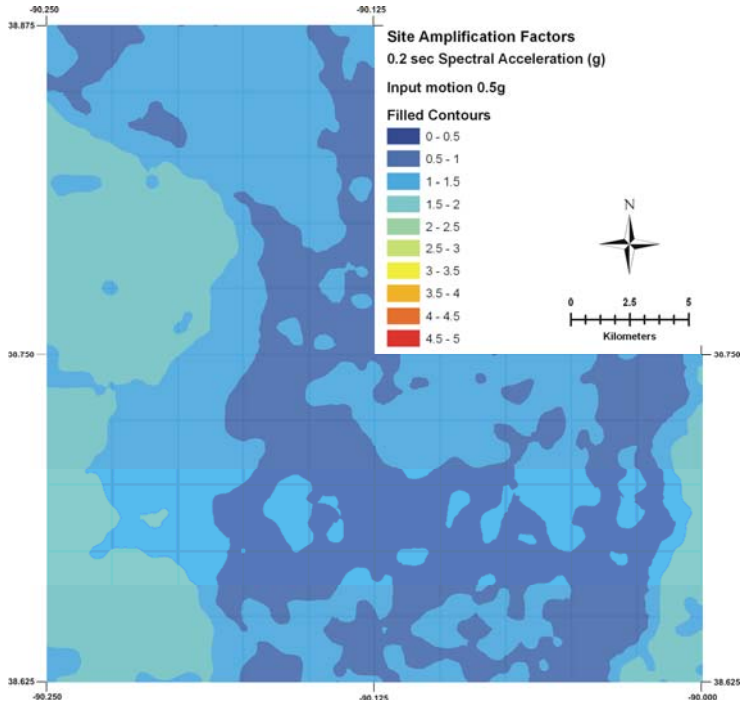

Figure 34. Site amplification map of 0.2 sec spectral acceleration for input ground motion level of 0.5g.

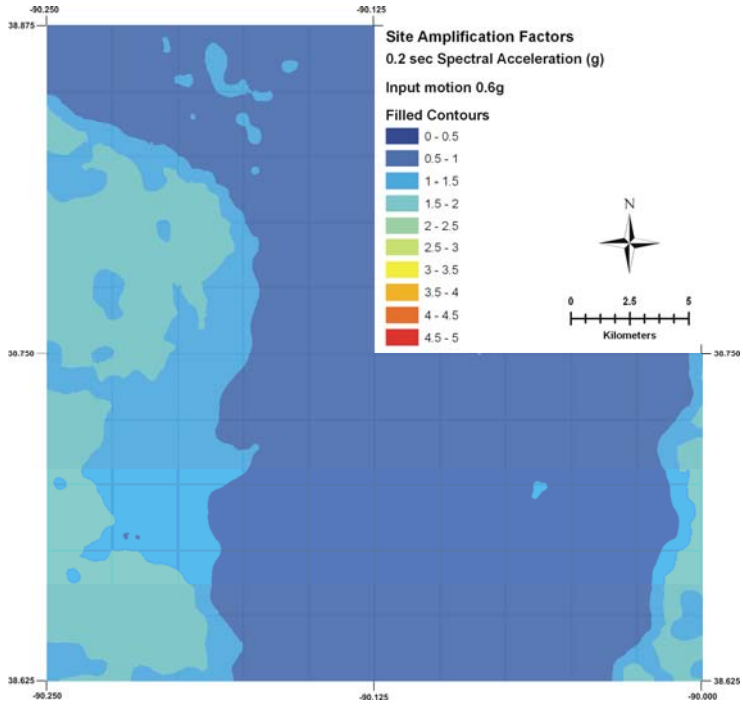

Figure 35. Site amplification map of 0.2 sec spectral acceleration for input ground motion level of 0.6g.

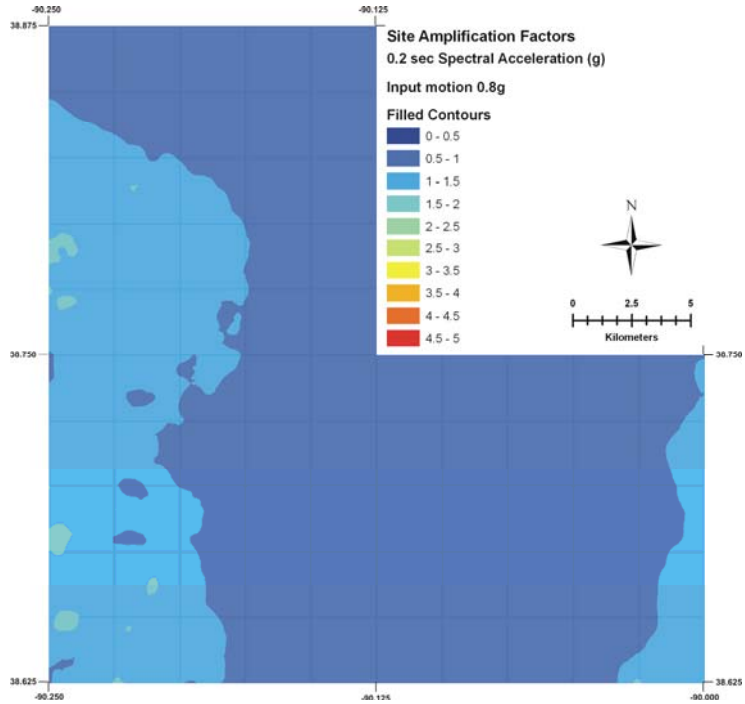

Figure 36. Site amplification map of 0.2 sec spectral acceleration for input ground motion level of 0.8g.

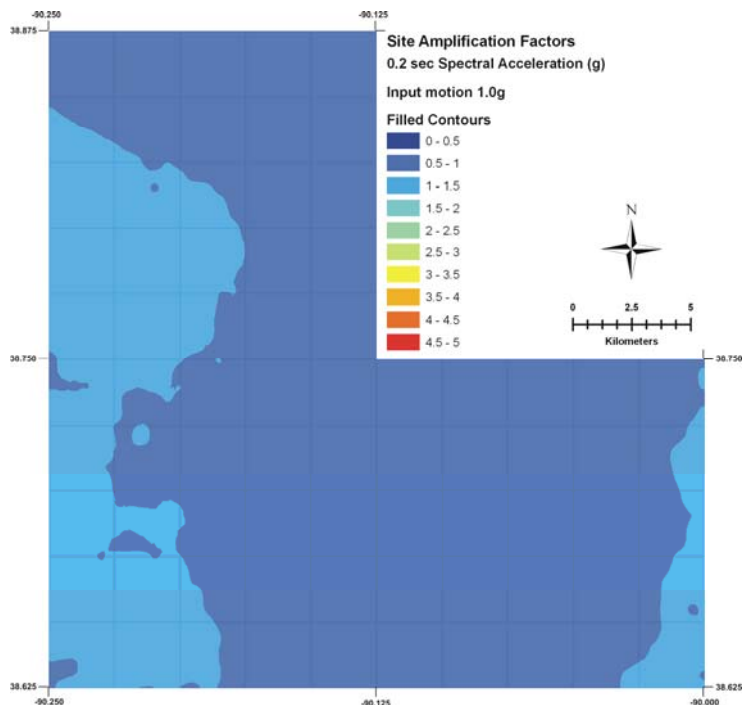

Figure 37. Site amplification map of 0.2 sec spectral acceleration for input ground motion level of 1.0g.

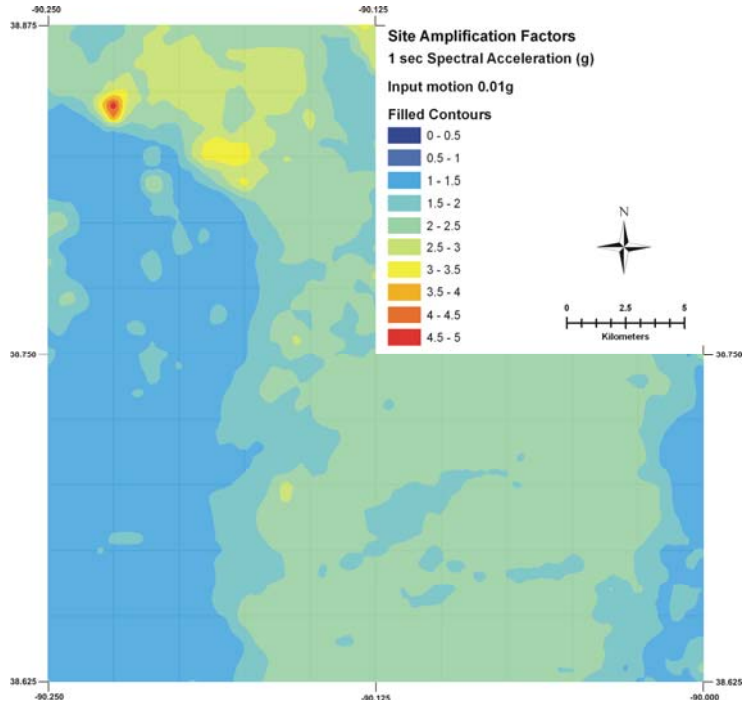

Figure 38. Site amplification map of 1.0 sec spectral acceleration for input ground motion level of 0.01g.

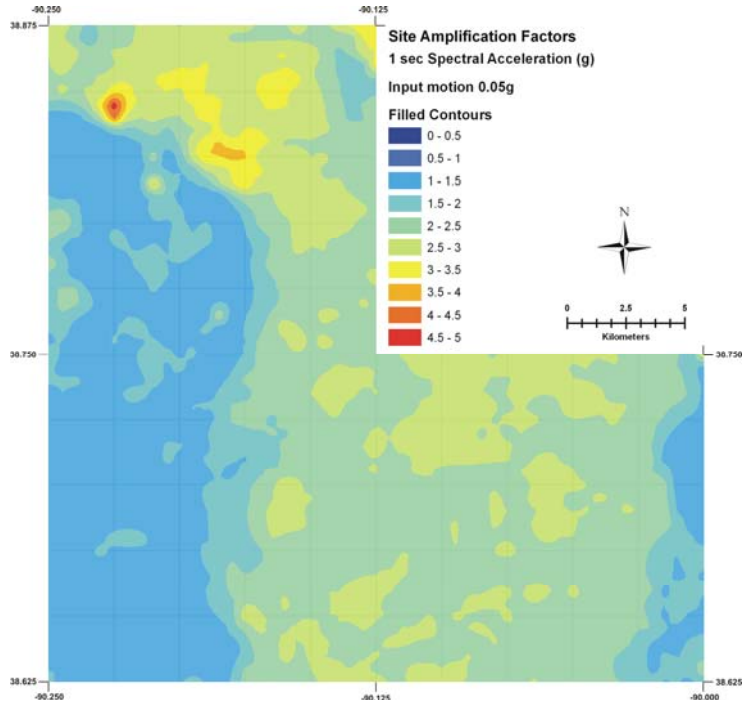

Figure 39. Site amplification map of 1.0 sec spectral acceleration for input ground motion level of 0.05g.

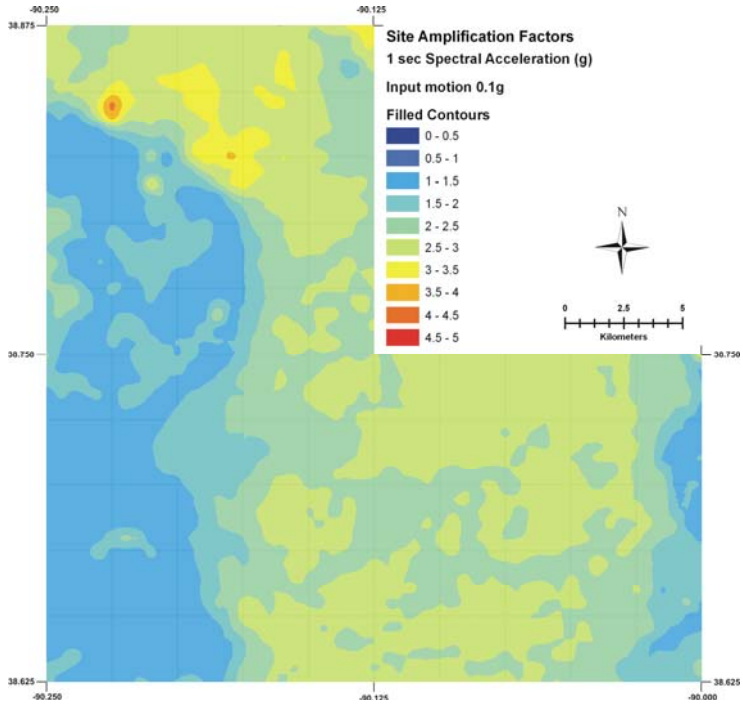

Figure 40. Site amplification map of 1.0 sec spectral acceleration for input ground motion level of 0.1g.

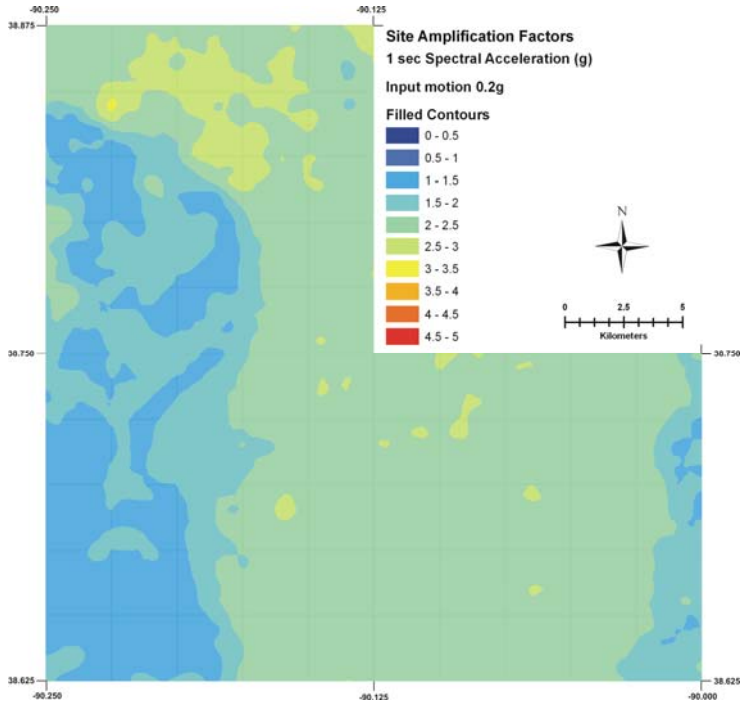

Figure 41. Site amplification map of 1.0 sec spectral acceleration for input ground motion level of 0.2g.

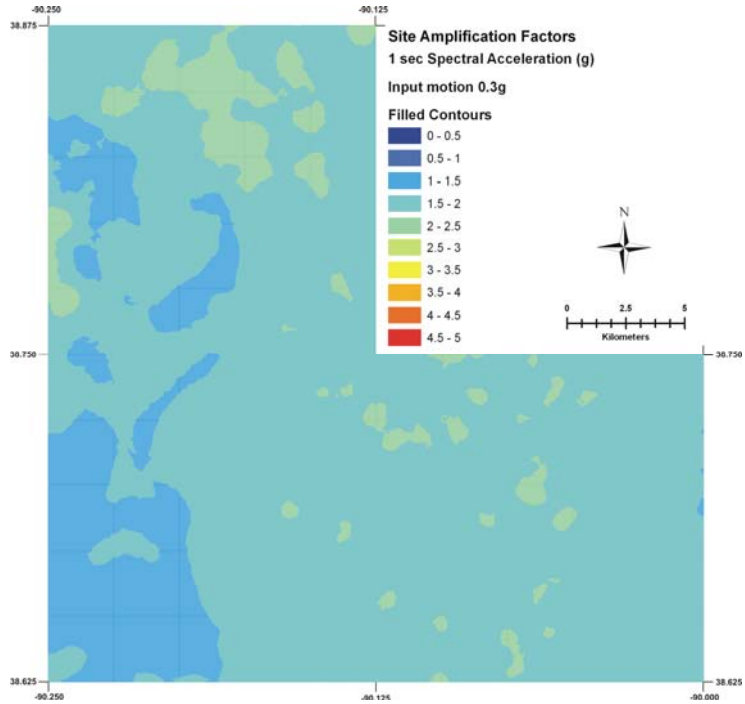

Figure 42. Site amplification map of 1.0 sec spectral acceleration for input ground motion level of 0.3g.

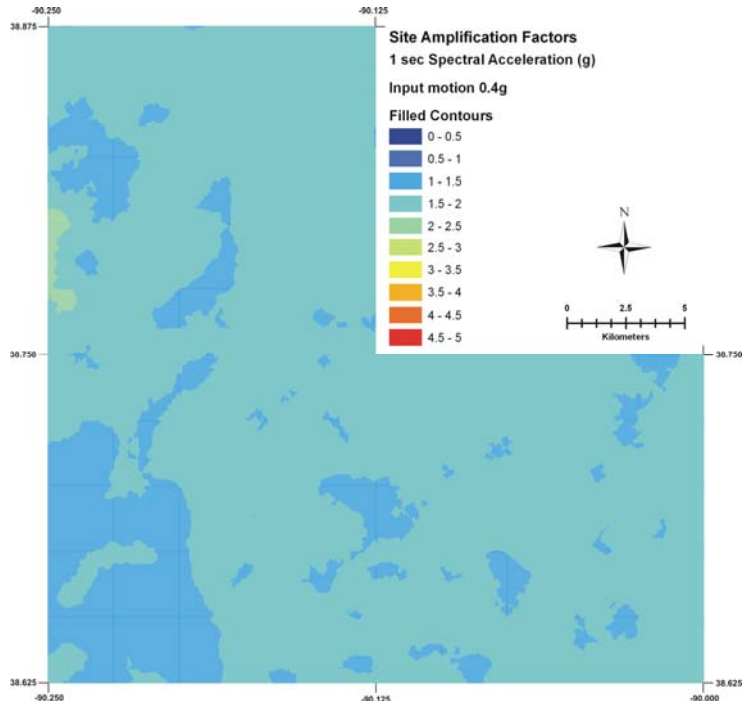

Figure 43. Site amplification map of 1.0 sec spectral acceleration for input ground motion level of 0.4g.

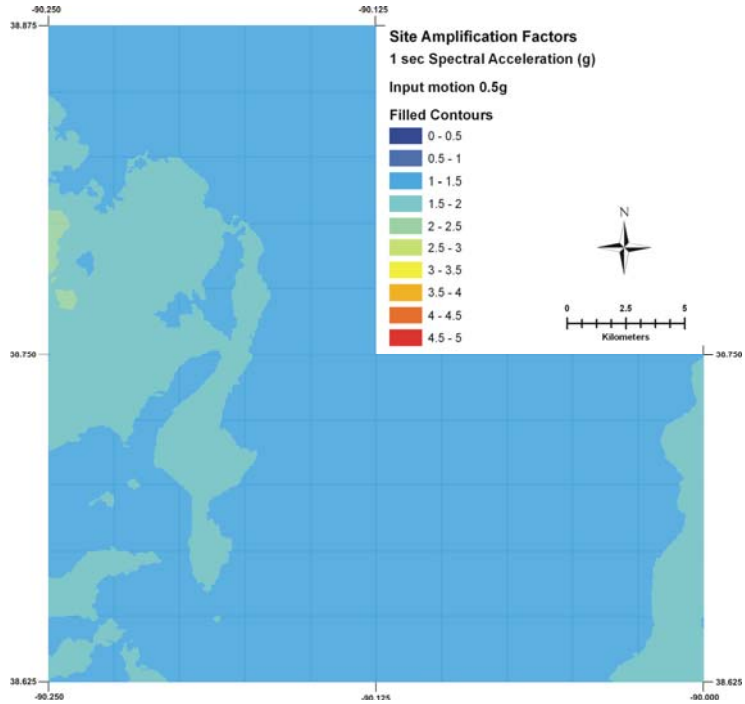

Figure 44. Site amplification map of 1.0 sec spectral acceleration for input ground motion level of 0.5g.

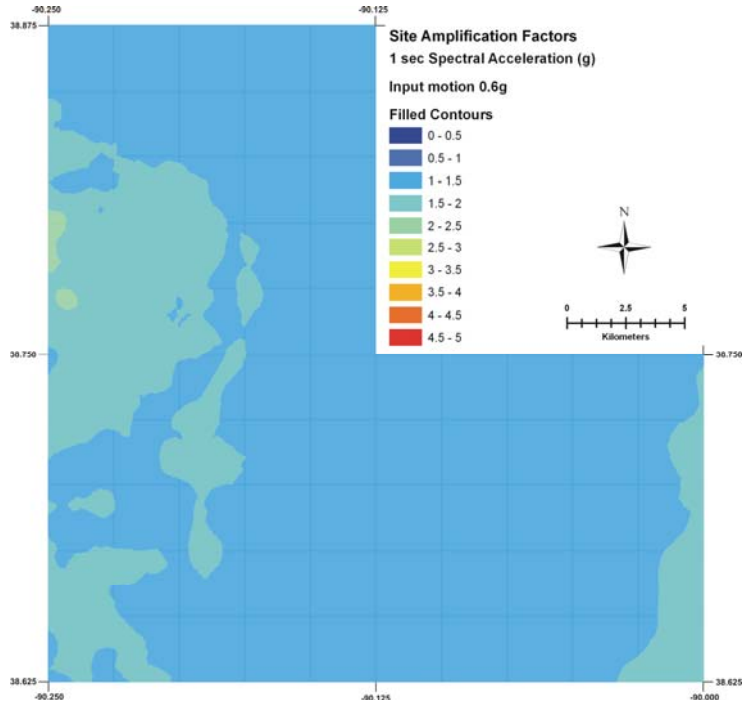

Figure 45. Site amplification map of 1.0 sec spectral acceleration for input ground motion level of 0.6g.

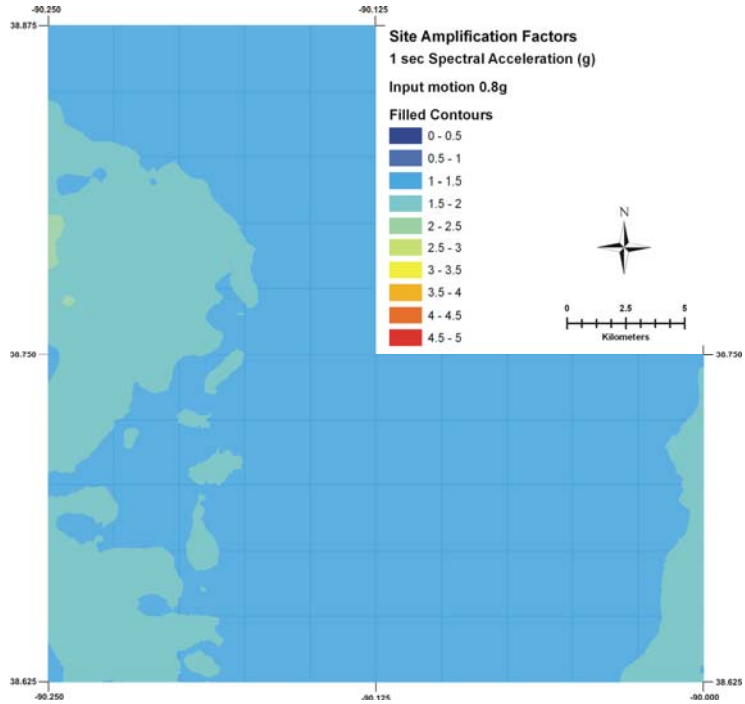

Figure 46. Site amplification map of 1.0 sec spectral acceleration for input ground motion level of 0.8g.

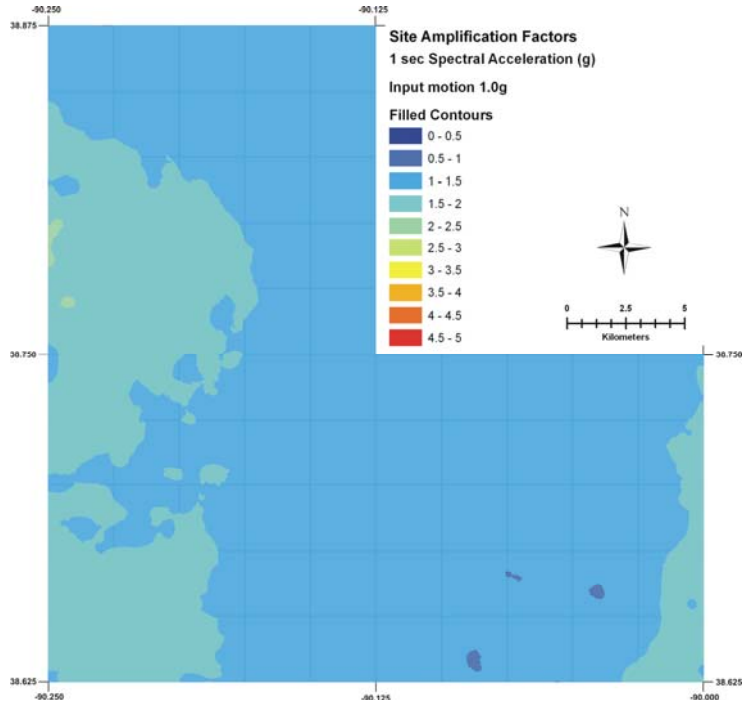

Figure 47. Site amplification map of 1.0 sec spectral acceleration for input ground motion level of 1.0g.

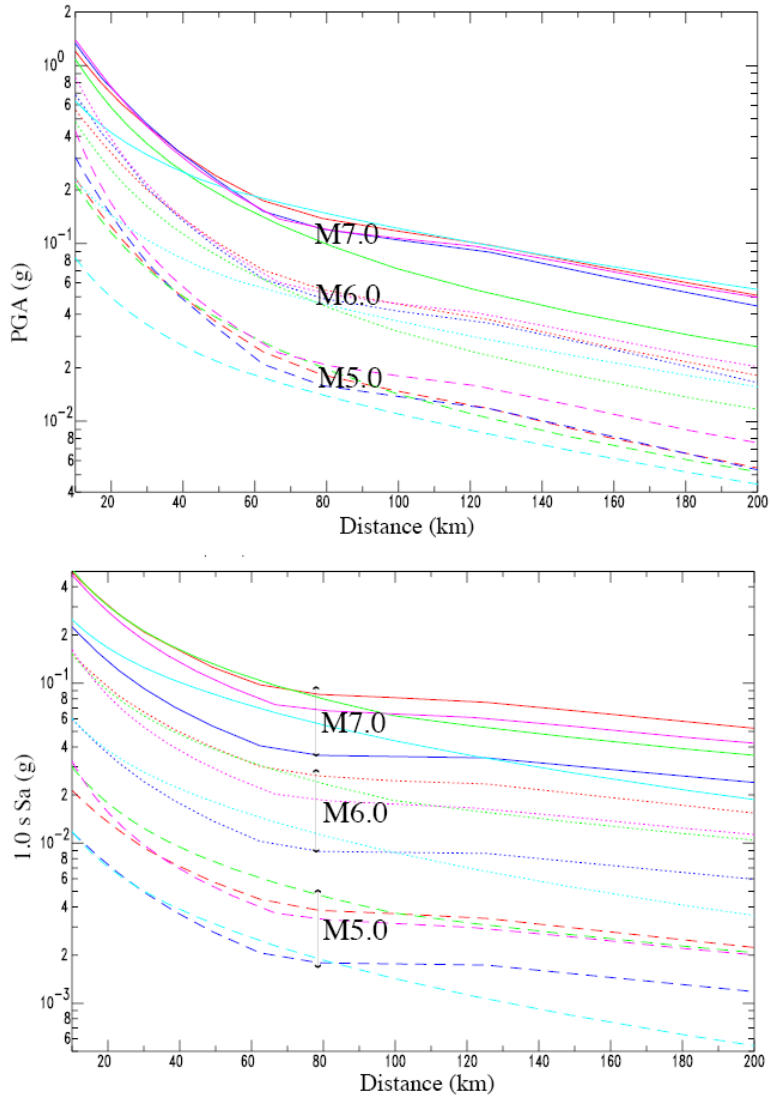

Figure 48. The comparison of the Eastern North America ground motion attenuation relationships in terms of PGA and 1 sec Sa for M 7.0 (solid lines), M 6.0 (dotted lines) and M5.0 (dashed lines) used in the USGS national maps and the Memphis seismic hazard maps. Colors indicate the used attenuation: Frankel et al. (1996) in red, Atkinson and Boore (1995) in blue, Toro et al. (1997) in green, Somerville et al. (2001) in light blue and Campbell (2003) in magenta (adopted from Cramer et al., 2004).

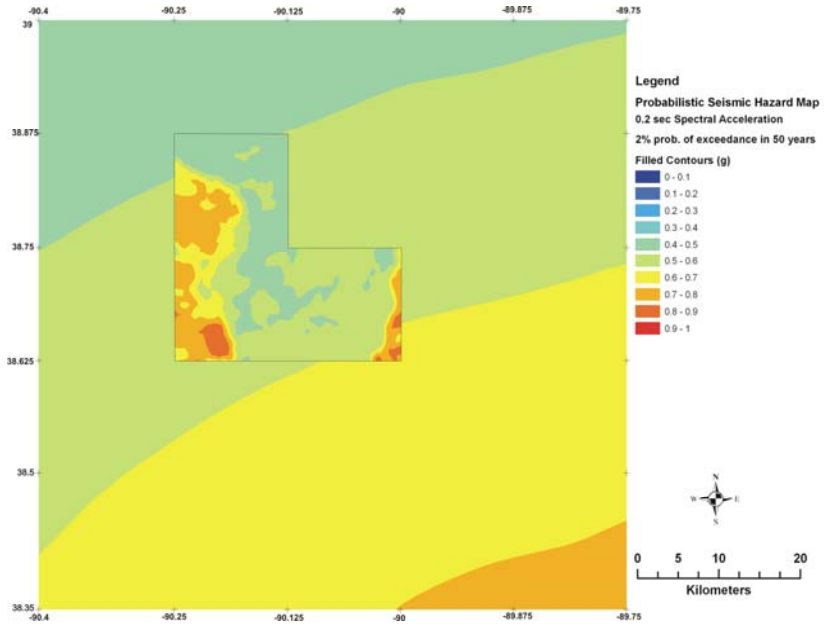

Figure 49. Probabilistic seismic hazard map showing 0.2 sec spectral acceleration with 2% probability of exceedance in 50 years. The L-shape area is the area under investigation, superimposed on the 2002 USGS national seismic hazard maps for the same ground motion level.

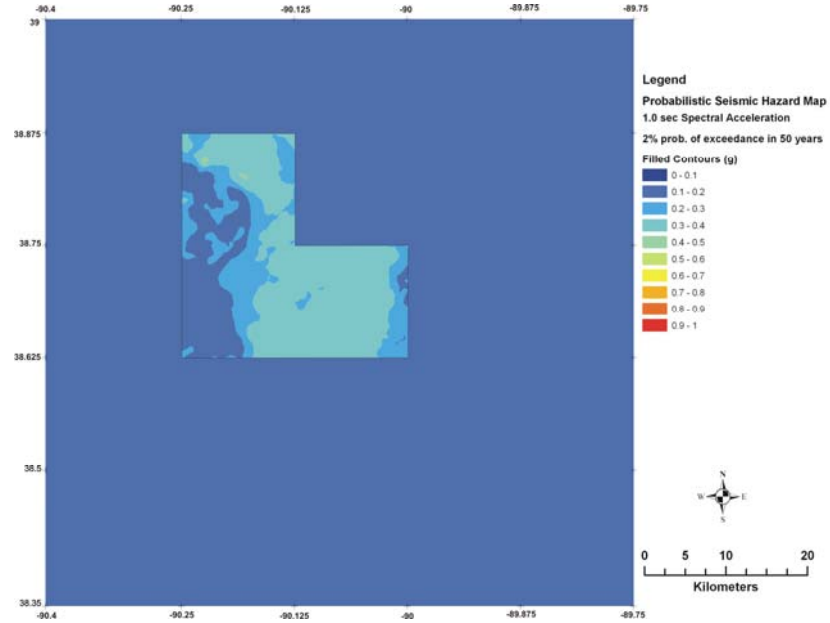

Figure 50. Probabilistic seismic hazard map showing 1.0 sec spectral acceleration with 2% probability of exceedance in 50 years. The L-shape area is the area under investigation, superimposed on the 2002 USGS national seismic hazard maps for the same ground motion level.

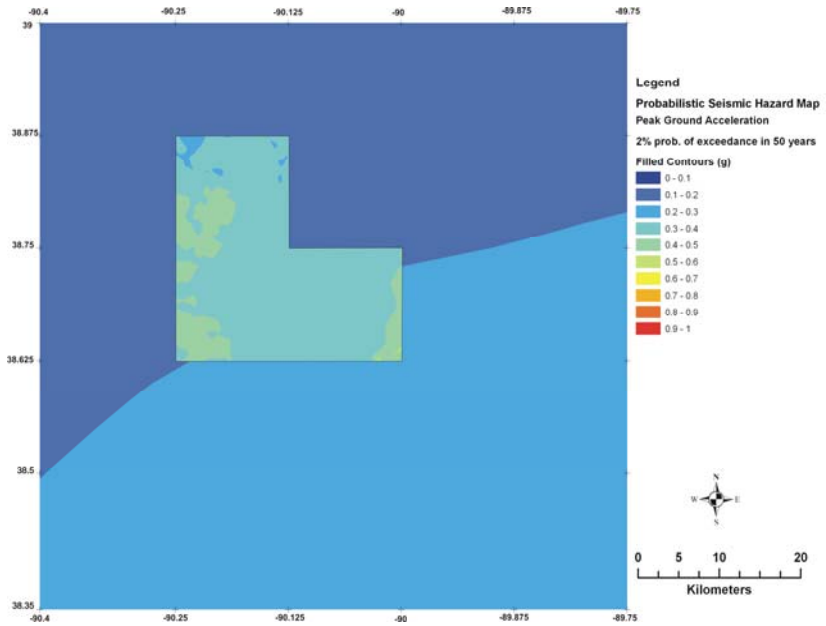

Figure 51. Probabilistic seismic hazard map showing PGA with 2% probability of exceedance in 50 years. The L-shape area is the area under investigation superimposed on the 2002 USGS national seismic hazard maps for the same ground motion level.

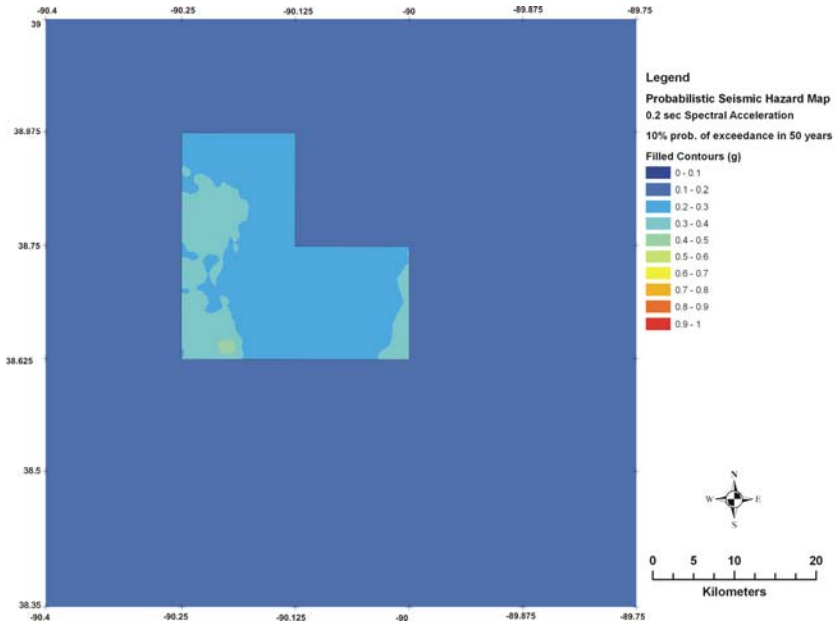

Figure 52. Probabilistic seismic hazard map showing 0.2 sec spectral acceleration with 10% probability of exceedance in 50 years. The L-shape area is the area under investigation, superimposed on the 2002 USGS national seismic hazard maps for the same ground motion level.

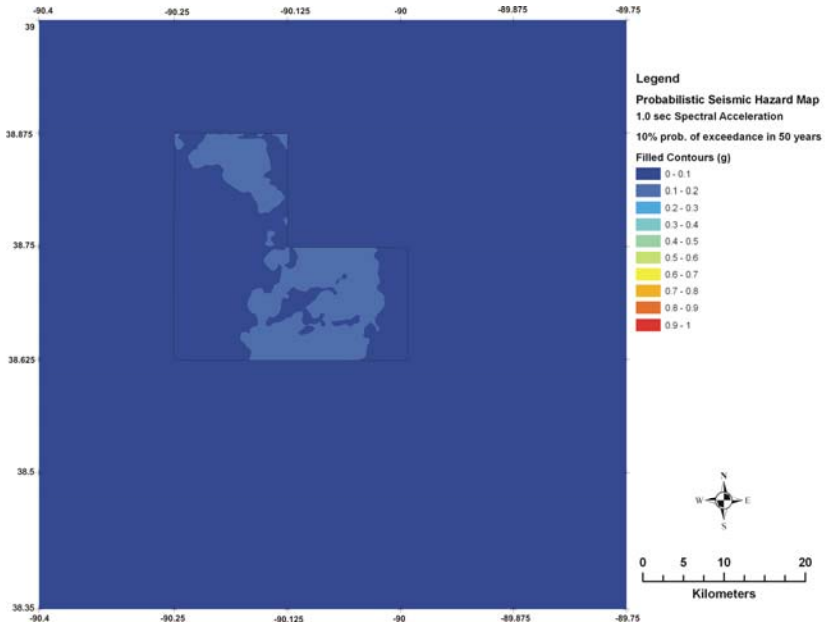

Figure 53. Probabilistic seismic hazard map showing 1.0 sec spectral acceleration with 10% probability of exceedance in 50 years. The L-shape area is the area under investigation, superimposed on the 2002 USGS national seismic hazard maps for the same ground motion level.

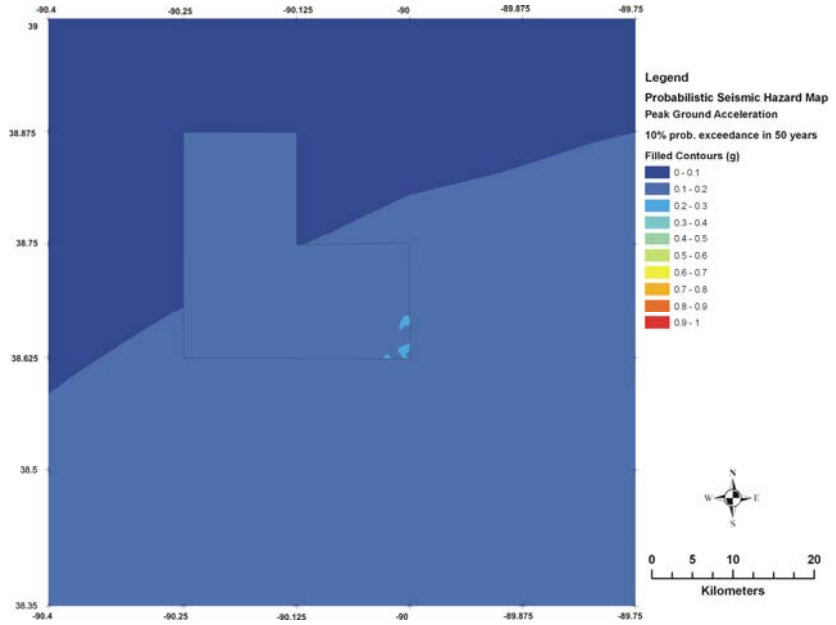

Figure 54. Probabilistic seismic hazard map showing PGA with 10% probability of exceedance in 50 years. The L-shape area is the area under investigation, superimposed on the 2002 USGS national seismic hazard maps for the same ground motion level.

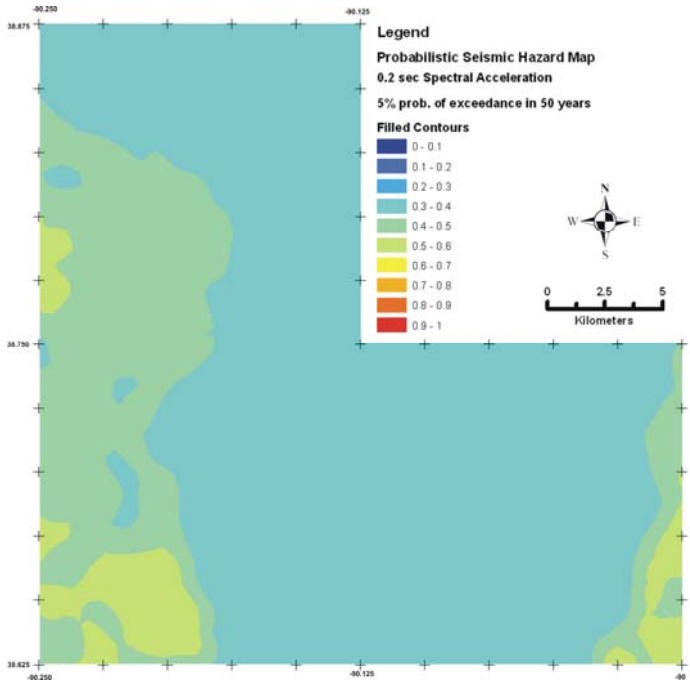

Figure 55. Probabilistic seismic hazard map showing 0.2 sec spectral acceleration with 5% probability of exceedance in 50 years.

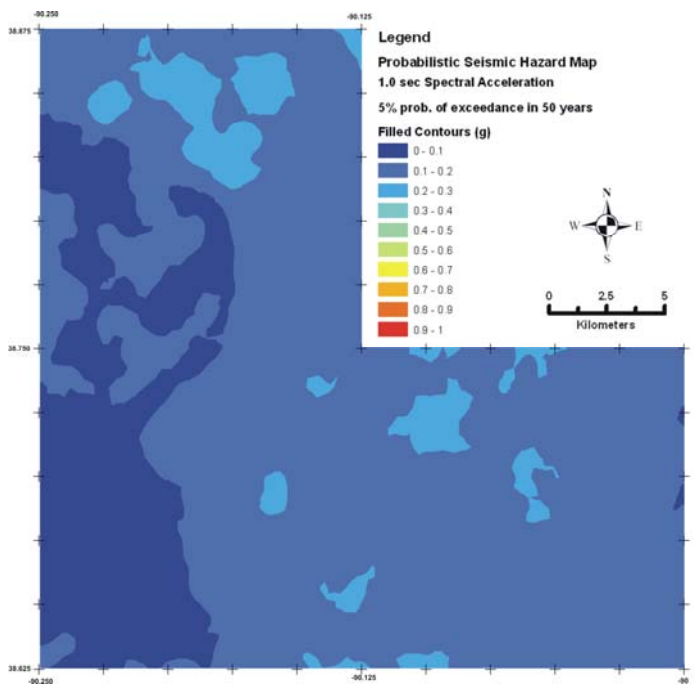

Figure 56. Probabilistic seismic hazard map showing 1 sec spectral acceleration with 5% probability of exceedance in 50 years.

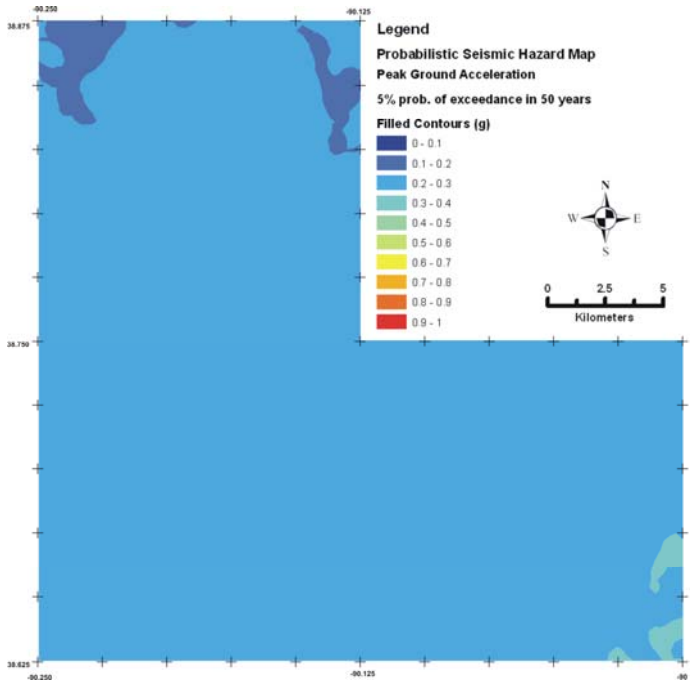

Figure 57. Probabilistic seismic hazard map showing PGA with 5% probability of exceedance in 50 years.

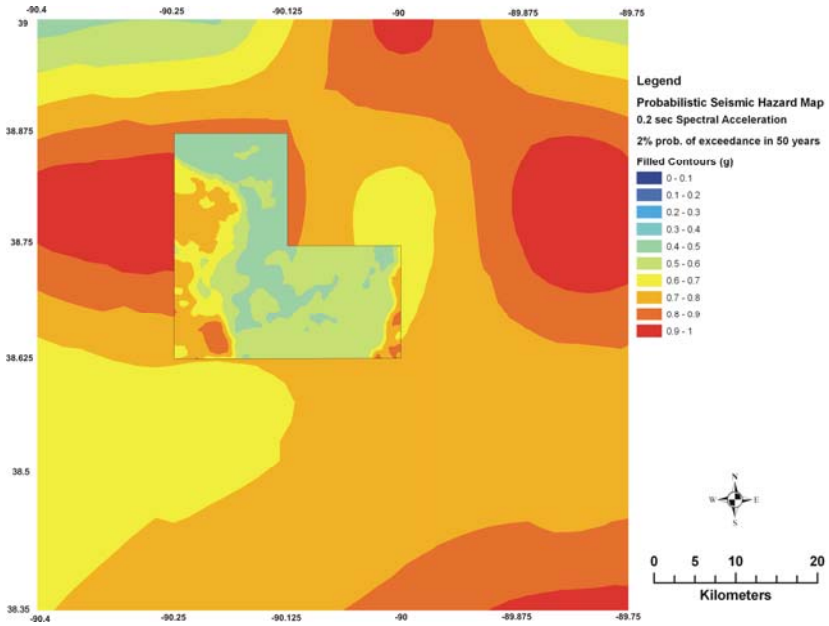

Figure 58. Probabilistic seismic hazard map showing 0.2 sec spectral acceleration with 2% probability of exceedance in 50 years. The L-shape area is the area under investigation, superimposed on Cramer's 2006c seismic hazard maps for the same ground motion level.

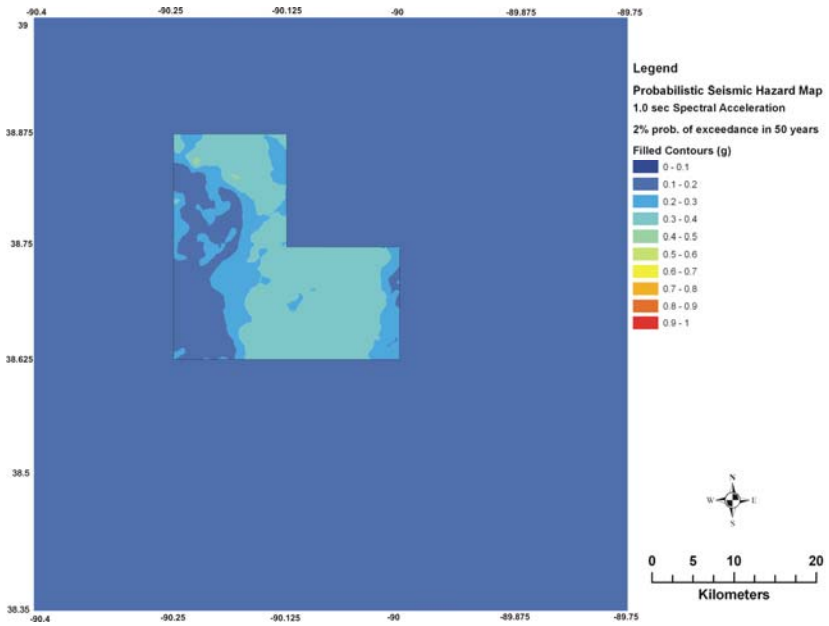

Figure 59. Probabilistic seismic hazard map showing 1.0 sec spectral acceleration with 2% probability of exceedance in 50 years. The L-shape area is the area under investigation, superimposed on Cramer's 2006c seismic hazard maps for the same ground motion level.

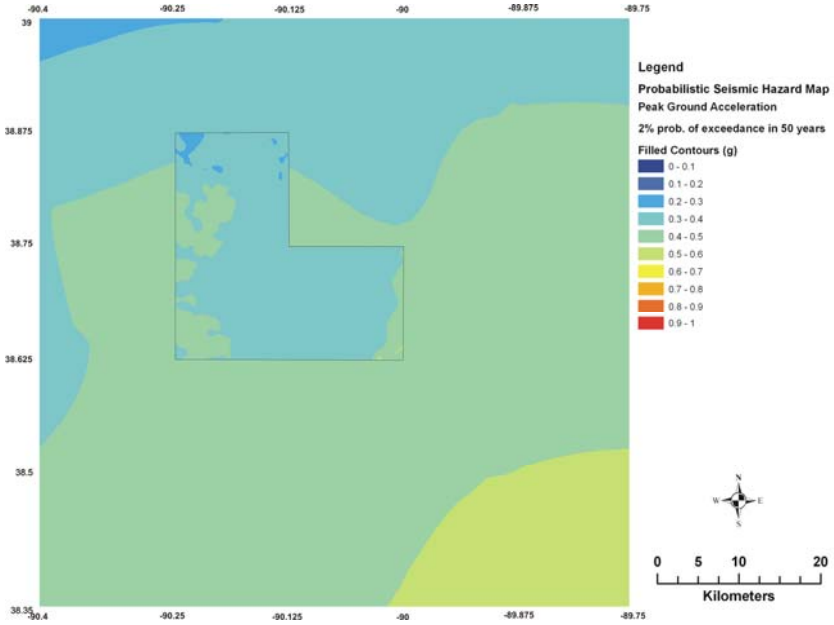

Figure 60. Probabilistic seismic hazard map showing 0.2 sec spectral acceleration with 2% probability of exceedance in 50 years. The L-shape area is the area under investigation, superimposed on Cramer's 2006c seismic hazard maps for the same ground motion level.

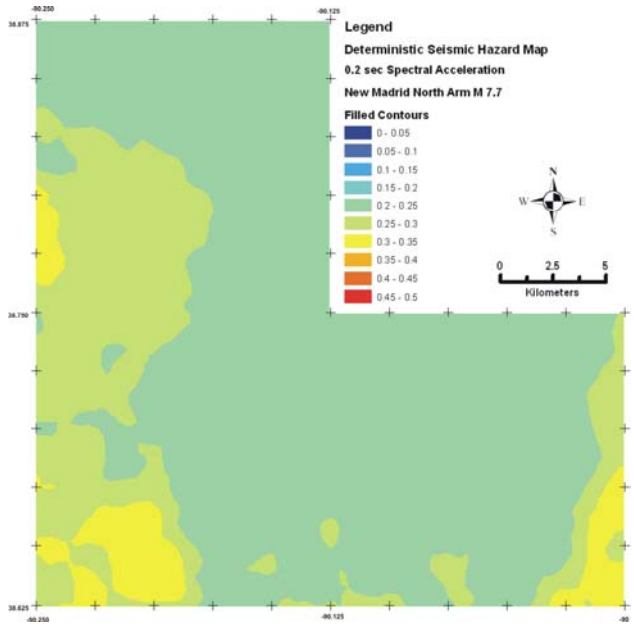

Figure 61. Deterministic seismic hazard map of 0.2 sec Sa for a M 7.7 earthquake originating from the New Madrid North arm at a distance of approximately 200 km. Notice that a different scale was employed in this map.

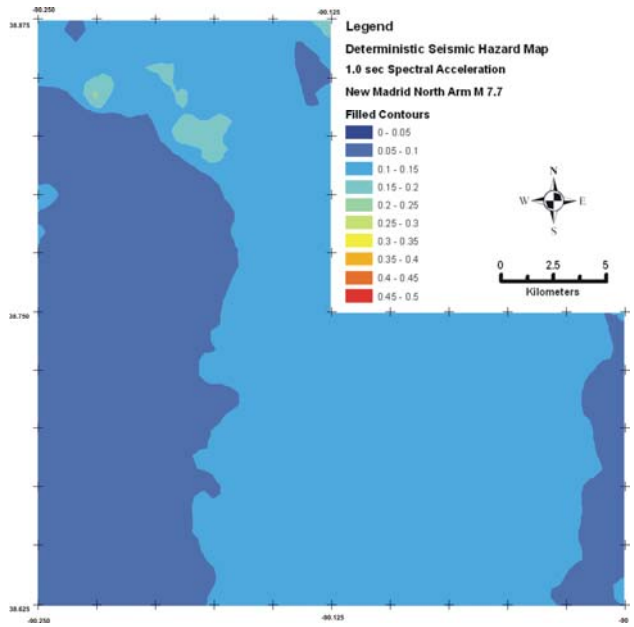

Figure 62. Deterministic seismic hazard map of 1 sec Sa for a M 7.7 earthquake originating from the New Madrid North arm at a distance of approximately 200 km. Notice that a different scale was employed in this map.

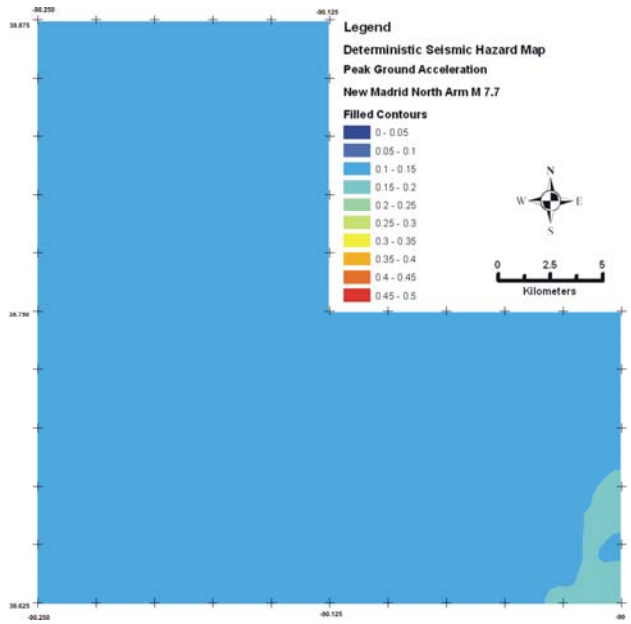

Figure 63. Deterministic seismic hazard map of PGA for a M 7.7 earthquake originating from the New Madrid North arm at a distance of approximately 200 km. Notice that a different scale was employed in this map.

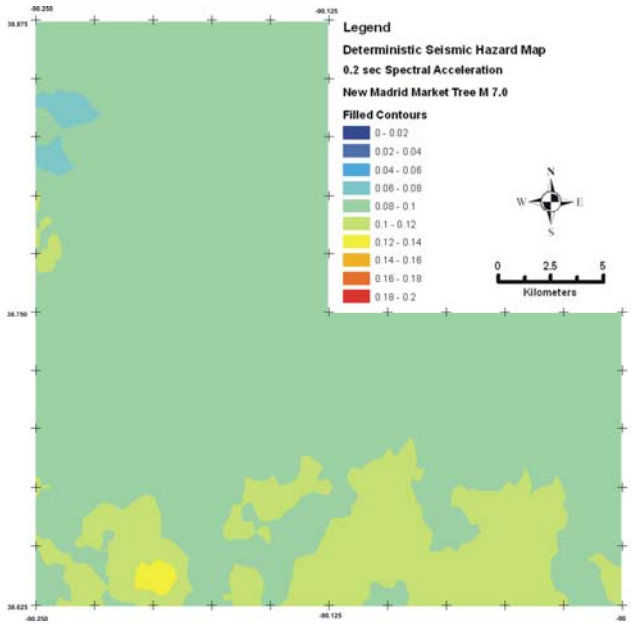

Figure 64. Deterministic seismic hazard map of 0.2 sec Sa for a M 7.0 earthquake originating from the New Madrid South arm at a distance of approximately 400 km. Notice that a different scale was employed in this map.

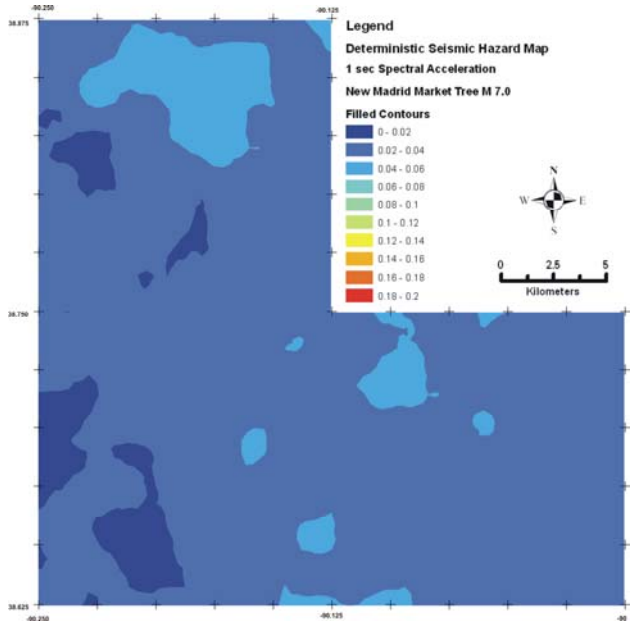

Figure 65. Deterministic seismic hazard map of 1 sec Sa for a M 7.0 earthquake originating from the New Madrid South arm at a distance of approximately 400 km. Notice that a different scale was employed in this map.

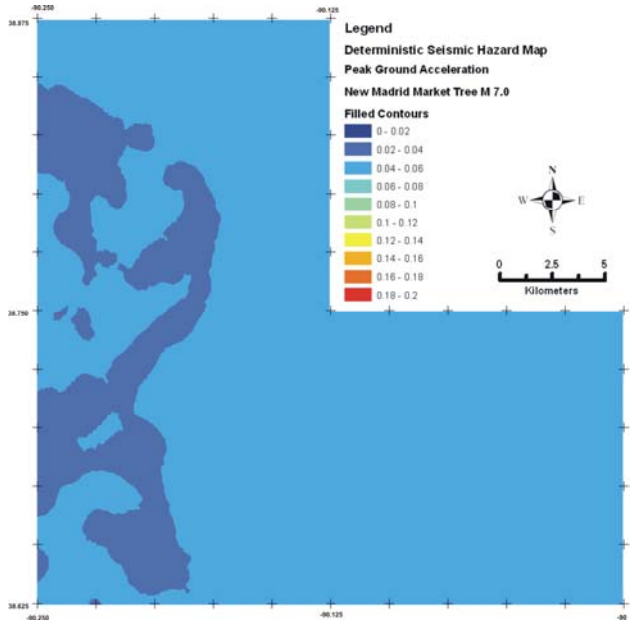

Figure 66. Deterministic seismic hazard map of PGA for a M 7.0 earthquake originating from the New Madrid South arm at a distance of approximately 400 km. Notice that a different scale was employed in this map.

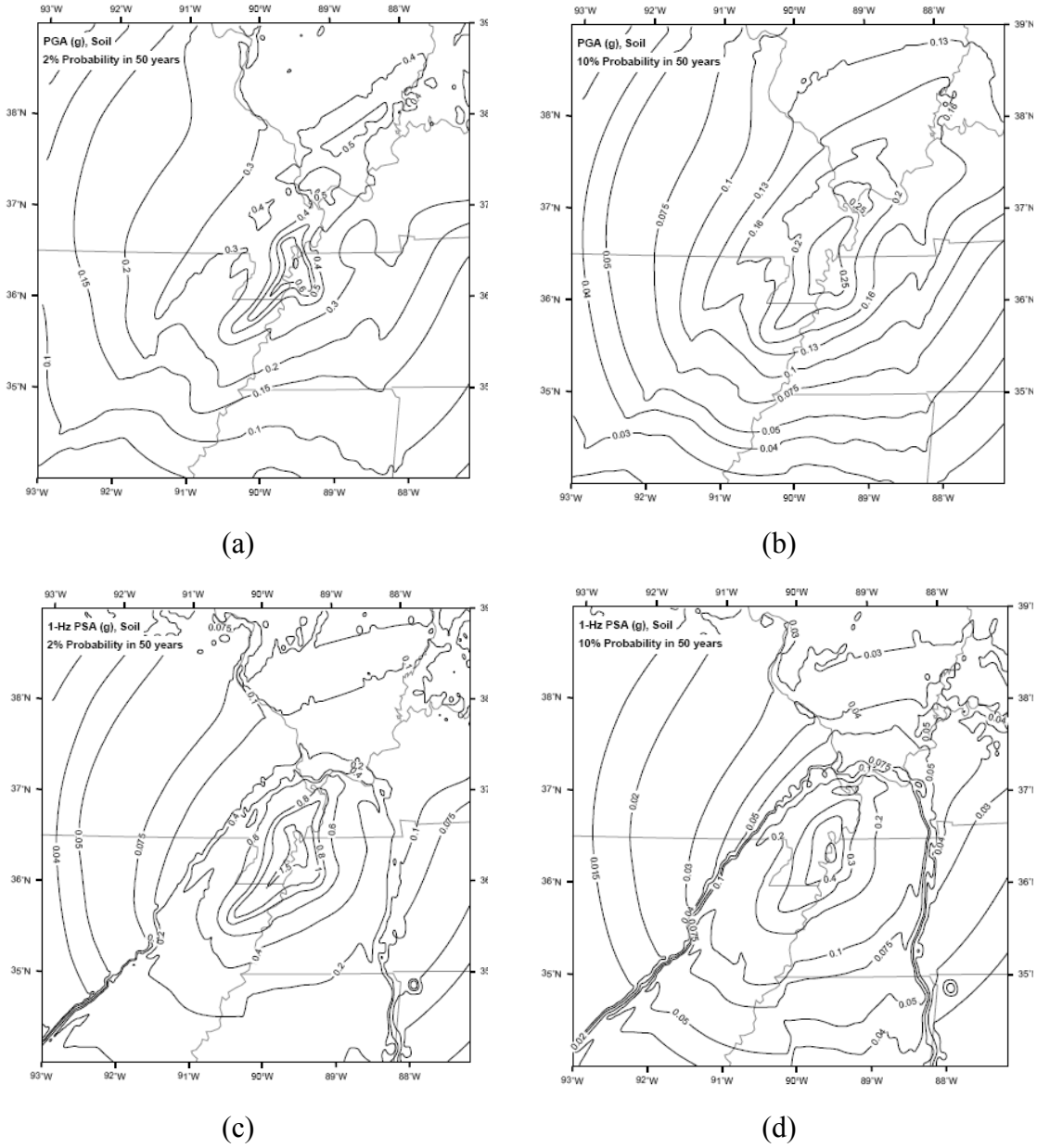

Figure 67. Probabilistic seismic hazard maps generated by Toro and Silva (2001) for PGA and 1 sec Sa; (a) PGA of soil for 2% probability of exceedance in 50 years; (b) PGA of soil for 10% probability of exceedance in 50 years; (c) 1 sec spectral acceleration for soil for 2% probability of exceedance in 50 years; (d) 1 sec spectral acceleration for soil for 10% probability of exceedance in 50 years.

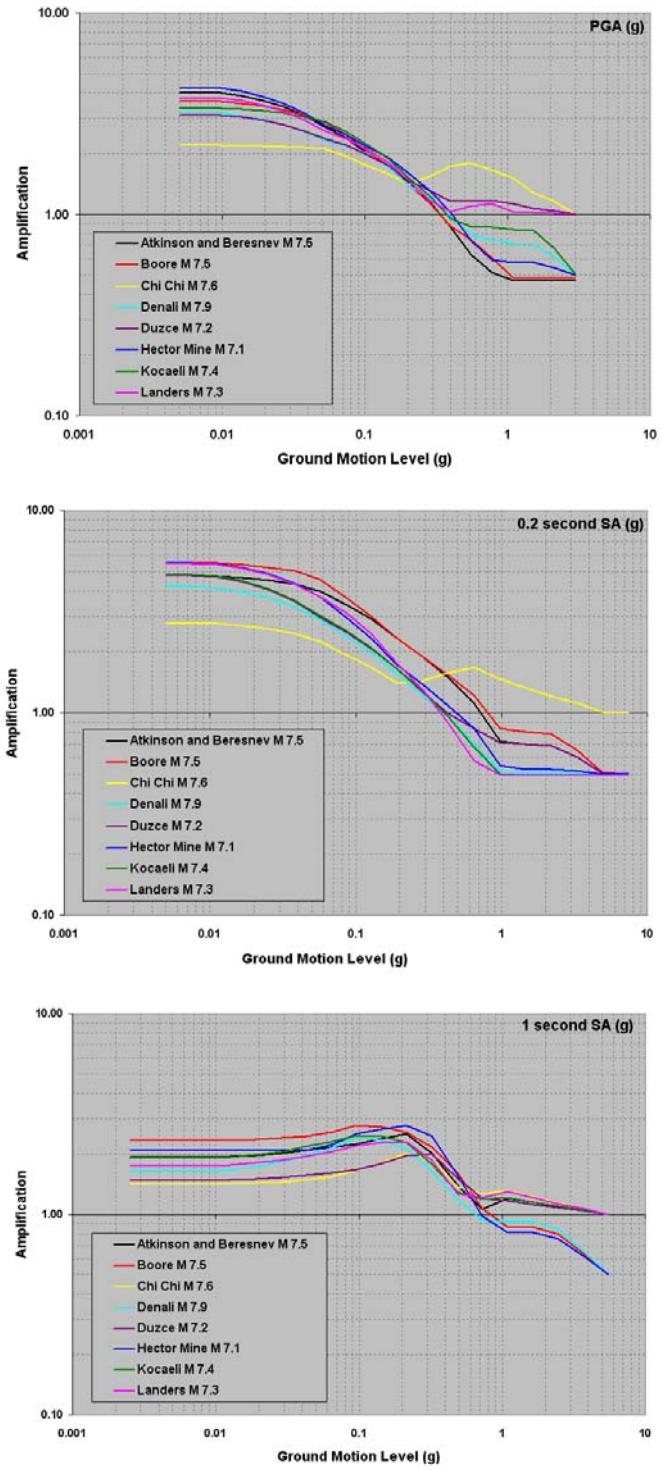

Figure 68. Variations in site amplification for PGA, 0.2 sec Sa and 1 sec Sa due to the choice of input time series.

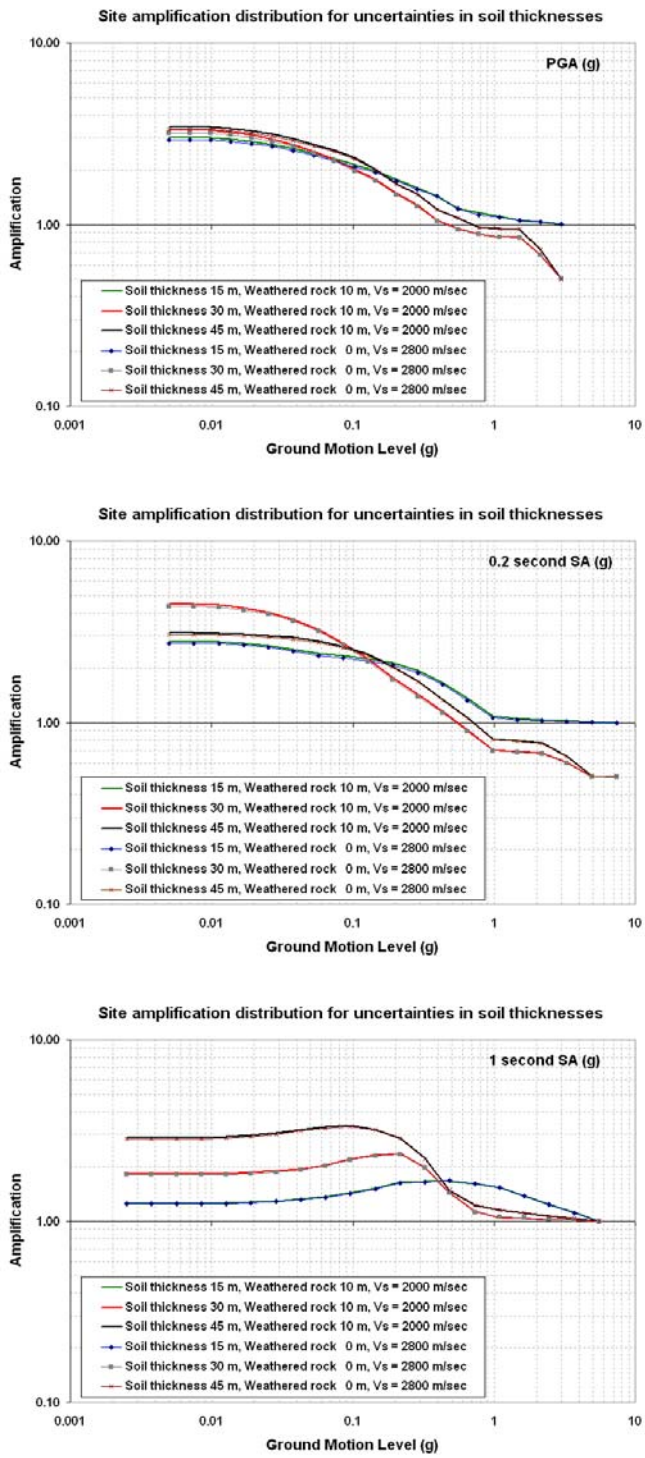

Figure 69. Sensitivity of the site amplification distributions to the variations in soil thickness (15m, 30 m and 45 m) for PGA, 0.2 sec Sa and 1 sec Sa.

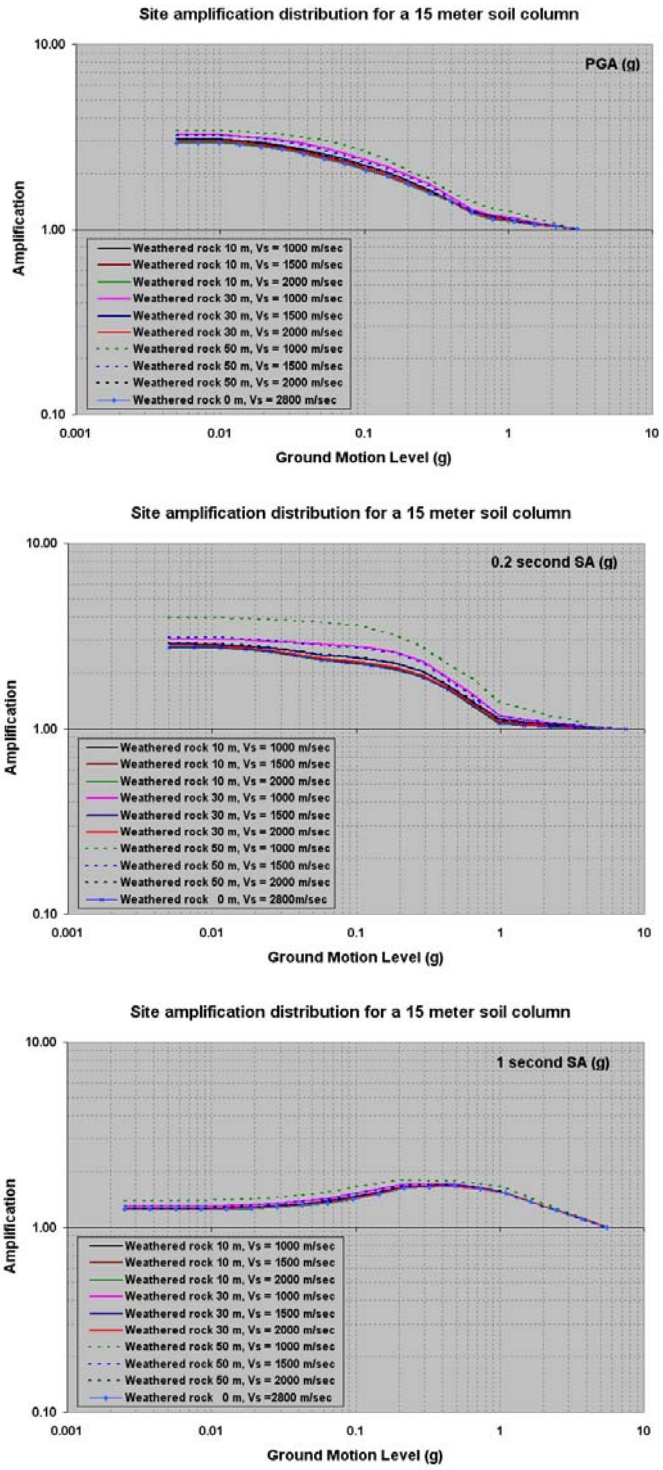

Figure 70. The effect of the variations in thickness and shear wave velocity of the weathered rock unit for a 15 meter thick soil column. The site response for zero thickness weathered rock unit is plotted as diamond shaped line for reference.

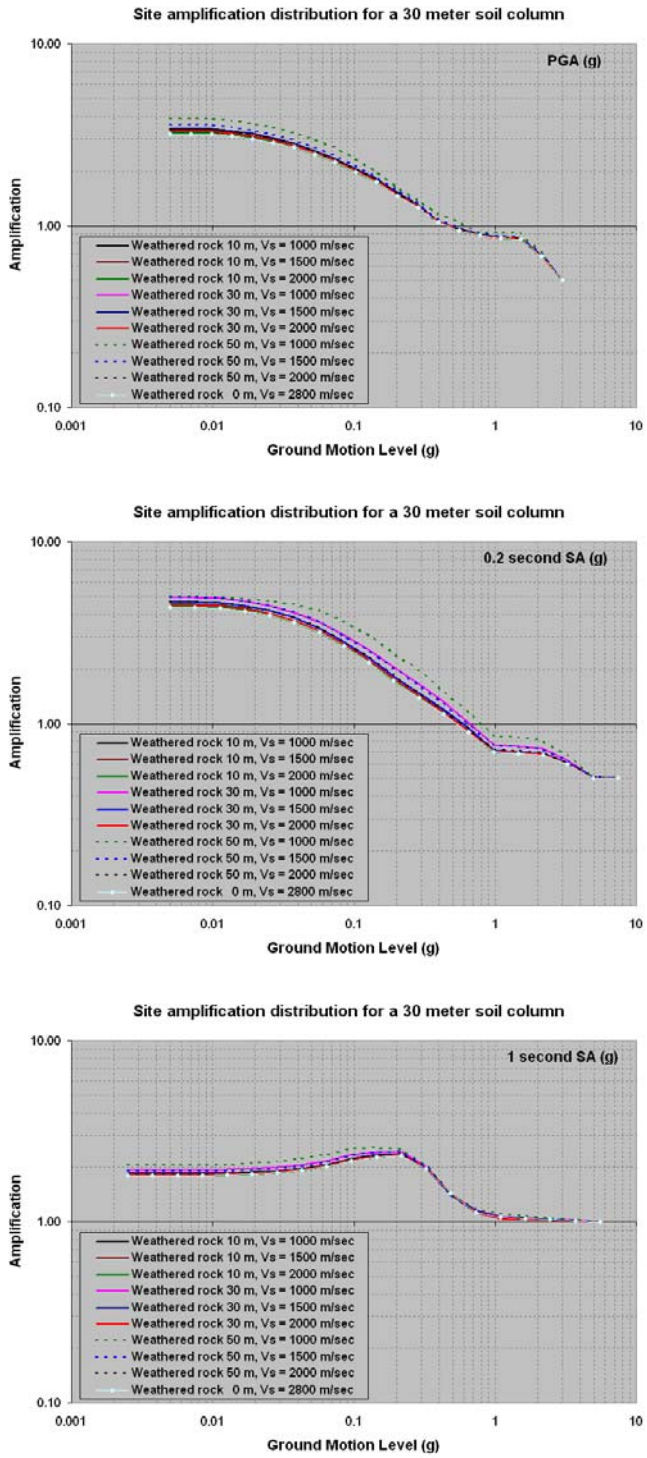

Figure 71. The effect of the variations in thickness and shear wave velocity of the weathered rock unit for a 30 meter thick soil column. The site response for zero thickness weathered rock unit is plotted as diamond shaped line for reference.

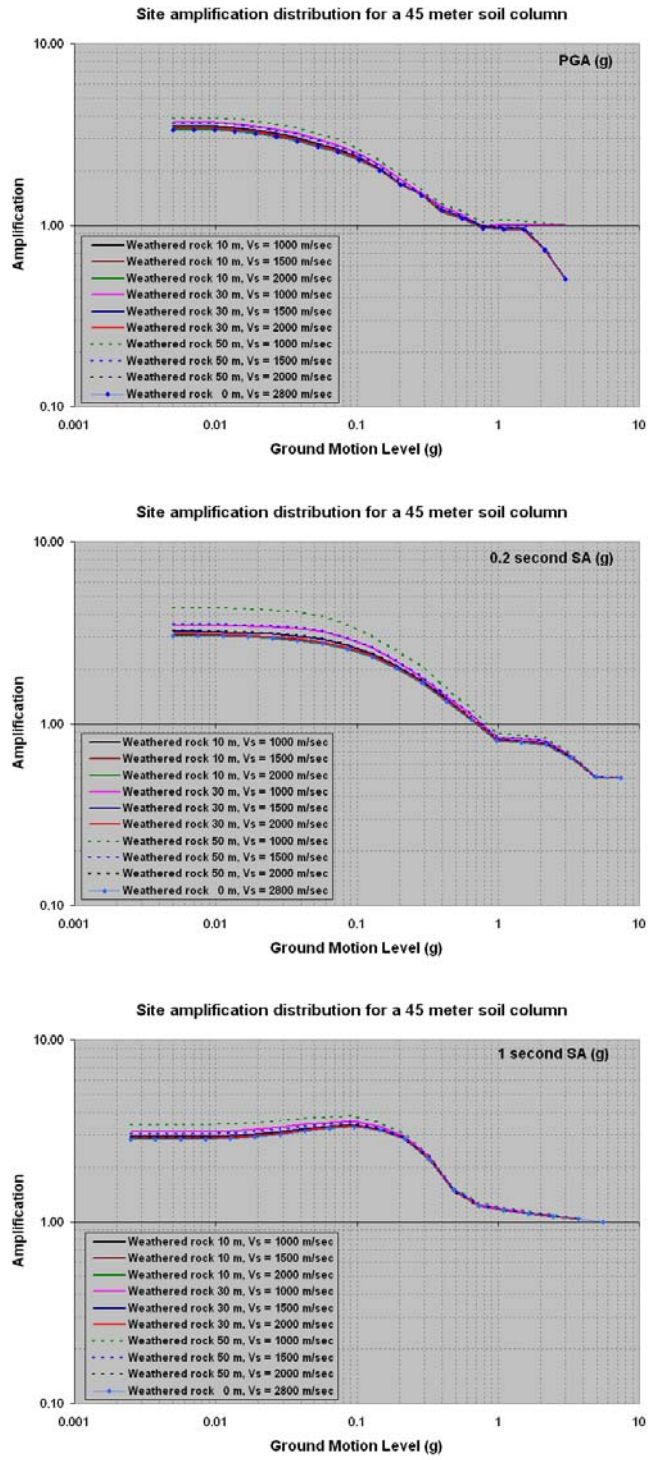

Figure 72. The effect of the variations in thickness and shear wave velocity of the weathered rock unit for a 45 meter thick soil column. The site response for zero thickness weathered rock unit is plotted as diamond shaped line for reference.

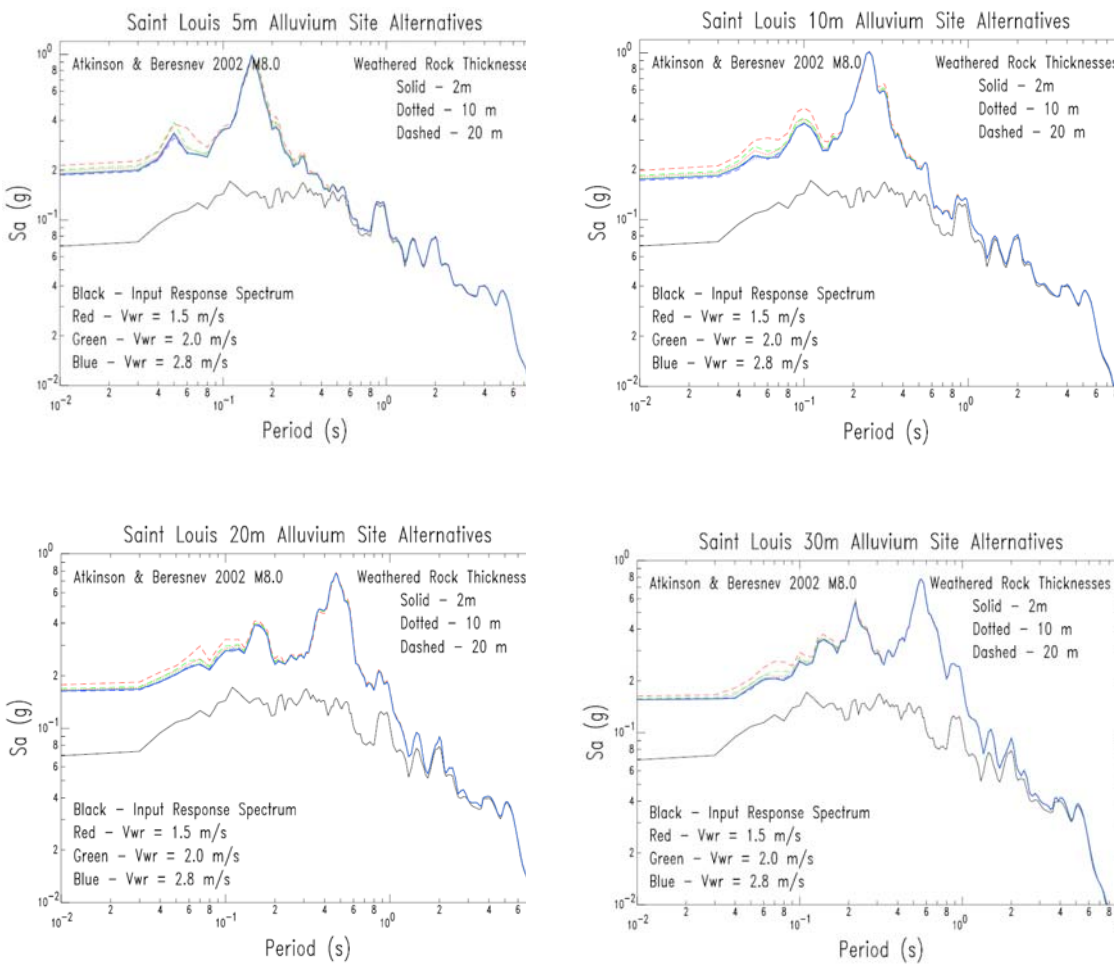

Figure 73. The response spectrum of the input record (an Atkinson and Beresnev, 2002 synthetic record representing a M8.0 in the NMSZ as recorded on hard rock in the St. Louis area) and nine alternative response spectra covering the above weathering layer thickness and shear velocity alternatives for each overall soil thickness of 5, 10, 20, and 30 m (Cramer, 2007).

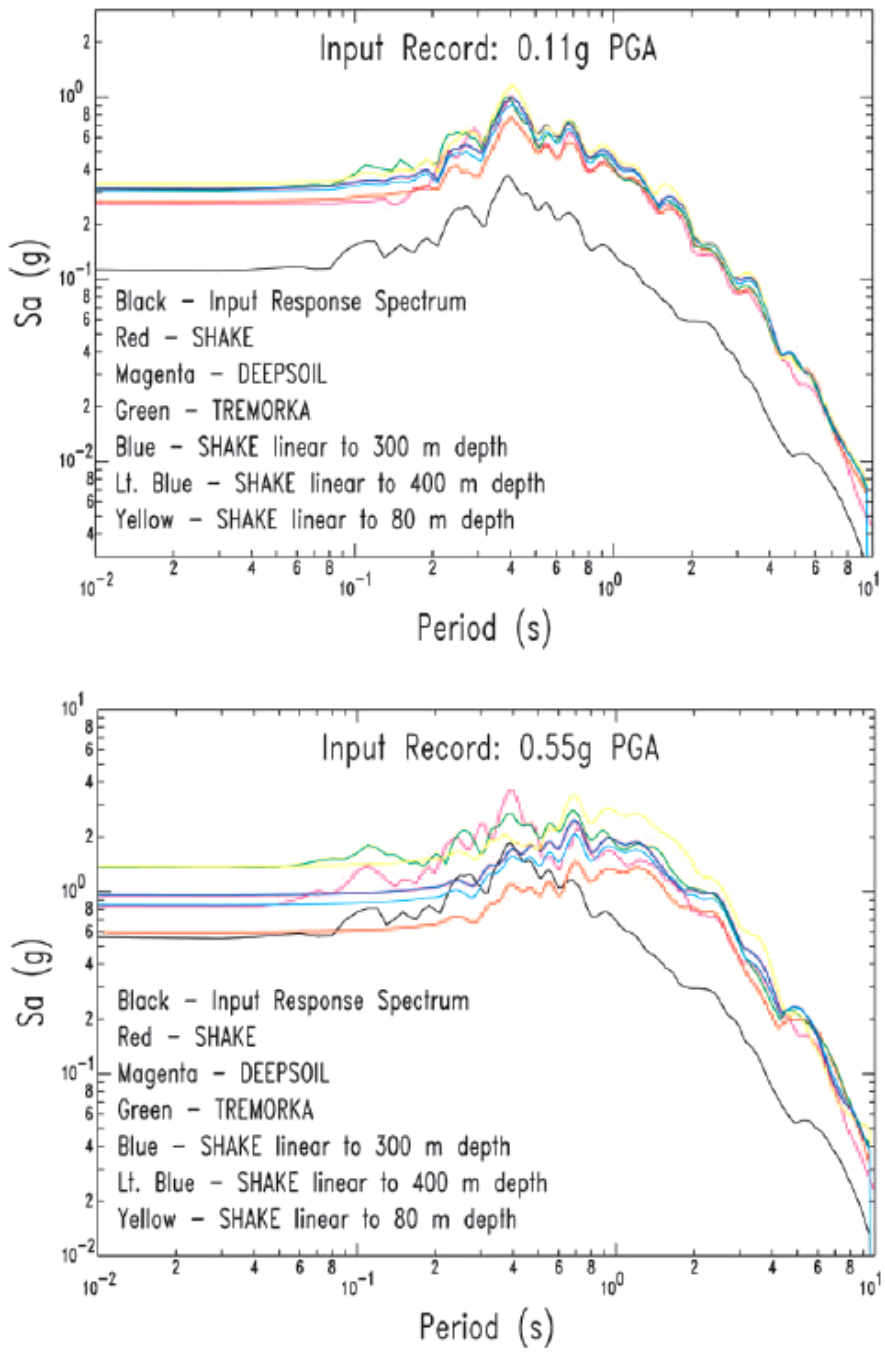

Figure 74. Comparisons of different site response softwares on the estimation of the response spectra for input motions of 0.1g and 0.5g (Cramer, 2006c).

BIBLIOGRAPHY

Aki, K., 1993, Local site effects on weak and strong ground motion, *Tectonophysics*, Vol. 218, p.93-111.

Anderson, J. G., Lee, Y., Zeng, Y., and Day, S., 1996, Control of Strong Motion by the Upper 30 Meters, Bulletin of the Seismological Society of America, Vol. 86, No. 6., pp. 1749-1759.

Anderson, 2003, Strong motion seismology, International Handbook of Earthquake and Engineering Seismology, Part B, pp. 937-966.

Ang, A., H-S., and Tang, W. H., 2007, Probability Concepts in Engineering, Emphasis on Applications to Civil and Environmental Engineering, 2nd Edition, John Wiley & Sons Inc., p. 406.

Atkinson, G. M., and Beresnev, I. A., 2002, Ground motions at Memphis and St. Louis from M 7.5–8.0 Earthquakes in the New Madrid Seismic Zone, Bulletin of the Seismological Society of America, Vol. 92, pp. 1015-1024.

Atkinson, G. M., and Boore, D. M., 2006, Earthquake ground-motion prediction equations for Eastern north America, *Bulletin of the Seismological Society of America*, Vol. 96, no. 6, pp. 2181-2205.

Bauer, R. A., 2007, Personal communications.

Boore, 2003, SMSIM –Fortran programs for simulating ground motions from earthquakes: Version 2.0 –a revision of OFR 96-80-A, United States Department of Interior United States Geological Survey, p. 56.

Building Seismic Safety Council (BSSC), 2001, *2000 Edition, NEHRP Recommended Provisions for Seismic Regulations for New Buildings and Other Structures, FEMA-368*, Part 1 (Provisions): developed for the Federal Emergency Management Agency, Washington, D.C.

Campbell, K. W., 2003, Prediction of strong ground motion using the hybrid empirical method and its use in the development of ground-motion (attenuation) relations in the eastern North America, *Bulletin of Seismological Society of America*, Vol. 93, No. 3, pp. 1003-1012.

Chopra, A. K., 2001, Dynamics of Structures: Theory and Applications to Earthquake Engineering, Prentice Hall, p. 844.

Cramer, C. H., 2001, A seismic hazard uncertainty analysis for the New Madrid seismic zone, *Engineering Geology*, Vol. 62., pp. 251-266.

Cramer, C. H., 2003, Site-specific seismic-hazard analysis that is completely probabilistic, *Bulletin of Seismological Society of America*, Vol. 93, No. 4, pp. 1841-1846.

Cramer, C. H, Gomberg, J. S, Schweig, E. S., Waldron, B. A., and Tucker, K., 2004, The Memphis Shelby County Tennessee Seismic Hazard Maps, United States Geological Survey Open File Report 2004-1294, p. 41.

Cramer, C.H., Schweig. E.S., and Tuttle, M.P., 2005a, The possibility of northeastward unilateral rupture for the January 23, 1812 New Madrid earthquake" (abstract), *Program for ES-SSA 2005 meeting, October 3-4, 2005, Memphis, Tennessee*, Eastern Section of the Seismological Society of America, 103.

Cramer, C. H., 2005b, Site-specific seismic-hazard analysis that is completely probabilistic, Errata, *Bulletin of Seismological Society of America*, Vol. 95, No. 5, p. 2026.

Cramer, C. H., 2006a, Personal communications.

Cramer, C. H., 2006b, An assessment of the impact of the 2003 EPRI ground-motion prediction models on the USGS national seismic hazard maps, *Bulletin of Seismological Society of America*, Vol. 96, No. 3, p. 1159-1169.

Cramer, C. H., 2006c, Quantifying the uncertainty in site amplification modeling and its effects on site-specific seismic hazard estimation in the upper Mississippi embayment and adjacent areas, *Bulletin of Seismological Society of America*, Vol. 96, No. 6, p. 2008-2020.

Cramer, C., 2007a, University of Memphis, Personal communication.

Cranswick, E., Ozel, O., Meremonte, M., Erdik, M., Safak, E., Mueller, C., Overturf, D., and Frankel, A., 2000, Earthquake Damage, Site Response, and Building Response in Avcilar, West of Istanbul, Turkey, International Journal for Housing science and Its Applications, ISSN 0146-6518, Special Issue: Kocaeli Earthquake 1999, Oktay Ural, Editor-In-Chief, Vol. 24, No. 1, 2000, pp. 85-96.

Curry, B. B., and Grimley, D. A., 2006, Provenance, age, and environment of mid-Wisconsinan slackwater lake sediment in the St. Louis Metro East area, USA, Quaternary Research, Vol. 65, pp. 108-122.

Denny, F. B., and Devera, J. A., 2001, Bedrock Geologic Map of Monks Mound Quadrangle, Madison and St. Clair Counties, Illinois, Department of Natural Resources, Illinois State Geological Survey, 1:24,000.

Denny, F. B., 2003, Bedrock Geology of Granite City Quadrangle, Madison and St. Clair Counties, Illinois and St. Louis County, Missouri, Department of Natural Resources, Illinois State Geological Survey, 1:24,000.

Dobry, R., Borcherdt, R. D., Crouse, C. B., Idriss, I. M., Joyner,W. B., Martin, G. R., Power, M. S., Rinne, E. E., and Seed, R. B., 2000, New site coefficients and site classification system used in recent building code provisions, *Earthquake Spectra,* Vol. 16, No. 1, 41–68.

Duke C. M., 1958, Bibliography of Effects of Soil Conditions on Earthquake Damage, Earthquake Engineering Research Institute

Dunlap and Spinazola, 1984, Interpolating water-table altitudes in west-central Kansas using kriging techniques: United States Geological Water-Supply Paper 2238, 19 p.

EPRI, 1993, Guidelines for determining design basis ground motions, Earthquake Engineering Research Institude, TR-102293.

Federal Emergency Management Agency (FEMA), 2001, HAZUS99 estimated annualized earthquake losses for the United States, p. 32.

Fehrenbacher, J. B., Jansen, I. J., and Olson, K. R., 1986, Loess thickness and its effect on soils in Illinois: University of Illinois Agricultural Experiment Station Bulletin 782, p.13.

Field, E. H., 2000, A modified ground motion attenuation relationship for southern California that accounts for detailed site classification and a basin depth effect, *Bulletin of Seismological Society of Americ*a, Vol. 90, No. 6B, S209-S221.

Finn, W.D.L., 2000, State-of-the-art of geotechnical earthquake engineering practice, *Soil Dynamics and Earthquake Engineering*, Vol. 20, p. 1-15.

Fisk, H.N., 1944, Geological investigation of the alluvial valley of the Lower Mississippi, War Department, Corps of Engineers. Mississippi River Commission, Vicksburg MS, 78 p.

Frankel A. D., 1999, How does the ground shake?, *Science*, v. 283, no. 5410, pp. 2032-2033.

Frankel, A., Mueller, C., Barnhard T., Perkins, D., Leyendecker, E. V., Dickman, N., Hanson, S., and Hopper, M., 1996, National seismic hazard maps: Documentation, *U.S Department of the Interior & U.S Geological Survey* Open-File Report 96-532, Denver, CO.

Frankel, A., Petersen, M. D., Mueller, C., Haller, K. M., Wheeler, R. L., Leyendecker, E. V., Wesson, R. L., Harmsen, S. C., Cramer, C. H., Perkins, D., and Rukstales, K. S., 2002, National seismic hazard maps: Documentation, *U.S Department of the Interior & U.S Geological Survey* Open-File Report 02-420, Denver, CO.

Grimley, D.A., 2000, Glacial and nonglacial sediment contributions to Wisconsin Episode loess in the central United States, *Bulletin Geological Society of America,* Vol. 112, pp. 1475–1495.

Grimley, D. A., Phillips, A. C., Follmer, L. R., Wang, H., and Nelson, R. S., 2001, Quaternary and environmental geology of the St Louis Metro East Area, Guidebook for Field Trips for the 35th Annual Meeting of the North-Central Section of the Geological Society of America, Editor: David Malone, ISGS Guidebook 33, p. 21-73.

Grimley, D. A., and Lepley, S. W., 2005, Surficial Geology of Wood River Quadrangle, Madison County, Illinois, Illinois State Geological Survey, Illinois Preliminary Geologic Map, IPGM Wood River-SG, 1:24,000.

Grimley, D. A., Phillips, A. C., and Lepley, S. W., 2007, Surficial Geology of Monks Mound Quadrangle, Madison and St. Clair Counties, Illinois, Illinois State Geological Survey, Illinois Preliminary Geologic Map, IPGM Monks Mound-SG, 1:24,000.

Grimley, D. A., and Lepley, S. W., 2005, Surficial Geology of Wood River Quadrangle, Madison County, Illinois, Illinois State Geological Survey, Illinois Preliminary Geologic Map, IPGM Wood River-SG, 1:24,000.

Gomberg, J., Waldron, B., Schweig, E., Hwang, H., Webbers, A., Van Arsdale, R., Tucker, K., Williams, R., Street, R., Mayne, P., Stephenson, W., Odum, J., Cramer, C., Updike, R., Hutson, S., and Bradley, M., 2003, Lithology and shear-wave velocity in Memphis, Tennessee, *Bulletin of Seismological Society of America*, Vol. 93, No. 3, p. 986-997.

Goodfield, A. G., 1965, Pleistocene and surficial geology of the city of St. Louis and the adjacent St. Louis County, Missouri, University of Illinois at Urbana-Champaign, p.207, unpublished.

Goodman, R. E., and Appuhn R. A., 1966, Model experiments on the earthquake response of soil-filled basins, *Geological Society of America Bulletin*, Vol. 77, No. 11 pp. 1315–1326

Gordon, D. W., Theron, J. B., Hermann, R. B., and Rogers, A. M., 1970, The south-central Illinois earthquake of November 9, 1968: Macroseismic studies, Bulletin of Seismological Society of America, Vol. 60, No. 3, p. 953-971.

Gutenberg, B., 1956, Great earthquakes 1876-1903, EOS, Transaction of the American Geophysical Union, Vol. 37, pp. 608-614.

Hajic, E.R., Wiant, M.D., and Oliver. J.J., 1995, *Distribution and Dating of Prehistoric Earthquake Liquefaction in Southeastern Illinois, Central U. S.* Final Technical Report Submitted to the U. S. Geological Survey National Earthquake Hazards Reduction Program. Contract No. 1434-93-G-2359. 33 p.

Holzer, T. L., 2005, Comment on 'comparison between probabilistic seismic hazard analysis and flood frequency analysis', *EOS*, Vol. 86, No. 33.

Musson, R. M. W., 2005, Comment on 'comparison between probabilistic seismic hazard analysis and flood frequency analysis', EOS, Vol. 86, No. 39.

Phillips, A. C., Grimley, D. A., and Lepley, S. W., 2001, Surficial Geology Map of Granite City Quadrangle, Madison and St. Clair Counties, Illinois and St. Louis County, Missouri, Illinois State Geological Survey, 1:24,000.

Reiter, L., 1990, Earthquake Hazard Analysis, Issues and Insights, Columbia University Press, New York, p. 254.

Resendiz, D., and Roesset, J. M., 1986, Soil-structure interaction in Mexico City during the 1985 Earthquake, *Proceedings of the International Conference, The Mexico Earthquakes-1985 Factors Involved and Lessons Learned*, Mexico City, p. 193-203.

Romero, S., and Rix, G. J., 2001, Regional variations in near surface shear wave velocity in the Greater Memphis area, Engineering Geology, Vol. 62, p. 137-158.

Romero, S., and Rix, G. J., 2005, Ground motions amplification of soils in the upper Mississippi Embayment, National Science Foundation Mid America Earthquake Center, Report No GIT-CEE/GEO-01-1, p. 461.

Rogers, J. D., and Figuers, S. H., 1991, Engineering geologic site characterization of the greater Oakland- Alameda Area, Alameda and San Francisco Counties, California, Final Report, National Science Foundation, *Grant BCS-9003785*.

Rogers, J. D., Karadeniz, D., and Kraig, C., 2007a, Seismic site response modeling for three Missouri river highway bridges, Journal of Earthquake Engineering, 11:3, p. 400-424.

Rogers, J. D., Karadeniz, D., and Chung, J. W., 2007b, The effect of site conditions in the amplification of ground motion in the St. Louis Area, 4th International Conference on Earthquake Geotechnical Engineering, Paper No. 1768.

Romo, M. P., and Seed, H. B., 1986, Analytical modeling of dynamic soil response in the Mexico Earthquake of Sept. 19, 1985, *Proceedings of the International Conference, The Mexico Earthquakes-1985 Factors Involved and Lessons Learned*, Mexico City, p. 148-162.

Seed, H. B., and Idriss, I. M., 1969a, Influence of soil conditions on ground motions during earthquakes, *Journal of the Soil Mechanics and Foundations Division,* Proceedings of the American Society of Civil Engineers, Proceeding paper 6347, Vol. 95, No. SM1, p. 99-137.

Seed, H. B., and Idriss, I. M., 1969b, Influence of local soil conditions on building damage potential during earthquakes, *Earthquake Engineering Research Center*, University of California Berkeley, Report No. EERC 69-15.

Seed, H. B., Ugas, C., and Lysmer, J., 1976, Site-dependant spectra for earthquake-resistant design, *Bulletin of the Seismological society of America,* Vol. 66, No. 4, pp. 221-243.

Seed, R. B., Dickenson, S. E., Reimer, M. F., Bray, J. D., Sitar, N., Mitchell, J. K., Idriss, I. M., Kayen, R. E., Kropp, A., Harder, L. F., and Power, M. S., 1990, Preliminary report on the principal geotechnical aspects of the October 17, 1989 Loma Prieta earthquake, Report UCB/EERC-90/05, Earthquake Engineering Research Center, University of California, Berkeley, p. 137.

Singh, S. K., Mena, E., and Castro, R., 1988, Some aspects of source characteristics of the 19 September 1985 Michoacan earthquake and ground motion amplification in and near Mexico City from strong motion data, *Bulletin of the Seismological society of America*, Vol. 78, pp. 451-477.

Schnabel, P.B., J. Lysmer, and Seed, H.B., 1972, SHAKE: A computer program for earthquake response analysis of horizontally layered sites, *Report EERC 72-12,* Earthquake Engineering Research Center, University of California, Berkeley, CA.

Smith, L. M., and Smith, F. L., Engineering geology of selected areas, U.S. Army Engineering Division, Lower Mississippi Valley, Report 1; The American Bottom, MO-IL, Volumes I and II: Technical Report GL-84-14:Vicksburg, Mississippi, U.S. Army Corps of Engineers, Geotechnical Laboratory, p. 24.

Somerville, P. G., and Moriwaki, Y., 2003, Seismic hazards and risk assessment in engineering practice, International Handbook of Earthquake and Engineering Seismology, Part B, pp. 1065-1080.

Tezcan, S. S., Kaya, E., Bal, I. E., and Ozdemir, Z., 2002, Seismic amplification at Avcilar, Istanbul, Engineering Structures, Vol. 24, pp. 661-667.

Toro, G. R., Abrahamson, N. A., and Schneider, J. F., 1997, Model of Strong Ground Motions from Earthquakes in Central and Eastern North America: Best Estimates and Uncertainties, *Seismological Research Letters*, Vol. 68, No. 1, pp. 41- 57.

USGS, 2002, Earthquake hazard in the heart of the homeland, *U.S. Geological Survey* Fact Sheet, FS-131-02.

Wang, Z., Woolery, E., Shi, B., and Kiefer, J. D., 2003, Communicating with uncertainty, a critical issue with probabilistic seismic hazard analysis, EOS, Vol. 84, No. 46.

Wang, Z., 2005a, Reply to comment by T. L. Holzer, EOS, Vol. 86, No. 33.

Wang, Z., 2005b, Response to comment by R. M. W. Musson, EOS, Vol. 86, No. 39.

Williams R. A., Wood, S., Stephenson, W. J., Odum, J. K., Meremonte, M. E., Street, R., and Worley, D. M., 2003, Surface Seismic Refraction/Reflection Measurement Determinations of Potential Site Resonances and the Areal Uniformity of NEHRP Site Class D in Memphis, Tennessee, Earthquake Spectra, Vol. 19, No. 1, pp. 159-189.

Williams R. A., Odum, J. K., Stephenson, W. J., and Hermann, R. B., 2007, Shallow P- and S-Wave velocities and site resonances in the St Louis Region, Missouri-Illinois, Earthquake Spectra, Vol. 23, No. 3, pp. 711-726.

Youd, T. L., and Carter, B. L., 2005, Influence of soil softening and liquefaction on spectral acceleration, Journal of Geotechnical and Geoenvironmental Engineering, Vol. 131, No. 7, pp. 811-825.

Zeevaert, 1991, Seismosoil dynamics of foundations in Mexico City earthquake, September 19, 1985, Journal of Geotechnical Engineering, Vol. 117, No. 3, pp. 376-428.

Zorapapel, G. T., and Vucetic, M., 1994, The effects of seismic pore water pressure on ground surface motion, Earthquake Spectra, Vol. 10, No. 2, pp. 403-438.